POLITECNICO DI TORINO

MASTER's Degree in Biomedical Engineering

MASTER's Degree Thesis

Unveiling the Influence of Stress and Mental Workload on Our Brain: An fNIRS Analysis

Supervisors

Prof. Danilo DEMARCHI

Ph.D Irene BURAIOLI

Candidate

MARZIA DE CARLO

December 2023

To those who believed in me from the beginning.

Abstract

Stress and workload are conditions that profoundly affect our cognitive and emotional processes, often hindering decision-making in various situations in daily life. These factors have a significant impact on our ability to make decisions, and in some contexts, such as aviation, making the wrong choice can entail significant risks.
Given the critical nature of decision-making in high-stress environments, recent years have seen a growing adoption of HMI systems (Human-Machine Interaction). These systems, designed to enable collaboration between humans and machines, allow the performance of specific functions and the achievement of precise objectives. In the future, they offer the possibility of monitoring the stress and cognitive load of pilots by supervising their work, providing support, or even replacing the pilots themselves in some tasks.
The human body is sensitive to these two conditions and reacts through alterations in physiological signals: electrodermal activity, body temperature, eye movements, brain activity, and cardiorespiratory signal.
Among these, the Functional Near-Infrared Spectroscopy signal (fNIRS) is an important source of information about stress and cognitive load, as it measures changes in light absorption in brain tissue, which reflects changes in the concentration of oxygenated (ΔHbO_2) and deoxygenated haemoglobin (ΔHbR), due, for example, to cognitive stimuli.
This thesis project aims to discover how stress and cognitive load influence the fNIRS signal, identifying which signal characteristics are discriminating in detecting these states of the subject.
Through a state-of-the-art analysis, 19 features were selected comprising 8 temporal, 7 statistical and 4 spectral features to be extracted from the two signals (ΔHbO_2 and ΔHbR).
Subsequently, an acquisition protocol was carried out on 64 subjects who underwent two types of tests namely: the Stroop test to induce stress and the N-back test to induce cognitive load. The signal was acquired using the Biosignalsplux fNIRS sensor, positioned in the center of the subject's forehead, this sensor output provides two digital raw data. These two outputs were subjected to processing operations, including artifact removal and the application of the Modified Lambert-Beer Law to obtain the concentrations of oxygenated and deoxygenated haemoglobin.
After features extraction, for each test phase, these were divided into classes based

on the answers given by the participants to a subjective questionnaire. In the questionnaire, subjects were required to express their perception of stress and cognitive load across four possible levels.
Finally, for each feature, a statistical approach based on the Kruskal-Wallis test and the Mann-Whitney test was carried out to discriminate which features presented a certain significance.
It emerged that 50% of the extracted features allowed a binary classification, distinguishing between a state of rest and one of stress or cognitive load. In particular, it was observed, in line with the state of the art, an increase in the mean value of oxygenated haemoglobin and a consequent decrease in deoxygenated haemoglobin during the execution of a task inducing stress or workload.
Although these are preliminary tests, they demonstrate a strong link between the fNIRS signal and the two cognitive conditions. Therefore, the results encourage us to continue investigating this context to provide efficient and reliable solutions to future HMI systems.

Keywords: *Functional near-infrared spectroscopy; Stress; Workload; HMI.*

Table of Contents

List of Tables

List of Figures

Acronyms

fNIRS
: Functional Near Infrared Spectroscopy

CLT
: Cognitive Load theory

CW
: Cognitive Workload

TMT
: Trail Making Test

SCWT
: Stroop Colour and Word Test

WL
: Working Memory

CBF
: Cerebral Blood Flow

CVR
: Cerebrovascular resistance

CPP
: Cerebral perfusion

CVP
: Central Venous Pressure

ICP
: Intracranial Pressure

MAP
: Mean Arterial Pressure

ECG

Electrocardiogram

DPF

Differential path length factor

PFC

Prefrontal cortex

HCI

Human-computer interaction

HMI

Human-machine interaction

UAVs

Operating unmanned aerial vehicle

NVC

Neurovascular coupling

MBLL

Modified Beer-Lambert Law

SPO

Single Pilot Operations

Chapter 1

Introduction

The evolution of technologies has brought about a significant change in the interaction between individuals and machines, influencing key sectors such as aviation, healthcare, the automotive industry, and other safety-critical areas. In these contexts, operational effectiveness and, above all, safety have become central priorities.
Human-Machine Interaction (HMI) systems are designed to facilitate the execution of specific functions and the achievement of defined objectives through collaboration between humans and machines. In some situations, they are created to relieve the operator by allowing the machine to perform certain tasks directly. However, in other circumstances, the operator often finds themselves managing multiple responsibilities simultaneously while interacting with the HMI system. This situation can lead to an increase in stress levels and workload for the operator, resulting in incorrect decisions that increase the risk of incidents.
Understanding and managing these two factors, cognitive workload and stress, are crucial to ensuring an adequate level of safety in these contexts. Workload refers to the amount of mental effort required for specific tasks, while stress can stem from various sources, including the complexity of operations and external factors.
As a result, the idea of developing next-generation HMI systems with safety mechanisms based on measuring and controlling operator stress and cognitive workload has emerged. These systems prevent the operator from performing functions or tasks if these two altered states become excessively pronounced. This allows the operator to work under optimal workload conditions, even in the most demanding situations, promoting safety and reducing the risk of incidents.
For example, in the field of civil aviation, there has been a growing adoption of Single Pilot Operations (SPO) in recent years. This term refers to the condition of flying an aircraft with only one pilot on board, assisted by advanced automation systems and, at times, ground operators providing piloting support. This transition poses significant challenges in terms of safety and pilot monitoring, making it essential to develop an intelligent Human-Machine Interaction (HMI) system capable of assessing both the operator's mental workload and stress to ensure flight safety.
Currently, three approaches are used for monitoring stress and cognitive workload and they are:

- Subjective questionnaires;
- Behavioral analysis;

- Physiological measurements.

Subjective questionnaires have limitations as they cannot be integrated into future systems due to the lack of real-time capabilities. On the other hand, large-scale behavioral analyses are challenging to scale. Therefore, there is a growing trend towards using physiological parameters to assess stress and cognitive workload, as these can be more easily integrated into future HMI system developments.
In particular, various physiological signals have been identified as sensitive to these conditions, including ECG, respiration, electrodermal activity, temperature, brain activity, and eye movements. Integrating these signals offers promising prospects for a more accurate and real-time assessment of stress and cognitive workload in HMI systems.
This thesis primarily focuses on the **Functional Near-Infrared Spectroscopy signal** (fNIRS), chosen for its promising potential as an indicator of brain activity, which is crucial for evaluating variations in stress and cognitive workload. The lack of comprehensive studies in this specific field has emphasized the importance of further exploring the relationship between the fNIRS signal, stress, and cognitive workload, providing the basis for in-depth analysis in this work. Additionally, the ease of integrating instrumentation for acquiring the fNIRS signal with Human-Machine Interface (HMI) systems has provided further incentive to fully understand the role of this signal.

1.1 Objectives of the thesis project

In light of this, the following thesis aims to achieve the following objectives:

- Conduct a state-of-the-art analysis regarding the relationship between the fNIRS signal and variations in stress and cognitive workload, identifying significant features.
- Perform experimental tests using the acquisition equipment to assess the variation of the fNIRS signal in relation to stress and cognitive workload.
- Process the obtained data to extract the most significant features identified earlier from the signal information.
- Finally, evaluate the correlation of these features with variations in stress and cognitive workload and assess whether it can be used as a reliable indicator to monitor the subject's cognitive state.

To achieve these objectives, a data acquisition protocol involving a population of 62 participants was executed. During this protocol, participants underwent the Biload Test, comprising the Stroop test to induce stress and the N-back test to induce cognitive load. Subsequently, a specific statistical analysis was conducted to evaluate whether the extracted features, previously identified through a state-of-the-art analysis, indeed demonstrated sensitivity to variations in cognitive load.
In this thesis, the acronyms HbO_2 and HbR will be used to refer to oxygenated and deoxygenated hemoglobin, respectively.

In the upcoming sections, a detailed presentation of the background with key concepts related to cognitive load, stress, and Functional Near-Infrared Spectroscopy (fNIRS) will be provided. Following that, the materials and methods used for the study will be described, the conducted statistical analysis will be presented, and the obtained results will be discussed.

Chapter 2

Background

This chapter provides an essential context for understanding the key elements of this thesis work.
It begins by defining stress and cognitive load, subsequently introducing the tests most commonly used in the literature to induce these two conditions in subjects.
This is followed by a brief overview of the physiological signals that have shown significance in previous studies on this topic, with a particular focus on the ***Functional Near-Infrared Spectroscopy signal*** (fNIRS), which is the main focus of this thesis by providing a description of the physiology behind this signal.
In a separate section, works in the literature exploring the link between stress, cognitive load, and fNIRS is reviewed.
Finally, the chapter proceeds to provide a detailed description of the acquisition protocol used to record the physiological signals, ensuring a clear understanding of the experimental context and measurement procedures adopted during the study.
The conclusion of the chapter includes an explanation of the two statistical tests that will be utilized in the statistical approach to obtain the results for this thesis work.

2.1 Stress

Approximately four decades ago, Hans Selye [1], widely regarded as the pioneer in stress, authored his inaugural publication on the subject. Since its inception, there has been an extensive body of literature consisting of numerous papers, research, and experiments dedicated to the exploration of stress, accompanied by a multitude of diverse definitions. According to Cofer and Appley (1964) [2], stress may be defined as the condition in which an organism perceives a threat to its well-being and responds by mobilizing all available resources to ensure its preservation. In an alternative use, stress was delineated as a category of circumstances that give rise to disruptions inside an individual, and it was conceptualized as a continuum of stimuli. In relation to Human-Machine Interface (HMI) systems, this term can be linked to the physiological response of an individual to stimuli that disrupt the normal equilibrium, resulting in physical, mental, or emotional strain [3]. The stress response is a subjective phenomenon [4], as it varies among individuals due to their unique capacity for handling a specific situation.
There are three distinct categories in which stress may be classified [5]:

- **Nuestress**: derived from the term "nue" meaning neutral, refers to a state in which the stress response is essential for daily adaption;

- **Distress**: characterized by the prefix "dis" indicating adverse emotions, refers to the stress response that is unfavorable and has the potential to induce disease. It is widely acknowledged as a type of stress that occurs when the level of excitement goes beyond a personally decided limit, either in terms of how strong or long it lasts, or in situations that are seen as risky or demanding.

- **Eustress**: derived from the word "eu" denoting happy or healthy emotions and shortened from euphoric, refers to a stress reaction that is advantageous and can provide beneficial outcomes for individuals. These advantages may include heightened focus and therefore increased productivity.

Stress can manifest in both short and long-term scenarios. In short-term situations, it triggers the body's response to a perceived threat or danger, known as the 'fight or flight' response. This reaction involves the release of chemicals such as adrenaline and cortisol, influencing various aspects of the autonomic nervous system and providing the body with a surge of energy and strength. This allows the individual to react, cope with the situation, and restore homeostasis, both psychologically and physiologically. On the other hand, when stress persists over time, it is referred to as chronic stress, which has a significant impact on the body, leading to lasting effects on the individual's health. Conditions such as diabetes, anxiety, depression [6], heart disease and digestive problems have been associated with stress.
Stressors are defined as stimuli or contexts that induce stress and cause chronic stress. Various aspects of life, such as work, finances, relationships, and daily inconveniences, can be stressors, as well as cognitive arithmetic tests, preparation for a public speech, and loud sounds.

Figure 2.1: Representation of a person during a stressful situation.

2.2 Workload

The concept of cognitive workload is related to the level of mental processing capability that a task places on an individual, as well as the amount of mental resources required for an individual to successfully complete a certain activity within a defined environment and time [7],[8]. The cognitive workload is shown to rise proportionally with the level of task complexity, mostly due to a decrease in the total number of cognitive resources that are accessible for use. When the cognitive workload reaches a level that is close to or exceeds an individual's cognitive capability, it can result in human mistakes and suboptimal decision-making.
This intricate relationship with cognitive processes is reflected in physiological signals, where the workload is strongly linked to the sympathetic nervous system.
Nevertheless, extended periods of engaging in low-intensity cognitive tasks, when the amount of task demand is constant, can also result in the depletion of cognitive resources. A low cognitive workload (CW) has been found to potentially result in negative consequences such as frustration, distraction, and human mistakes [9].
Considering the inherent limitations of human cognitive abilities, it is of utmost significance to strive for the optimization of these resources in order to enhance performance and achieve superior outcomes [10],[11]. Instances characterized by high cognitive workload (CW) should be particularly circumvented in crucial decision-making contexts, such as air traffic control or military operations when it isn't possible to commit errors [12]. An excessive workload has the potential to result in several negative consequences, such as weariness, memory impairments, diminished thinking abilities, irritability, and difficulties in learning [10]. Moreover, those experiencing fatigue are more susceptible to making mistakes.
Two distinct components contribute to the cognitive load, namely the mental load and the mental effort. The mental effort is connected to the nature of a task, such as how complicated it is and the way it is presented. In contrast, mental effort pertains to the amount of cognitive resources requested by the job [7].

Figure 2.2: A representation of the workload

According to Mulder (1986) [13], there are two distinct categories of cognitive exertion: one that pertains to the processing of information in a deliberate manner (referred to as computational effort), and another that is necessary when the operator's energy level is compromised (known as compensatory effort). The first mode is employed to ensure consistent task outcomes in response to changes in task difficulty

or the addition of supplementary tasks. Conversely, the second mode is activated when performance deteriorates to a specific threshold as a result of weariness. The phenomena under consideration is commonly referred to as dissociation, which occurs when there is an inability to meet an overwhelming demand, leading to a decline in the completion of tasks. The feasibility of compensatory effort is limited because excessive amounts of exertion might escalate job complexity and mental burden. Instead of exerting substantial levels of effort, the operator has the option to employ adaptive techniques [14]. Hence, the implementation of a real-time cognitive workload monitoring system holds considerable potential in mitigating task errors and managing workloads during periods of excessive demand. This technology has the potential to be applied in a range of contexts, including but not limited to safety measures, Smart Technology advancements, driver awareness enhancement, mental health monitoring, and Human Machine Interface (HMI). In this thesis study, the terms "mental workload" and "cognitive load" are used as synonymous, as explained in the review of Luzzani et al. [15].

2.3 Stress and Mental Workload relationship

Stress and Mental Workload are not two distinct concepts that have nothing in common with each other. According to Luzzani et al. [15], stress is a factor that can influence activity performance with the mental workload.

In Figure 2.3, it is possible to observe the elements characterizing the concept of

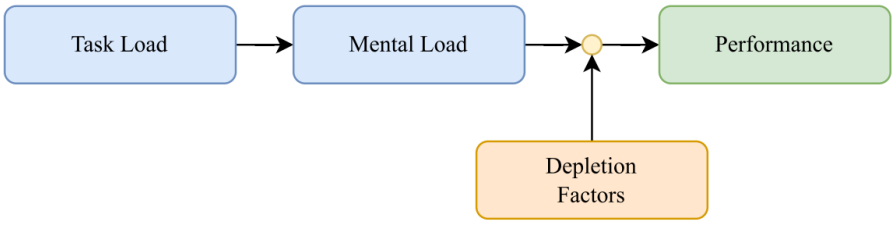

Figure 2.3: Stress and Mental workload relationship

mental workload. The initial block labeled "Task Load" signifies the specific tasks and duties that an individual is required to do. The subsequent block, labeled "Mental Load" reflects the level of cognitive load needed to execute these tasks at a high level of performance successfully. The third concept is "Depletion Factors", the subject must deal with concerns, fatigue, and motivation, leading to the fourth block, "Performance", which represents how the individual is executing the assigned cognitive tasks.

2.4 The tests

In the literature, various tests for psychological and cognitive assessment are available. Among these, there are tests for attention and concentration, involving the examination of visual and auditory reaction times using visual or auditory stimuli and logic games. Additionally, cognitive tests, such as the arithmetic Montreal Imaging Stress

Task, are found. Similarly, there are tests designed to measure various cognitive skills, particularly attention and cognitive flexibility, as demonstrated in the Trail Making Test (TMT).
In the following thesis work, two widely utilized tests in the literature have been selected. The first chosen test is the **Stroop Colour and Word Test** (SCWT), known for its ability to induce stress in participants [16]. The second chosen test is the **N-back Test**, commonly used to assess cognitive overload in individuals [17].

2.4.1 The Stroop Colour-Word Test

The Stroop Color-Word Test (SCWT) is a psychological experiment and cognitive test meant to assess a person's ability to focus on a specific task while suppressing interference from a conflicting, automatic response. John Ridley Stroop created the test in 1935 [18], and it has since become a popular tool in the realms of psychology and neuroscience.

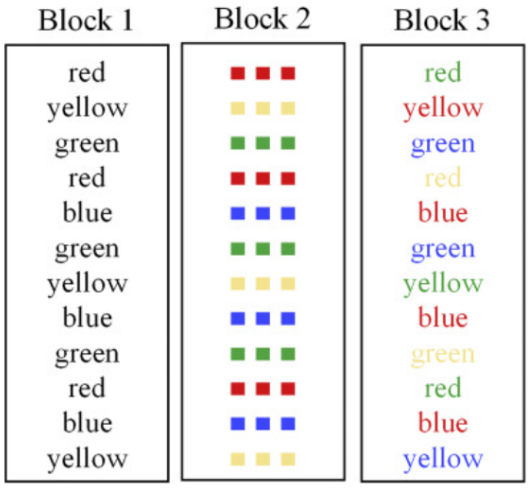

Figure 2.4: The schema of the first version of the Stroop Color-Word Test.

The Stroop effect was discovered in the eighteenth century and was first reported in 1935 by American psychologist John Ridley Stroop[18]. The original Stroop Color and Word Test consists of three phases or blocks. In the first phase, individuals are presented with color terms printed in black ink and are instructed to read the colors aloud as quickly as possible. In the second phase, random colored squares are displayed, and individuals are instructed to call out the color of each square as rapidly as possible. In the third block, a sequence of color words is presented with a randomly mismatched color.
The three test blocks are shown schematically in Figure 2.4. Blocks 1 and 2 are control circumstances, whereas Block 3 is the experiment condition. Individuals are slower to name the ink color when the meaning of the word is a different color than the ink (for example, the word red written in green ink) than when the word's color and the ink color match.
The difficulty in blocking the automatic reaction (reading the word) in favor of the

necessary response (identifying the ink color) explains this impact. Williams et al.[19] showed that the amplified Stroop effect may be utilized to evaluate a variety of psychopathologies.
The Stroop test has been translated into other languages, as well as a "neutral language" variant that uses numbers rather than words. Despite its usefulness, the main issue related to the test is represented by the presence of various versions.
Furthermore, multiple research have been conducted to study various aspects that may impact performance, including age, gender, nationality, language, brain injury, and IQ.[20]

2.4.2 The N-back Test

The N-back Test is widely utilized in research publications as a working memory (WM) paradigm, and its application as a measure of individual differences is growing. The N-back test is a reliable cognitive assessment tool that modifies working memory load, one of the key elements and a reliable indicator of mental workload. By analyzing the changes in biosignals during each activity, this test tries to change the mental workload and determine how it affects people on a mental and physical level [21]. It was first presented as a visual-spatial problem with four load factors ('0-back' to '3-back') by Kirchner in 1958 [22] and as a visual letter task with up to six load factors by Mackworth in 1959 [23]. N-back tasks are continuous recognition assessments where a stimulus, like letters, images, or shapes, is presented in succession at intervals of many seconds. For every item in the sequence, the participant must determine if the stimulus being shown now matches the stimulus that was presented n items ago. According to Au et al., 'n' is a variable that can be adjusted up or down to either increase or decrease the cognitive load.[24]. An alternative was suggested by Susanne Jaeggi et al. in 2003 [25] and is known as the dual-task n-back task. The dual-task paradigm involves the simultaneous presentation of two independent sequences, usually with distinct stimuli modalities, such as visual and auditory. An illustration of a dual-n-back test is shown in Figure 2.5, in which the auditory and visual stimuli are presented simultaneously and at the same rates.

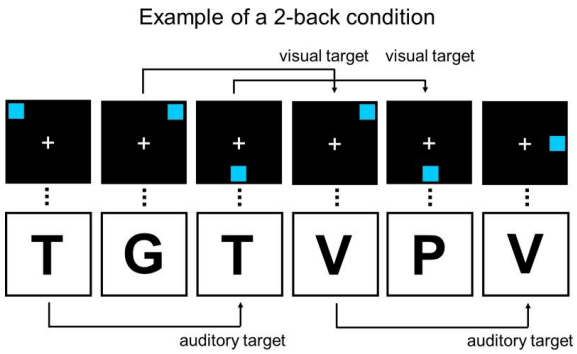

Figure 2.5: An illustration of a dual n-back task under the 2-back condition.

Response delay to targets or the application of dependent variables from signal detection theory, such as hits, false alarms, accurate rejections, and misses, are used to quantify performance in the n-back task. The performance level declines with

increasing N in terms of signal discrimination and reaction delay.

2.5 Biosignals for Stress and Cognitive Load Assessment

Based on the literature [26][27], it was possible to identify six biosignals that can be sensitive to variations in stress and cognitive load:

- **Electrocardiography (ECG)**: it provides information on the electrical activity of the heart. This activity is detected on the surface of the body. The Heart Rate (HR) and Heart Rate Variability (HRV) are derived from this signal to assess stress.

- **Electrodermal Activity (EDA)**: it is a measure of the electrical conductance of the skin's surface. EDA values tend to rise and display greater fluctuation when negative emotional states are present.

- **Temperature**: it is measured on the fingers and during times of stress, it tends to decrease due to vasoconstriction, which is the narrowing of blood vessels. This physiological response is aimed at diverting blood flow to the muscles in preparation for physical activity, which is a common reaction in fight-or-flight situations.

- **Eye movements**: They include saccades (rapid eye movements between fixation points), fixations (periods of gaze fixation), and pupil size changes, which are highly sensitive to variations in stress levels. The increased saccadic activity and changes in pupil size may indicate heightened cognitive load.

- **Breathing**: Breathing patterns can provide insights into an individual's emotional state, with negative emotions often resulting in irregular rhythms. Stress can lead to a heightened respiratory rate, along with potential instances of apnea and irregular inhaled air volume.

- **functional Near-Infrared Spectroscopy Signal (fNIRS)**: it measures changes in the concentration of oxygenated and deoxygenated hemoglobin in the brain, offering insights into the level of brain activity. During stress or cognitive load situations, significant changes in brain oxygenation levels can occur, detected through the fNIRS signal. This provides an indication of the brain's response to stressful stimuli or cognitive demands.

In this context, the fNIRS signal serves as a valuable indicator for assessing brain activity related to stress and cognitive load, complementing the information provided by the other biosignals listed.

2.6 Selected signal: fNIRS

In this study, the last signal mentioned in the previous section, **functional Near-Infrared Spectroscopy** (**fNIRS**), has been selected and analyzed to assess stress and cognitive load. This choice has been motivated by the fact that it represents a highly promising signal, which has not yet been studied in this context and shows interesting prospects for integration into HMI systems.
The following sections will introduce the underlying anatomy, a detailed description of this signal, and finally an analysis of previous work in which an influence of stress and cognitive load on the fNIRS signal was observed.
In the preceding sections, the underlying physiology of this signal will be introduced, followed by a description of its functioning.

2.7 Anatomy and physiology of cerebrovasculature

The human brain is a very important part of the nervous system. Even though it only makes up 2% of the body's mass, it gets a lot of resources: 12–15% of the heart's output, 20% of the body's oxygen needs, and 25% of the body's glucose needs.
Nonetheless, the human brain has a limited storage capacity, making careful management of cerebral hemodynamics critical for maintaining a stable supply [28]. Since the brain nearly completely lacks glucose storage and mostly relies on aerobic metabolism to create energy, a healthy blood perfusion and subsequently an appropriate oxygen and glucose supply are essential for sustaining a state of awareness.
The brain is fed with blood via two major artery sets:
-carotid arteries internal;
-vertebral arteries.
These two complexes flow into the internal jugular veins through the dural venous sinuses and the cerebral veins. An anastomosis called the **Polygon (or Circle) of Willis** (see Figure 2.6) is formed by both of these arterial systems and it is located at the base of the brain. Even in the presence of an occlusion, this arterial system can provide the brain with an adequate blood supply: when the canonical pathway encounters an obstacle, the blood can choose an alternative route thanks to the total interconnection of the components.
The brain accounts for 20% of the body's total oxygen use, making it the organ with the greatest metabolic requirement. The equation below illustrates the relationship between *Cerebral Blood Flow* (**CBF**) and *Cerebral Metabolic Rate of Oxygen* ($\mathbf{CMRO_2}$):

$$\mathrm{CMRO_2} = \mathrm{CBF} \cdot (A - V)_{\mathrm{O_2}} \tag{2.1}$$

where $(A - V)_{O_2}$ represents the difference in oxygen content between the vein and the artery.
Grey matter and white matter are the two main tissue types that make up the encephalon. The two tissues carry out quite distinct tasks: the grey matter is responsible for choosing and starting motor and informational actions, while the white matter is in charge of connecting and interacting with motor impulses. As a result, the grey matter has a higher oxygen need than the white matter because cerebral blood flow changes in response to metabolic demand.

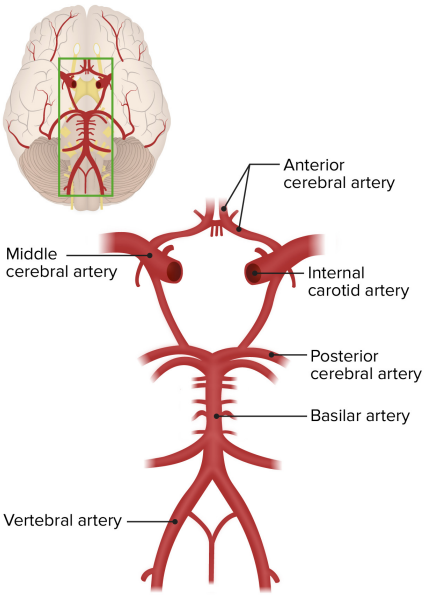

Figure 2.6: Circle of Willis

The energy generated by the conversion of glucose into ATP is essential for maintaining both cell homeostasis (which accounts for 40% of the energy produced) and brain functions (60% of the total energy produced).

2.7.1 Cerebral Blood Flow and Cerebral Perfusion Pressure

Since Kety and Schimdt's ground-breaking discovery[29], CBF has been recognized to be a crucial factor in the proper supply of nutrients and oxygen to the brain, proving essential to its function.
CBF can be defined mathematically in steady state as:

$$CBF = \frac{CPP}{CVR} \tag{2.2}$$

where CVR is the cerebrovascular resistance to flow and CPP is the cerebral perfusion pressure. The CPP of an adult is calculated using the following equation:

$$CPP = MAP - (CVP + ICP) \tag{2.3}$$

where MAP corresponds to Mean Arterial Pressure, CVP is Central Venous Pressure, and ICP equals Intracranial Pressure.
In a healthy adult, MAP is between 70 and 90 mmHg, and CBF is constant; if MAP drops below 50 mmHg, the risk of cerebral ischaemia rises.
According to the equivalent equation for a single vessel, the resistance of a vessel may be represented by the Poiseuille Equation of fluid dynamics, which is given by:

$$\text{CVR} = \frac{8\mu L}{\pi r^4} \tag{2.4}$$

where μ is the blood viscosity, L is the length of the vessel, and r is the radius [30].

The resistance of a blood artery is proportional to its radius, length, and hematocrit, as shown in Equation 2.4. Assuming that the last two remain mostly constant throughout time, blood flow is primarily regulated by variations in vessel radius. Furthermore, Equation 2.4 demonstrates that vascular resistance is inversely proportional to the radius of the fourth power, implying that even little changes in vessel radius can result in significant changes in blood flow.
CBF and Cerebrovascular Resistance, (CVR), are inversely related, as shown in Equation 2.2, thus when vasodilation occurs, CVR lowers and CBF increases; conversely, when vasoconstriction occurs, the opposite event happens. There are several mediators capable of affecting CBF (including hydrogen ions, potassium, and CO_2), but their impact is minor when compared to changes induced by local metabolic demand.

2.7.2 Autoregulation mechanism

The cerebrovascular tree has a mechanism capable of protecting the brain from changes in arterial pressure to maintain appropriate CBF during fluctuations in systemic arterial pressure. As a result, CBF remains constant within the range of 60 to 140 mmHg. In the Figure 2.7, it is possible to observe how cerebral autoregulation, despite variations in systemic pressure, allows for maintaining a constant cerebral blood flow of approximately 50-54 ml/100g/min within the range of 60-140 mmHg.

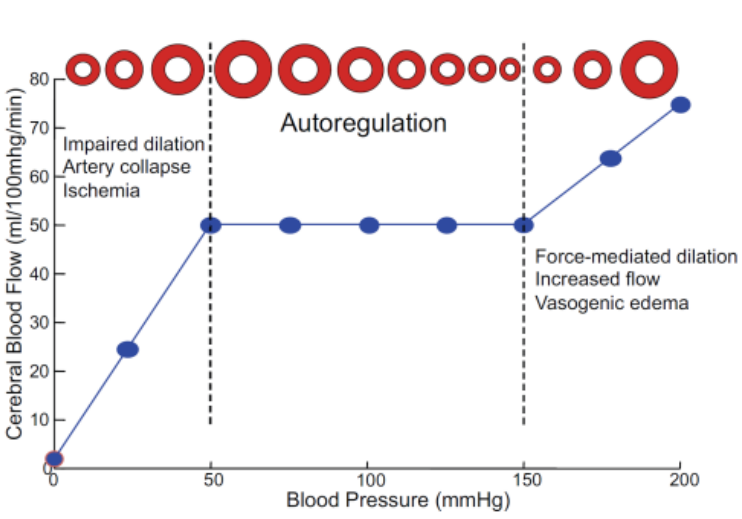

Figure 2.7: Flow-Pressure Curve

Autoregulation is a physiological mechanism in which the cerebral circulation raises or reduces its resistance in order to maintain constant cerebral blood flow without changing the cerebral perfusion pressure. Blood has two tasks in the cerebral autoregulation mechanism:

1. It supplies oxygen and nutrients to the brain tissue;
2. It eliminates carbon dioxide and other waste products.

This regulating system is based on three distinct yet synergistic mechanisms:

- **Myogenic autoregulation** is the ability of arteries and arterioles to adapt to changes in blood pressure while maintaining constant blood flow inside the vessels;

- **Metabolic autoregulation** is the principal factor capable of controlling the arteriolar caliber of brain arteries in response to variations in locally generated carbon dioxide concentration. An increase in metabolic demand in one body location causes a local rise in CO_2 and acidic metabolites, which causes vasodilation and an increase in CBF. This guarantees that blood flow is increased immediately in more actively engaged brain regions.

- Vasoconstrictive impulses from sympathetic-adrenergic nerve fibers that innervate blood vessels influence **neurogenic autoregulation.**

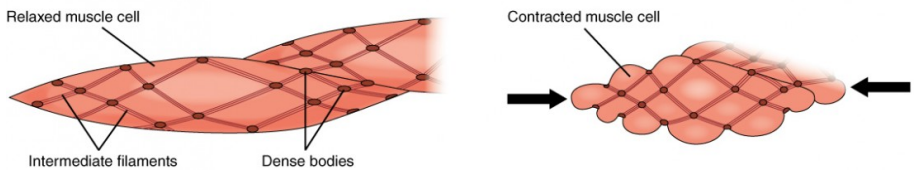

Figure 2.8: Representation of smooth muscle cells. At the top, cells in a relaxed conformation are depicted. At the bottom, the contracted conformation is shown. Intermediate filaments consist of actin and myosin held together by dense bodies. These proteins are responsible for the contraction of this muscular tissue.

The processes mentioned above are supplemented by the endothelial function of smooth muscle cells (Figure 2.8), which are smooth muscle cells found in the walls of blood vessels that control vasodilation or vasoconstriction to increase or reduce blood pressure. Because of the minimal oxygen consumption required, these smooth muscle cells are encased in a protein matrix, giving them a high contraction capability that can be sustained over time.
Cortical autoregulation takes place at the regional level, as various cortical regions may or may not use this process. A hemodynamic response can be induced by a task and analyzed to determine the oxygenation status of a specific location. Arithmetic exercises, for example, might generate a hemodynamic response in the left dorsolateral prefrontal cortex. When stimulated, these regions vasodilate, enabling more oxygen to enter, this happens because the activated brain area demands more oxygen.
The functional investigation of such regional hemodynamic responses is carried out through Near-Infrared Spectroscopy (NIRS), which may identify the activation or deactivation of the autoregulation mechanism by analyzing variations in hemoglobin concentration within the examined brain section.

2.8 The principles of functional near-infrared spectroscopy

In 1977, Francis Jobsis, an American researcher, made an important discovery based on the knowledge of the relative transparency of various tissues, including the skull, within the near-infrared spectrum. This finding enabled the development of a non-invasive method for monitoring the concentrations of oxygenated hemoglobin (HbO_2) and deoxygenated hemoglobin (HbR) in the brain [31]. The individual's groundbreaking contributions established to the basis of near-infrared spectroscopy (NIRS). The discovery made by Jobsis involved the observation that bone, with a thickness of up to 4 mm, could be penetrated by red light.
This insight, coupled with the evolution of optical technologies, significantly advanced the study of brain activity [32].
In particular, the emerging optical neuroimaging technique known as Functional Near-Infrared Spectroscopy (fNIRS) plays a pivotal role in this context. Grounded in the theory of neurovascular coupling (NVC) and optical spectroscopy [33], the fNIRS allows the non-invasive measurement of changes in oxyhemoglobin (HbO_2) and deoxyhemoglobin (HbR) concentrations in the brain in response to neuronal activity.
As depicted in Figure 2.9, an increase in neural activity results in a corresponding augmentation in oxygen metabolism, a process that fulfills the energetic requirements of the neuronal tissue through neurometabolic coupling[34],[35],[36]. In the context of neuronal oxygen metabolism, the process of energy production involves the consumption of oxygen. This results in a reduction in the concentration of oxyhemoglobin (HbO_2) and an increase in the concentration of deoxyhemoglobin (HbR) [35] [36].

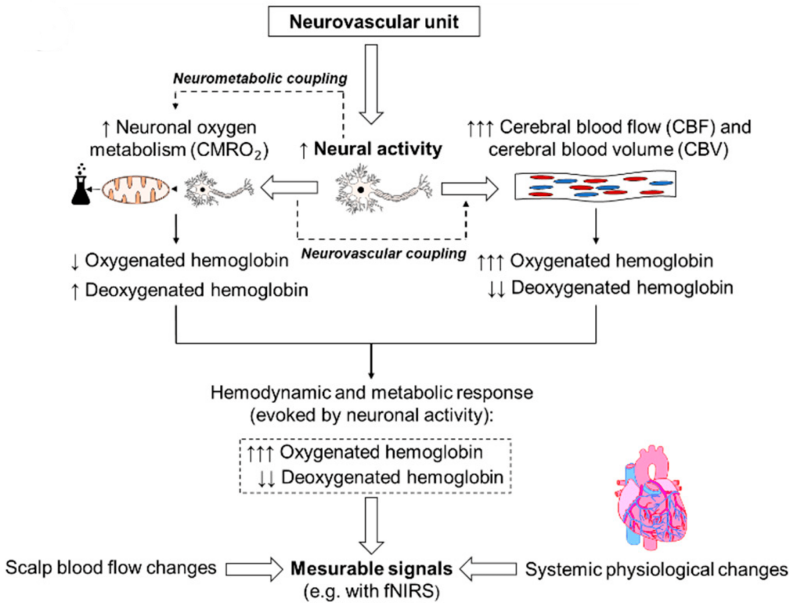

Figure 2.9: Hemodynamic and metabolic response during neural activity

The production of energy in the form of adenosine triphosphate (ATP), which is necessary for neural tissue to function, relies on the utilization of glucose and oxygen,

these essential nutrients are continuously delivered to the tissues via the bloodstream. The activation of neural activity leads to localized alterations in cerebral hemodynamics, resulting in a significant increase in the energy needed to support electrochemical processes, along with an increase in cerebral blood flow (CBF) and cerebral blood volume (CBV) in the specific stimulated brain regions.
The brain region that is activated by the stimulation receives a supply of oxygen and glucose within a few seconds, facilitated by the transportation of oxygen through haemoglobin.
In these regions of the brain, it is expected to observe a higher concentration of oxyhemoglobin and a reduction in deoxyhemoglobin due to the total amount of oxygen transferred being greater than that consumed in the process, resulting in an imbalance between cerebral blood flow (CBF) and oxygen consumption [37], characterizing the hemodynamic response in a recognizable manner.
As previously mentioned, the fNIRS enables the assessment of localized hemodynamic response by analyzing changes in the concentration of oxy- and deoxy-hemoglobin across time. These two forms of haemoglobin exhibit distinct optical characteristics. The information is deduced from the attenuation in the intensity of a beam of light. When adopting functional Near Infrared Spectroscopy (fNIRS), a source located on the scalp emits light of varying wavelengths within the near-infrared spectrum. This emitted light passes through several layers, such as the skull and cerebrospinal fluid, before reaching the neuronal tissue [34], [38]. Within the tissue, the light undergoes absorption and scattering that contributes to light attenuation [38],[39]. During the process of absorption, the energy carried by photons is converted into internal energy within the medium under consideration. The phenomenon of scattering caused the photons to diverge from their initially linear courses, resulting in an extension of the distances they traveled [34],[39]. The detector positioned on the surface of the head can be used to measure the non-absorbed constituents of the scattered light (see Figure 2.10) [38].

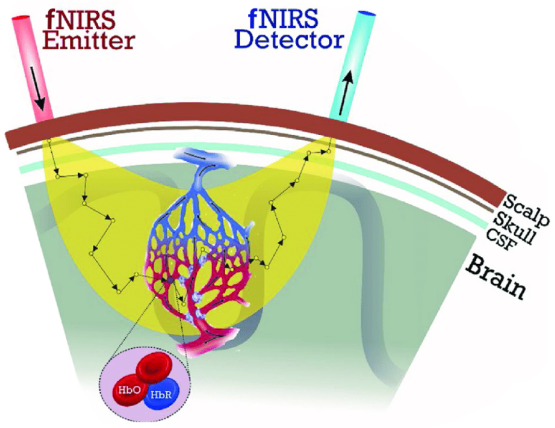

Figure 2.10: The "banana shape" trajectory of photons within the scalp following scattering phenomena.

The behavior of photons as they propagate through tissues is sensitive to both their wavelength and the optical characteristics of the tissue.

It has been shown that human tissue exhibits a comparatively high level of transparency to near-infrared light. The absorption spectra of the observed substance (Figure 2.11) indicate that throughout the near-infrared spectral region (650-950 nm), the absorption coefficients are rather low. Consequently, light can propagate through the tissue for a considerable distance, extending up to several centimeters. Water, an essential component of biological tissue, exhibits significant absorption in the ultraviolet region of the electromagnetic spectrum. Additionally, it demonstrates absorption at longer wavelengths, primarily in the medium and far infrared ranges.

On the other hand, alterations in the relative concentration of oxyhemoglobin

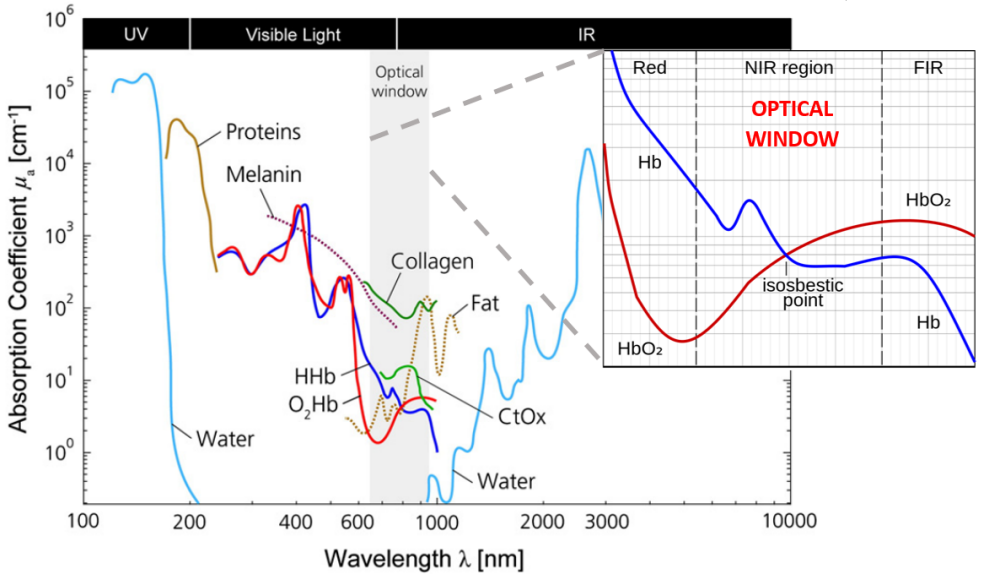

Figure 2.11: Absorption spectra for several chromophores found in human tissue, using a natural logarithmic basis, with a focus on the spectrum related to oxygenated hemoglobin (HbO_2) and deoxygenated hemoglobin (Hb)

and deoxyhemoglobin impact the optical response of the tissue. When examining the optical window, it becomes apparent that HbO_2 and HbR display contrasting behaviors at the boundaries, except for the isosbestic point where they demonstrate identical absorption coefficients. To discern their respective contributions, it is imperative to examine the tissue using light at two distinct wavelengths, deliberately selected on opposing ends of the isosbestic point.

The Modified Beer-Lambert Law (MBLL) (section 2.8.2) allows for the calculation of changes in concentration of the two chromophores through the analysis of light attenuation measurements. When examining the properties of biological tissues, it is important to note that scattering events play a significant role in determining the course of photons. These scattering events occur more frequently than absorption events [40].

Due to scattering events, a fraction of the photons emitted from a localized source undergoes scattering in the opposite direction, towards the scalp, where they can be detected. These scattered photons follow a trajectory that resembles the shape of a banana, as depicted in Figure 2.10. The photons have the capability to convey valuable data regarding the tissue they traverse during their trajectory from the

source to the detector.
Laser diodes and light-emitting diodes (LEDs) are commonly employed as sources of light, whereas photomultipliers and avalanche photodiodes are utilized to facilitate the precise detection of attenuated light that scatters back to the scalp. The depth of penetration is contingent upon the relative placements of the source and detector, which constitute a channel. In 2005, Cui et al. [41] utilized photon migration models to estimate the penetration depth in adult heads, which is between one-third and one-half of the distance between the source and detector.
The distance between the detector and the source is a crucial factor to consider, as the signal obtained encompasses the hemodynamic response originating from the cerebral areas, physiological and measurement noise, and also superficial physiological components.
When the separation between the linked source and detector is less than 1 cm, the signal obtained no longer contains cerebral information. Instead, it provides information solely about the physiological activity occurring in the superficial layers of the skull. In contrast, exceeding the optimal separation between channels results in a significant reduction in signal quality, as indicated by a decreased Signal-Noise Ratio value (cita).
Each detector can be coupled with many light sources, allowing for measurements to be taken in various regions or at varied distances. The configuration of both sources and detectors together referred to as the optical probe, is typically consolidated into a cap or strip. This design is tailored to accommodate the specific measurement requirements and ensure proper fitting on the subject's head. The allocation of accessible optodes plays an important role in the examination of specific regions of interest inside the brain.

2.8.1 Lambert Beer Law

The Beer-Lambert equation says that the amount of light that is absorbed (A) by a substance is related to the quantity of light absorbers in the substance (C), the light absorber's optical properties (ε), and the length of the light beam's optical path (L).

$$A = -\log_{10}\left(\frac{I}{I_0}\right) = \varepsilon c L \tag{2.5}$$

Where:

- **I**: intensity of the signal transmitted through the medium;
- $\mathbf{I_0}$: intensity of the incident light on the medium;
- $\boldsymbol{\varepsilon}$: molar extinction coefficient;
- **c**: concentration of the chromophore;
- **L**: optical pathlength.

The direct application of the Beer-Lambert equation to biological tissue is not feasible due to the significant scattering properties exhibited by human tissue when exposed to near-infrared light.

In 1988, Delpy et al. incorporated the phenomenon of light scattering and formulated the **Modified Beer-Lambert Law** (MBLL) [42].

2.8.2 Modified Beer-Lambert Law

Equation 2.6 shows the Modified Beer-Lambert Law (MBLL), which is an extension of the Beer-Lambert law that includes a light intensity loss parameter, indicated as G, which is dependent on scattering.
The phenomenon of light intensity reduction (I) in tissue, also known as optical density (OD) or attenuation (A), is described by the law. This law is dependent on various factors including the concentrations of chromophores (c, $[M]$), molar extinction coefficients (ε, $[M^{-1}cm^{-1}]$), the differential path length factor (DPF, unitless) which takes into account the increased distance traveled by light due to the reduced scattering coefficient (μ_s'), the separation between the light source and detector (d, [cm]), and the factor G[36]:

$$OD(t,\lambda) = -\log_{10}\left(\frac{I(t,\lambda)}{I_0(t,\lambda)}\right) = \sum_i \varepsilon_i(\lambda)c_i(t)DPF(\lambda)d + G(\lambda) \tag{2.6}$$

The index "i" represents all the chromophores used, which in the case of fNIRS are two, namely, oxygenated hemoglobin and deoxygenated hemoglobin. In the equation, a base 10 logarithm is used along with molar extinction coefficients (i.e., $I = I_0 * 10^{-\varepsilon cd}$), but absorption coefficients, related to the natural logarithm, could also be used. The molar extinction coefficients and absorption coefficients both quantify the degree of absorption per unit concentration (μM/mM) and per unit length (cm), however, they change by a scaling factor of the natural logarithm of 10 ($\ln(10)$).
The factor "G" is challenging to estimate a priori. It is predominantly a geometric factor, and studies have shown that it strongly depends on the geometry of the examined body region. Furthermore, this factor varies depending on the geometry of the source and detectors used by the sensor. It can be considered a time-invariant factor since, at the beginning of the acquisition, the geometric aspects of the source, as well as the cranial configuration, remain the same and additionally, scattering changes are minimal compared to absorption changes.
Therefore, this element may be omitted when calculating the alteration in optical density between time points t_1 and t_0. In addition, it is assumed that the emitted intensity I_0 remains constant, resulting in the cancellation of this term.[36]
The change in optical density is given by:

$$\Delta OD(\Delta t,\lambda) = OD(t_1,\lambda) - OD(t_0,\lambda)) \tag{2.7}$$

$$\Delta OD(\Delta t,\lambda) = -\log_{10}\frac{I(t_1,\lambda)}{I(t_0,\lambda)} = \sum_i \varepsilon_i(\lambda)\Delta c_i(t)DPF(\lambda) \tag{2.8}$$

where Δc_i represents the temporal variation in chromophore concentration ($\Delta c_i = c_i(t_1) - c_i(t_0)$).
The MBLL is applicable to uniform changes in HbO_2 and HbR concentrations within homogeneous tissue. The presence of tissue inhomogeneity is not a concern, as the

constant term G accounts for it, effectively canceling it out for concentration change measurements. Although concentration changes in HbO_2 and HbR are not uniform (occurring only in the brain and not in other tissues like skin and skull), this results in a quantification error. The MBLL tends to underestimate variations in HbO_2 and HbR size. Typically, this error is mitigated by considering partial differential path lengths, although it's not always necessary, especially when the signal trend is correct and quantification isn't crucial in brain research. Detecting activation presence and location suffices. This enables signal comparison across locations and under different stimulation conditions [36].
Within Equation (2.8), there is the differential path length factor (**DPF**), a dimensionless correcting factor that quantifies the effective distance traveled by light, which is d times larger than the source-detector separation. This factor, multiplied by the source-detector separation, estimates the actual path length traversed by light [33], so it accommodates the increase in optical path length due to light scattering within biological tissue. This variable is known to be dependent on age, sex, and wavelength, and it exhibits variability among people and various tissues.
Ultimately, the changes in hemoglobin concentration are calculated by solving (2.9) to determine Δc, representing $\Delta[HbO_2]$ and $\Delta[HbR]$.

$$\begin{bmatrix} \Delta\left[HbR\right] \\ \\ \Delta\left[HbO_2\right] \end{bmatrix} = d^{-1} \begin{bmatrix} \varepsilon(\lambda_1)^{\mathrm{HbR}} & \varepsilon(\lambda_1)^{\mathrm{HbO_2}} \\ \\ \varepsilon(\lambda_2)^{\mathrm{HbR}} & \varepsilon(\lambda_2)^{\mathrm{HbO_2}} \end{bmatrix}^{-1} \begin{bmatrix} \frac{\Delta OD(\lambda_1)}{DPF(\lambda_1)} \\ \\ \frac{\Delta OD(\lambda_2)}{DPF(\lambda_2)} \end{bmatrix} \tag{2.9}$$

2.8.3 Classification of fNIRS techniques

Depending on the measurement method employed and the type of instrumentation, it is possible to classify three main fNIRS techniques[36]:

1. **Continuous Wave** (CW-fNIRS) injects constant intensity light (constant amplitude and frequency) and measures the attenuation of transmitted light. Unlike other techniques, it is not possible to determine the absolute concentrations of oxygenated and deoxygenated hemoglobin; only changes in the concentration of their respective chromophores can be measured.

2. **Frequency Domain** (FD-fNIRS) uses modulated light sources with sinusoidal intensity and frequencies ranging from tens to hundreds of MHz. This technique, through the direct measurement of the absorption and scattering effects of tissues, allows for the quantification of the absolute concentration of oxygenated and deoxygenated hemoglobin.

3. **Time Domain** (TD-fNIRS) is based on measuring the time of flight of photons in tissue by emitting an extremely short pulse of light on the order of hundreds of picoseconds. This technique provides more information and offers the possibility of determining, through the emission of different pulses with varying frequencies, the optical properties of tissues and a precise assessment of scattering and absorption coefficients.

The choice of using one method over another strictly depends on the nature of the study being conducted. Continuous wave instruments are the most popular on the

market and are the predominant choice in both clinical and research settings. This preference is motivated by their ease of use, ability to miniaturize instrumentation, portability, and cost. Moreover, they presented superior temporal resolution and the measurement of radiation intensity is a less noisy parameter than time-of-flight, which does not allow the detection of small functional activations. As a result, the CW-fNIRS technique is particularly suitable for functional studies of the brain, despite having a lower penetration depth than the other two methods[43].

2.8.4 Available fNIRS devices

The fNIRS, discovered in 1992, has undergone considerable technological advances, moving from low-sensitivity single-channel systems to modern multi-channel systems with high temporal resolution[43]. The use of sources and detectors arranged at different distances has enabled the development of tomographic techniques for the three-dimensional reconstruction of brain images. Although continuous wave technology is predominant, in the clinical setting fNIRS is only reliable for group analysis, given the anatomical variability of brain and extracerebral structures between individuals contributing to the acquired signal, motivating current research towards instrumental and methodological improvements to increase reliability and individual applicability. The selection of optimal wavelengths, improvements in sensor arrangement, and the use of mathematical algorithms are key areas of development [36]. The wide range of continuous wave fNIRS devices currently on the market

Device	(Manufacturer), country	Time-res, Hz	#Emitter	#Detector	MUX	SDS (mm)	E-tech	Wavelengths (nm)	D-tech	Data	Wear	CE
OXYMON MkIII	(Artinis), Netherlands	250	32	16	t	a	LD	760, 850*	APD	Raw	n	y
PortaLite	(Artinis), Netherlands	50	3	1	t	20+25/ 30+35+40	LED	760, 850*	PD	Raw	y	y
fNIR1 100	(fNIR Devices), USA	2	1/1/4	2/4/12	t	20/25/25	LED	730, 850		Hb	n	n
fNIR1 100w	(fNIR Devices), USA	2	1	2/4	t	20/25	LED	730, 850		Hb	y	n
ETG-4000	(Hitachi), Japan	10	18	8	f	20/30	LD	695, 830	ADP	Raw	n	y
ETG-7100	(Hitachi), Japan	10	40	40	f	20/30	LD	695, 830	ADP	Raw	n	y
WOT	(Hitachi), Japan	5	8	8	t + f	30	LD	705, 830	PD	Raw	y	n*
Genie	(MIRRA), USA	5.02	4 to 16	8 to 32	c	a	LED	700, 830	PD	Raw	y	n
NIRScout	(NIRx), USA	6.25 to 62.5	8 or 16	4 to 24	t + f	a	LED	760, 850	PD	Raw	n	y
NIRScoutX	(NIRx), USA	6.25 to 62.5	48	32	t + f	a	LED	760, 850	PD	Raw	n	y
NIRSport	(NIRx), USA	6.25 to 62.5	8	8	t + f	a	LED	760, 850	PD	Raw	y	y
Brainsight NIRS	(Rogue Research), Canada	100	4 to 16	8 to 32	f	a	LD	685, 830, (808)*	ADP	Raw	n	n*
FOIRE-3000	(Shimadzu), Japan	7.5 to 40	4 to 16	4 to 16	t	a	LD	780, 805, 830	PMT	OD	n	n
OEG-SpO2	(Spectratech), Japan	1.52/12.2	6	6	c	30/25/15-40	LED	770, 840	PD	Raw	y*	n*
CW6	(TechEn), USA	10 to 50	4 to 48	8 to 32	f	a	LD	690, 830*	APD	Raw	n	y
UCL Optical Topography System	(University College London), UK	10 to 160	16	16	f	a	LD	780, 850	APD	Raw	n	n
Imagent	(ISS), USA	16 to 60	16 or 32	4 or 8	f	a	LD	690, 830	PMT	Raw	n	y

Figure 2.12: Commercially available fNIRS devices [36]

(Reported in Table 2.12) offer the possibility of different biomedical applications

depending on the nature of the study. These instruments feature dedicated software for analyzing haemodynamic changes and are often based on MBLL to derive relative changes in haemoglobin HbO_2 and HbR concentrations, varying in the number and type of emitters, detectors, and channels. The channels constitute the possible paths between an emitter and a detector for the different wavelengths used by the device and are variable depending on the arrangement of the electrodes.
Another important parameter is the time resolution, indicated in Hz, which can vary depending on the activation of the sources and the specific use of the channels; the minimum value indicated represents the maximum sampling rate when all sources are activated, while the maximum indicates the use for a limited set of channels. Another parameter enabling the classification of devices is the source-detector separation (SDS), which can be fixed or manually adjustable (a).
The distinction of signals from different emitters and different wavelengths is achieved through multiplexing methods such as time multiplexing (t), frequency multiplexing (f), and code multiplexing (c).
It is also possible to choose the emission wavelength, a possibility that is left to the researcher and limited to specific intervals in the NIR region.
For signal recording, some devices focus on the calculation of HbO_2 and HbR concentrations, while others allow the detection of light intensity, identified as optical density (OD) or raw light (raw). In addition, some of these devices on the market feature wearable systems to allow acquisitions on the move.

2.9 State-of-the-art of fNIRS assessment

As part of the research, a considerable number of paper has been dedicated to investigating the use of the Functional Near-Infrared Spectroscopy (fNIRS) signal for the purpose of evaluating mental stress and mental workload in individuals.
One notable characteristic of these approaches is the frequent use of a multi-modal approach, in which the fNIRS signal is acquired simultaneously with other physiological signals. Alternatively, some studies have focused on the use of fNIRS devices equipped with a large number of acquisition channels; this strategy allows detailed mapping of the areas of the prefrontal cortex that are particularly active during specific cognitive tasks.
This trend towards a multi-modal approach reflects the growing awareness of the importance of integrating different sources of physiological information to obtain a more complete understanding of the response to stress or cognitive load. At the same time, the use of multi-channel devices allows for greater accuracy in localizing the brain activities involved, thus offering a detailed analysis of the regions of the prefrontal cortex where signal variations are greatest.

2.9.1 fNIRS and stress

The need to understand the influence of stress on physiological signals is crucial, considering that stress is a major contributor to several diseases, including heart attacks, depression, and strokes (as highlighted in the previous section 2.1).

This correlation underlines the importance of thoroughly investigating the physiological response to stress through approaches such as the use of fNIRS. The ability to detect and understand alterations in brain signals during stressful situations may offer key elements for anticipating and managing stress-related health conditions.
In the research conducted by Al Shargie et al. [44], they presented a method for evaluating stress by concurrently measuring electroencephalography (EEG) and fNIRS activity on the prefrontal cortex (PFC). In this paper, stress was induced using the Montreal Imaging Stress Task (MIST), a mental arithmetic task under time pressure with negative feedback. The fNIRS signal was acquired using the 23-channel OT-R40 system (Hitachi Medical Corp, Japan).
Participants underwent a control condition where they had to perform the arithmetic test without time limits and without receiving feedback on the correctness of their answers. Subsequently, they were exposed to stressors such as time limits for answering questions and negative feedback for incorrect responses.
The presence of mental stress was verified through the salivary alpha-amylase test. The experimental findings showcased that integrating EEG and fNIRS measurements improved the accuracy of mental stress classification by +3.4% compared to utilizing EEG alone and +11% compared to relying solely on fNIRS.
In particular, it was observed that during the control phase, the average concentration of oxygenated hemoglobin showed a significant increase in many areas of the PFC. However, during the stress condition, a slightly lower amplitude increase was observed, varying depending on the analyzed channel. In both cases, the hemoglobin concentration returned to the baseline value within 20 seconds from the start of the rest phase.
Furthermore, Al Shargie et al. noted that the right region of the prefrontal cortex (PFC) is particularly sensitive to mental stress. Analyzing the topographic maps of the response of oxygenated hemoglobin (HbO_2) in all participants during both the control and stress phases revealed a significant decrease concentrated in this area during stressful conditions.
Another study adopting a multimodal approach is the one conducted by Murayama et al. [45], in which the fNIRS signal is recorded using a two-channel device during an arithmetic test. The main objective was to assess the possible relationship between respiratory rhythm and prefrontal cortex activity. To measure the asymmetry of cortical activity, the lateral index was calculated, defined as the ratio of the difference in oxygenated hemoglobin concentrations recorded between the right and left sides of the PFC to the total HbO_2 concentration.
The results showed that arithmetic tasks induced more activity in the right PFC than in the left PFC. In particular, a significant increase in the concentration of oxygenated hemoglobin and a simultaneous decrease in deoxygenated hemoglobin were observed during the performance of the task. These results suggest a differentiated involvement of prefrontal regions during the performance of arithmetic tasks, highlighting the importance of the multimodal approach for a deeper understanding of brain dynamics in response to specific stimuli.
The study conducted by Schroeter et al.[46] differed from the previously described research by focusing exclusively on the fNIRS signal to explore the practicability of the event-related approach in functional brain activation research using cognitive paradigms.

While performing the Stroop task, a heightened hemodynamic response was noted, characterized by an elevation in HbO_2 concentration and a reduction in HbR concentration during incongruent trials in contrast to congruent and neutral trials. The intensified hemodynamic reaction observed was construed as a more prominent cerebral activation specifically during the incongruent trials of the Stroop test, attributable to interference.

2.9.2 fNIRS and Mental workload

In the context of research on the correlation between mental workload and fNIRS signals, several studies have helped to delineate the complex relationship between brain activity and cognitive demands. One widely adopted approach to induce and assess cognitive load is the use of the n-back test.
The fNIRS studies conducted on this approach have examined the effect of varying the n-back task on brain activation signals. In general, such research has found that a higher cognitive load tends to produce greater activation within the dorsolateral part of the prefrontal cortex ($dPFC$). This area is known to be related to working memory, allowing mental manipulation of information in a short period.
One important example is the study by Ogawa et al.[47], which found that people who did better on a visuospatial working memory task had higher amounts of oxygenated haemoglobin activation.
Similarly, the work of Peck et al.[48] contributed to this line of research by focusing on validating the application of functional near-infrared spectroscopy (fNIRS) in detecting workload during a human-computer interaction (HCI) involving an n-back visuospatial task. In their experiment with sixteen participants, fNIRS signals were recorded from the prefrontal cortex. By changing the variable n, the researchers induced individuals to retain n patterns in their short-term visuospatial memory, causing a corresponding increase in cognitive load on their visual short-term memory. fNIRS sensors were utilized on the prefrontal cortex of the forehead to examine alterations in deoxygenated hemoglobin (HbR) levels between the 1-back and 3-back situations.
Consistent with findings from functional magnetic resonance imaging (fMRI) investigations, they observed a greater magnitude of reduction in the average change in HbR levels for both the 1-back and 3-back tasks, including all trials and subjects. Furthermore, the participants in the study indicated that the 3-back task was seen as more cognitively challenging compared to the 1-back task. Moreover, the participants' performance declined as they engaged with the 3-back task in contrast to the 1-back task.
The findings presented in this study are consistent with previous research on the n-back task and provide support for the application of functional near-infrared spectroscopy (fNIRS) as a viable method for measuring alterations in visuospatial working memory within the prefrontal cortex.
Moreover, Ayaz et al. [49] employed a comparable methodology to ascertain the extent of cognitive demand experienced by individuals operating unmanned aerial vehicles (UAVs). During this experiment, individuals were instructed to sit at workstations and assume the role of air traffic controllers in a virtual environment. Their

objective was to effectively manage air traffic flow and minimize the occurrence of accidents. The quantity of unmanned aerial vehicles (UAVs) was systematically manipulated between trials, specifically with three different conditions (6, 12, 18). Subsequently, the average alteration in oxyhemoglobin (HbO_2) levels was computed for each trial. As the number of unmanned aerial vehicles (UAVs) that users were required to monitor rose, functional near-infrared spectroscopy (fNIRS) measurements revealed elevated levels of HbO_2 in the prefrontal cortex (PFC).
The researchers discovered that these alterations were similar to those observed during engagement with the n-back task. The NASA-TLX (NASA Task Load Index) is a subjective workload assessment tool that measures six dimensions of workload, including mental demand, physical demand, temporal demand, performance, effort, and frustration. A positive correlation was observed between elevated levels of HbO_2 and self-reported NASA-TLX workload assessments, providing additional support for the identification of workload-related signals.
In some research work, a significant focus has been placed on the classification of rest periods versus activity periods. In particular, the work of Herff et al. [50] stands out for exploring this dynamic exclusively through fNIRS data. In this study, it was found that workload from relatively simple tasks, such as the n-back test, can be strongly discriminated against during a rest period.
The authors used the Oxymon Mark III system from Artinis Medical Systems with 8 channels to record the average course of oxygenated and deoxygenated haemoglobin. Analyzing the HbO_2 results on all channels, they found a significant increase in activity in the 3-back condition, with slightly lower activity in the 1-back and 2-back conditions. Simultaneously, HbR levels decreased in all three conditions, with negative and steeper slopes in the 3-back condition. These results demonstrate that the haemodynamic responses measured in the prefrontal cortex can be successfully used to discriminate between three levels of workload.
Continuing in this line of research, Kesedzic et al. [51] further investigated the classification of cognitive load levels in the context of the n-back task. In his study, he took an innovative approach by simultaneously recording both the fNIRS signal with the Imager 1100 system with 16 optodes and the ECG signal.
A total of 30 features were extracted and the accuracy in classifying the cognitive load was assessed using different classifiers. The results indicate that the exclusive use of fNIRS data leads to an accuracy of 52-58%, whereas the multimodal approach shows a significant 10% increase in classification accuracy. Among the most relevant features selected for the 3 level cognitive load classification were: the mean and peak value of HbO_2 and the mean value of HbR.
This finding demonstrates that fNIRS-based features, associated with the central nervous system, and ECG-based features, associated with the autonomic nervous system, may have distinct impacts on the precision of cognitive load classification at varying levels of difficulty.
The Table 2.1 presents the trends of some features used in the literature, as this information is not available for many of them.

Feature	Trend
Mean ΔHbO_2	$\uparrow$
Mean ΔHbR	$\downarrow$
Slope ΔHbO_2	$\uparrow$
Slope ΔHbR	$\downarrow$

Table 2.1: Features trend showed by the literature

2.10 Experimental setup: Biosignalsplux sensors

In the following study, the Professional Kit from Biosignalsplux [52] was used for acquiring fNIRS signals. This kit comprises a trigger, a hub, and sensors, including the ECG sensor, the EDA sensor, the fNIRS sensor, the temperature sensor, and the respiratory activity sensor. In Figure 2.13, the experimental setup employed is illustrated.
The 8-channel Biosignalsplux hub receives and digitizes all the signals from the sensors and accessories. It then sends these signals to the computer via Bluetooth, where they are stored and shown in real time. The channels are capable of handling up to 16 bits of data and 3000 Hz sampling frequency per channel, or 4000 Hz sampling frequency per channel when only 3 channels are being used at the same time.

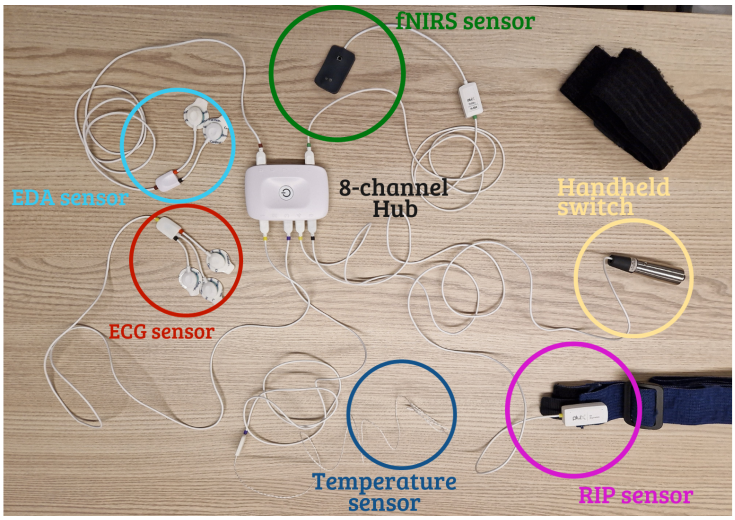

Figure 2.13: Professional Biosignalsplux kit, experimental setup

During the acquisition protocol, several physiological signals were recorded simultaneously: heart activity, temperature, electrodermal activity, respiration, brain activity, and eye movements. For the last signal, the Tobii Glasses 3 eye-tracking system was used.[53]
As this thesis work focuses on the analysis of brain activity, the specifications of the sensor used for this purpose will be detailed below, and a mention will be made of the sensor used to record cardiac activity as it was used to process the fNIRS signal.

2.10.1 Functional Near-Infrared Spectroscopy sensor

fNIRS sensor is equipped with two light-emitting LEDs, one in the red emission spectrum region (660 nm) and the other in the infrared with an emission spectrum peak of 860 nm. In addition, at a distance of 2 cm, there is a photodiode acting as a detector of light reflected from biological tissue, which has 850 nm as its wavelength of maximum sensitivity. In the Table 2.2, the main specifications of the sensor are listed. Using API, it is possible to adjust the output current of each LED and achieve a high signal-to-noise ratio for reliable results.
In Figure 2.14, it is possible to observe the fNIRS sensor from Biosignalsplux used in the study while its specifications are detailed in the Table 2.2.

Figure 2.14: The Biosignalsplux fNIRS sensor

Specification	**Value**
Infrared Emitter	
Peak Emission	860nm
Half Intensity Beam Angle	±13 deg
Spectral Bandwidth	30nm
Radiant Intensity	750mW/sr
Red Emitter	
Peak Emission	660nm
Half Intensity Beam Angle	±18 deg
Spectral Bandwidth	25nm
Power Output	7mW
Detector	
Wavelength of Max Sensitivity	850nm
Range of Sensitivity	400nm-1100nm
Radiant Sensitive Area	7.0 (mm^2)
Dimension of Radiant Sensitive Area	2.65mm x 2.65mm
Infrared/Red Emitter	
Duty Cycle	25%

Table 2.2: fNIRS Sensor Specifications

2.10.2 Electrocardiography sensor

The Biosignalsplux ECG sensor presents a differential triode configuration, designed to reduce noise to a minimum and improve the accuracy of ECG readings. The electrode marked in red constitutes the positive pole, the black electrode the negative pole and the third electrode constitutes the reference. As shown in Figure 2.15.

Characteristic	**Value**
Gain	1019
Range	±1.47mV (with VCC=3V)
Bandwidth	25-100 Hz
Input Impedance	>100 $G\Omega$
CMRR (Common Mode Rejection Ratio)	100 dB
Cable Length	100 cm ±0.5 cm

Table 2.3: ECG sensor specifications

In the Table 2.3, the specifications of this sensor have been reported.
This sensor allows ECG data to be collected from a single lead in an accurate and minimally invasive way, offering medical-quality raw sensor data.

Figure 2.15: The Biosignalsplux Electrocardiography (ECG) Sensor

2.10.3 OpenSignals software

Opensignals is a versatile software that allows the simultaneous acquisition of biomedical data from several sensors, enabling the visualization and recording of data for later analysis. It is user-friendly software and is compatible with PLUX devices.
One of the main features of OpenSignals is the data processing toolset, which includes signal filtering and numerous advanced analysis capabilities. These advanced capabilities make it possible to perform frequency analysis, calculate detailed statistics, and extract relevant parameters directly from acquired signals. A final feature is the ability to export acquired data in various formats such as .hdf5 and .txt for further analysis in other software such as MATLAB.

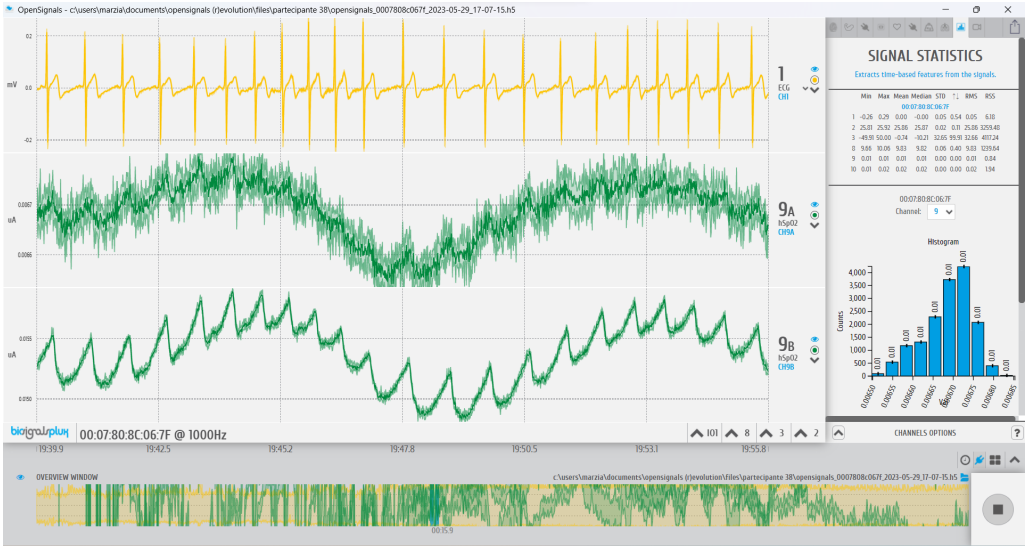

Figure 2.16: OpenSignals visual interface

2.11 Experiment

In this section of the chapter, the participant sample involved in the test and the adopted acquisition protocol will be introduced. Additionally, a detailed description of the Biload Test will be provided, an application developed in a previous project [15], that proves to be crucial for the execution of this study.

2.11.1 Sample

The volunteers who took part in the signal collecting were recruited from the university; there were a total of 64 persons, including 32 males and 32 females, aged approximately 23.53 ± 3.2 years, unfortunately, two subjects were excluded.

2.11.2 Acquisition protocol: the Biload Test

For all participants recruited for the following study, to record various physiological signals while performing cognitive tasks, it was decided to adopt the same acquisition protocol described below.
At the beginning of each session, after being invited to sit in front of the computer, each participant was described the rationale and the objective of the study and then asked to sign the informed consent, where they had to indicate their consent to participate to the study and to agree to the processing of their personal data.
Once this was done, the application where the test was going to be carried out, called Biload Test, was shown to them; this custom-made application was developed on Matlab during a previous project.
The first step required for the subject was to enter personal data such as first name, last name, age, and gender within the application's initial interface. Although they were going to be stored anonymously, they were essential to integrate the test results with the recorded physiological signals.
After that, sensors were placed on the subject, following the datasheet specifications:

in particular, the fNIRS sensor 2.10.1 was placed in the center of the forehead with the help of an elastic band included in the Biosignalsplux professional kit, while three ECG sensors 2.10.2 electrodes were placed on the left side of the chest. After

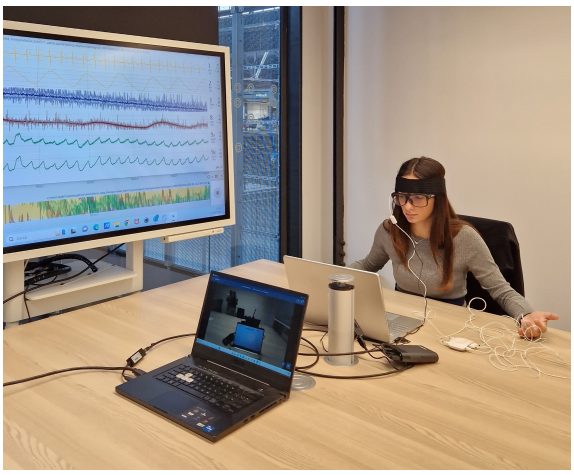

Figure 2.17: Subject performing the test with fNIRS sensor on forehead

the sensor's placement was finished, the structure of the Biload test, including how each individual step would work, was shown to the subject.
The test mainly consists of two types of tests: the Stroop Color and Word Test 2.4.1 to induce stress and the Nback test 2.4.2 to induce cognitive load:

- The Stroop test takes advantage of the discrepancy between the color name and the color of the character ink used to represent the word to create a conflict in the subject who needs more time to give the correct answer;
- N-back test that requires keeping in memory a piece of information presented N previous steps;

After this explanation, the subject was allowed to practice through two demos, one for each test type, which was useful both to get familiar with the platform and to make sure that they understood how the tests would work.
Once the training phase was over, the first phase (**REST 1**) was started, which constituted the initiation of signal recording using Opensignals software and the placement of an initial marker simultaneously using a trigger device.
During this first 3-minute phase, the subject was asked to be as relaxed as possible and remain silent.
After completing this initial phase, the subject was instructed to click the 'TEST' button in the application interface, as depicted in Figure 2.18, to initiate the Stroop test. At this specific moment, an additional marker was placed, which proved useful later for defining the durations of the various test phases.
The Stroop test was structured as follows: three levels of increasing difficulty corresponding to 3 different stages of the test (Stroop 1, Stroop 2, and Stroop 3). These had the same number of questions, equal to 90, with a maximum time to click the correct answer equal to 2.5 s, accompanied by an annoying clock ticking. In addition, an acoustic sound was generated for each incorrect or missed answer, with the aim of inducing stress. The colors used were RED, YELLOW, BLUE GREEN and BLACK.

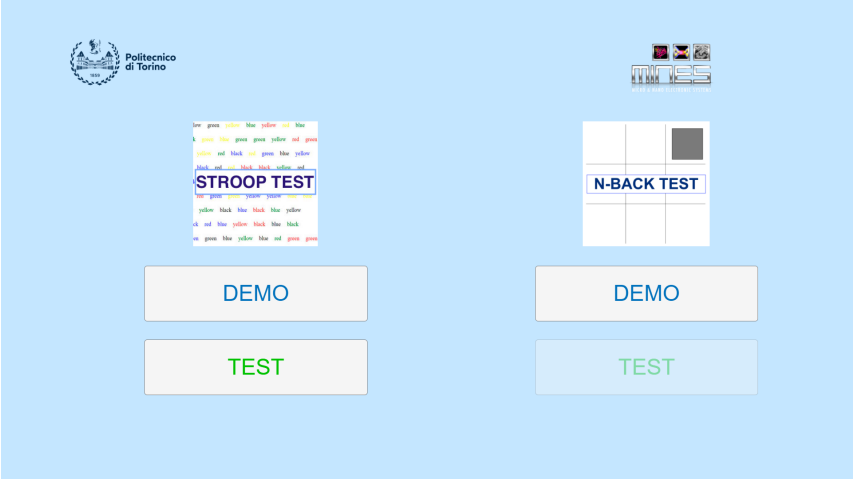

Figure 2.18: Initial interface of custom-made Biload application

- **Stroop 1**: First the simplest level, congruent questions were presented. The meaning of the word corresponds to the color with which it was written; in addition, the various answer buttons from one question to the next maintained the same position;
- **Stroop 2**: Intermediate-level, incongruent questions were presented. The colors of the word characters did not match the meaning of the word; this could lead to the subject taking more time to process the answer. In addition, the positioning of the answer keys changed from one question to another, which meant additional difficulty for the subject;
- **Stroop 3**: Last level and final stage of the Stroop test, incongruent questions were presented with noise. Compared to the previous level, an auditory-type distractor was introduced, repeating the color names randomly inducing further conflict.

When this first part of the test was finished, 3 additional minutes of rest (**REST2**) were acquired to allow physiological signals to return to the basal state; this is important not to affect the physiological data that will be acquired in the second part of the test.
The second part of the acquisition protocol consisted of the Nback test. It was made of 3 different tests, presented in the following order: 1) visual, 2) auditory 3) dual. Each consisted of three increasing levels: 1-back, 2-back and 3-back. In each, 30 questions were presented. Not all of them required an answer: in those cases, it was necessary to wait until the time ran out.

1. In the **visual N-Back** on the application grid interface for each question, one square at a time was enlightened; the subject had to click the "POSITION" button whenever the position of the enlightened square corresponded to the position it had in the N previous step. In case of no matches, the subject had to wait until the time ran out.
2. In the **auditory N-Back** on the application grid interface no square was enlightened, but an audio track of the letters of the English alphabet was played.

Each question corresponded to a letter: if the letter spoken was the same as in N previous steps, the subject had to click the "AUDIO" button.

3. In the **dual N-Back** both visual and auditory stimuli were present. The subject had to both remember the position of the square in N previous steps and pay attention to the letters pronounced by the audio track in N previous questions. In this case, both the "POSITION" and the "AUDIO" buttons could be clicked; in some cases, matching could occur for both, and both buttons needed to be clicked.

For all three of the above tests, visual (button highlighted in green or red, respectively) and auditory feedback were returned whenever the user responded correctly or incorrectly.
After the three n-back tests were finished, another 40 s were acquired to have a final rest phase (**REST3**) after which the recording on the Opensignals software was stopped.
A summary of the test procedure is shown in Figure 2.19.

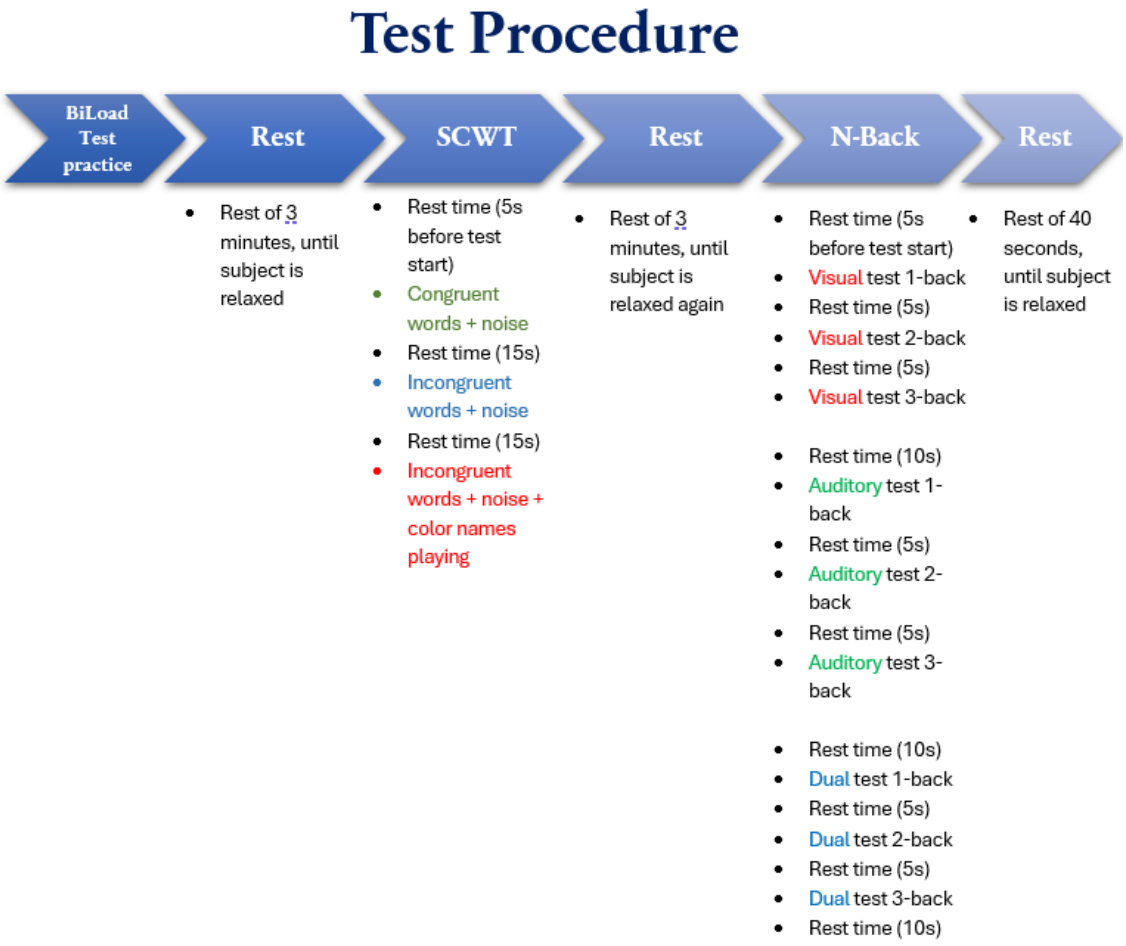

Figure 2.19: BiLoad test structure

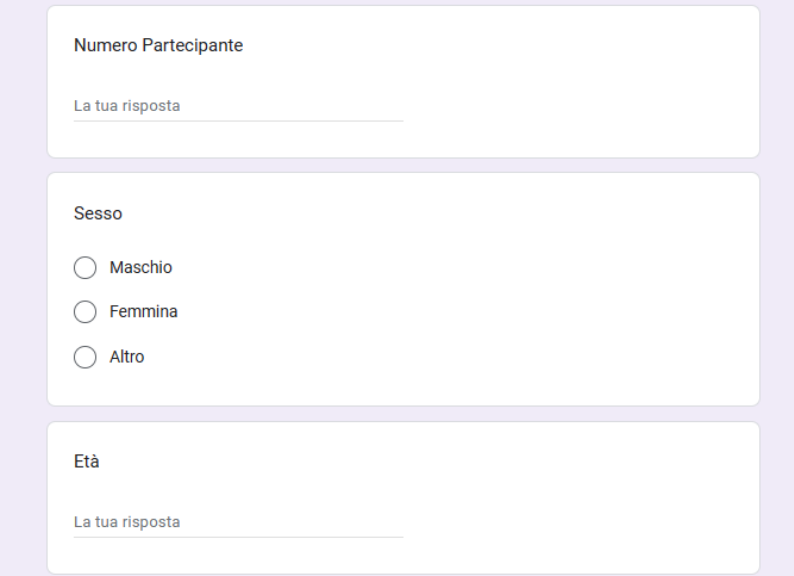

Figure 2.20: The first part of the questionnaire: personal data

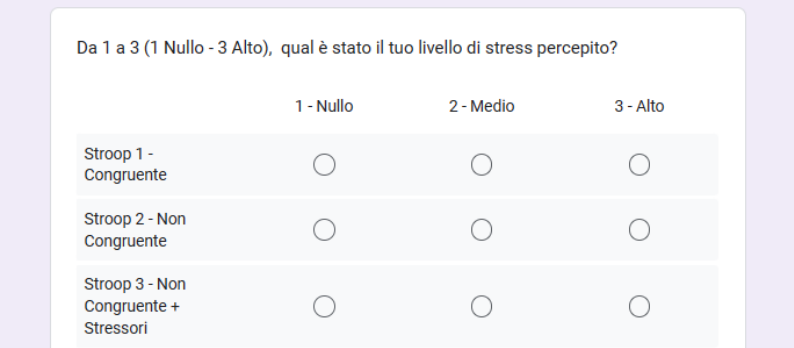

Figure 2.21: The second part of the questionnaire: perceived stress level

Finally, the various participants were asked to answer a subjective questionnaire called the Self-Assessment Questionnaire (SAQ) to identify their level of stress and workload load during the various phases of the test.
The questionnaire is structured as follows:

- In the first session, the subject was asked to enter personal information to associate the signals acquired with the questionnaire responses, as depicted in Figure 2.20.

- Second session in which the subject was asked to indicate a stress or workload value from 1 to 3 for each phase of the test described above (Stroop test and N-back test) where 1 means low, 2 means medium and 3 means high.this part is shown in Figure 2.21

2.12 Types of normalization

In the continuation of the thesis, a crucial aspect, as will be seen in Section 4.1 was the evaluation of normalization methods, which is based on the following approaches:

- **Z-score standardization**:
$$z_i = \frac{x_i - \mu}{\sigma}$$
where:
  - z_i represents the standardized value, and it is the distance of a data point from the mean in terms of the standard deviation.
  - x_i represents the original value.
  - μ represents the mean of the original data.
  - σ represents the standard deviation of the original data.

  This standardization provides a zero mean and a standard deviation of 1, preserving the shape properties of the original dataset (skewness and kurtosis). It is particularly robust to outliers and is recommended when the data distribution is approximately Gaussian.

- **Min-max scaling**:
$$s_i = \frac{x_i - \min(X)}{\max(X) - \min(X)}$$
where x_i represents the i-th value of the original data vector X to be normalized. This approach scales the data into a range between 0 and 1. However, it's important to note that this normalization might be influenced by outliers, and therefore, its effectiveness may vary in the presence of extreme data. It is a common choice when aiming to maintain a uniform distribution of data within a specific range.

- **Euclidean norm**:
$$s_i = \frac{x_i}{\|X\|_2} \tag{2.10}$$
where:
  - x_i represents the i-th value of the original vector X;
  - $\|X\|_2$ represents the Euclidean norm of the data vector X to be normalized.

  The Euclidean norm (or L2 norm) of a vector X of length N is defined as the square root of the sum of the squares of the vector's elements:
$$\|X\|_2 = \sqrt{\sum_{i=1}^{N} |x_i|^2} \tag{2.11}$$
where x_i is the i-th element of the vector X.
This type of normalization scales the data so that the normalized vector has unit length with respect to the Euclidean norm.

- **Mean scaling**:

$$s_i = \frac{x_i - \mu}{\max(X) - \min(X)}$$

where:

- x_i is the i-th element of the vector X to be normalized;
- μ represents the mean value of the vector X of the original data.

2.13 Statistical tests

Following data normalization, another crucial aspect of this thesis work involves conducting a statistical test on the data. It will be based on two non-parametric methods: the Kruskal-Wallis test and the Mann-Whitney U test.

2.13.1 Kruskal-Wallis Test

The Kruskal-Wallis test, introduced in 1952 by Kruskal [54] is a non-parametric statistical method designed to assess whether there are significant differences among three or more independent groups regarding a variable measured on an ordinal or at least interval scale. This test, sometimes referred to simply as the H test, is an extension of the Mann-Whitney U test for more than two groups. Unlike parametric tests such as one-away analysis of variance (ANOVA), Kruskal-Wallis does not assume a normal distribution of the data, making it suitable for situations where such assumptions may not be met or when dealing with ordinal data.
The test involves ranking and comparing the data from different groups without assuming a specific distribution.
The test follows a systematic procedure:

1. Calculation of ranks: all data, regardless of group membership, are sorted in ascending order, and each of them is assigned a rank based on their position in the order;

2. Calculation of mean rank for individual group: for each group, the sum of ranks is calculated and divided by the number of cases in the respective group;

3. Calculation of rank variance:

$$\sigma_R^2 = \frac{n^2 - 1}{12}$$

4. Calculation of the expected value of the ranking:

$$E_r = \frac{\sum i = 1^k (n_i + 1)}{2}$$

3. Calculation of the H Statistic: the H statistic is a measure of the difference between the average ranks of the groups under consideration and it is calculated

using the following formula

$$H = \frac{n-1}{n} \sum_{i=1}^{k} \frac{n_i \left(\bar{R}_i - E_R\right)^2}{\sigma_R^2}$$

where:
- n is the total number of cases (sum of elements in all groups);
- σ_R is the variance of the ranks;
- $\bar{R}_i$ is the mean rank for group i;
- E_R is the expected value of the ranking

H indicates how much the observed mean ranks differ from what would be expected under the null hypothesis of no differences between groups. Higher values of H provide stronger evidence in favor of the alternative hypothesis of significant differences between groups.

5. Comparison with chi-value distribution: the H statistic follows a chi-square distribution with $k-1$ degrees of freedom, where k is the number of groups. Critical values from the chi-square distribution are used to obtain the p-value associated with the H statistic.

6. Comparison of p-value with chosen significance level: the p-value is compared with the chosen significance level, α (e.g., 0.05). If the p-value is below the significance level, the null hypothesis is rejected, indicating significant differences among the groups. Conversely, if the p-value exceeds the significance level, there is insufficient evidence to reject the null hypothesis.

2.13.2 Mann-Whitney U Test

The Mann-Whitney test (1947)2.13.2 represents another non-parametric statistical approach, distinct from the Kruskal-Wallis test. Its application is focused on comparing two independent groups, aiming to determine whether they stem from the same population (null hypothesis) or if their distributions exhibit significant differences (alternative hypothesis).
Similar to the Kruskal-Wallis test, the Mann-Whitney test relies on the calculation of rank sums within the two groups. However, it differs in the use of the U statistic. This statistic is computed and subsequently compared with the expected probability distribution under the null hypothesis. When the number of observations is sufficiently large, it is possible to approximate the distribution of the U statistic to a normal distribution, allowing the use of the Z distribution to obtain the associated p-value.
The interpretation of the result involves comparing the obtained p-value with the pre-established significance level (e.g., 0.05). If the p-value is lower than the significance level, it suggests rejecting the null hypothesis, indicating significant differences in the distributions of the two groups. Conversely, if the p-value exceeds the significance level, there is insufficient evidence to reject the null hypothesis.

Chapter 3

Materials and Methods

In this chapter, the various methods implemented through the use of MATLAB R2022b software [55] for processing the signals recorded through the Biosignalsplux sensors are presented. Next, 19 significant features are extracted from the preprocessed fNIRS signals.
Finally, a statistical analysis was conducted on the extracted features using the Python programming language within the Visual Studio Code editor.

3.1 Signal pre-processing: pipeline

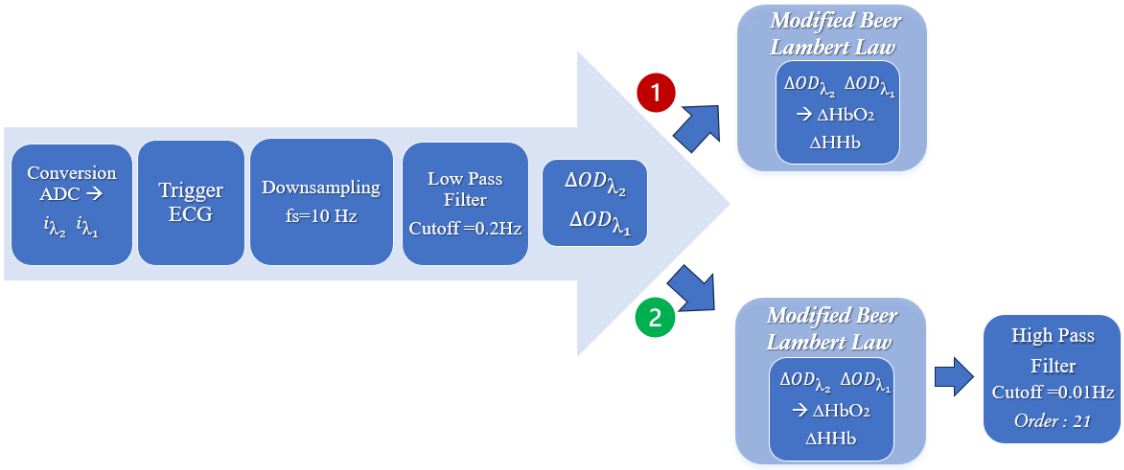

Figure 3.1: Pipeline pre-processing signal

The fNIRS and other physiological signals were acquired following the protocol described in the section 2.11.2. Regarding the functional Near-Infrared Spectroscopy signals, by literature review 2.9, on the acquired raw data it was necessary to perform pre-processing operations to allow conversion to changes in oxygenated and deoxygenated hemoglobin concentration.
In addition, since feature extraction from these signals was crucial for this study, to obtain hemoglobin concentration changes as reliably as possible, it was considered

essential to remove artifacts that could corrupt the fNIRS signal.
Figure 3.1 shows the pre-processing pipeline applied to the two fNIRS sensor outputs, consisting of these steps:

1. Conversion from digital to current values for both wavelengths;
2. Detection of a physiological trigger by ECG signal. This signal has its pipeline, which consists of only two steps:
   (a) conversion from digital values to voltages; (b) application of Pan-Tompkins algorithm; It is not the object of this study to understand the variations of this signal.
3. Low-pass type filtering with a cutoff frequency of 0.2 Hz;
4. Calculation of optical density variations for both wavelengths;
5. Application of modified Lambert Beer's law to obtain the concentration changes of oxygenated and deoxygenated hemoglobin.

These steps will be explained in detail in the subsequent sections.
As indicated in the figure 3.1 the pipeline was ultimately divided into two different paths. This separation has been integrated because, for some features extraction, it was necessary to add an additional filtering step: a high-pass filter with cutoff =0.01Hz (path 2).
For the other features like mean value, slope, entropy, total energy, and area under the curve, the high-pass filter was not applied because it turned out that the trend of the signal was crucial: with high-pass filtering the mean value was removed and it would not be meaningful to analyze the trend of such temporal features.
The following subsections give the implementation details of these steps for the fNIRS signal.

3.1.1 Data convertion

As mentioned in the section on OpenSignals software 2.10.3, the Biosignalsplux sensor output file is `.hdf5`. Through the h5read function, it is possible to read the acquired signals and save them within a `raw_data.mat` matrix. This matrix, concerning the data recorded by the fNIRS sensor, consists of 2 rows ('hSpO2' for the red emitter and infrared emitter) and n columns, where n is equal to the acquisition time multiplied by the sampling frequency. For data acquired through the ECG sensor, however, the matrix is composed of a single row named 'ECG' and as many columns as the samples recorded with the fNIRS sensor.
Furthermore, the extraction of the positions of the three markers is fundamental for the subsequent analysis: the start marker of the REST1 phase, the start marker of the SWCT, and finally the start marker of the N-back test.
The raw data acquired through Biosignalsplux sensors are in digital form, represented as Analog-to-Digital Converter (ADC) values. It is necessary to apply the specific transfer functions provided in the datasheets of these sensors to convert the fNIRS signals into current values. These values are associated with the two channels: one for the red emitter and the other for the infrared emitter, as outlined in Formula 3.1.

For the ECG signals, a different transformation Formula 3.2 is employed to extract voltage values.

$$\text{fNIRS\_data } [\mu\text{A}] = \frac{0.15 \cdot ADC}{2^n} \tag{3.1}$$

$$\text{ECG\_data } [\text{mV}] = 1000 \cdot \left(\frac{\text{ADC}}{2^n} - 0.5 \right) \cdot \frac{\text{VCC}}{G_{\text{ECG}}} \tag{3.2}$$

Where n is the number of bits per channel, ADC is the i-th value sampled from the channel under test, $fNIRS\_data$ is the resulting matrix containing the sample values in microamperes, VCC is the operating voltage set at $3V$, and G_{ECG} is the sensor gain, with a value of 1019. The variable ECG_data represents the resulting matrix containing the sampled values in millivolts.
In the Figure 3.2, it is possible to observe the two outputs of the fNIRS sensor after applying the transfer function.

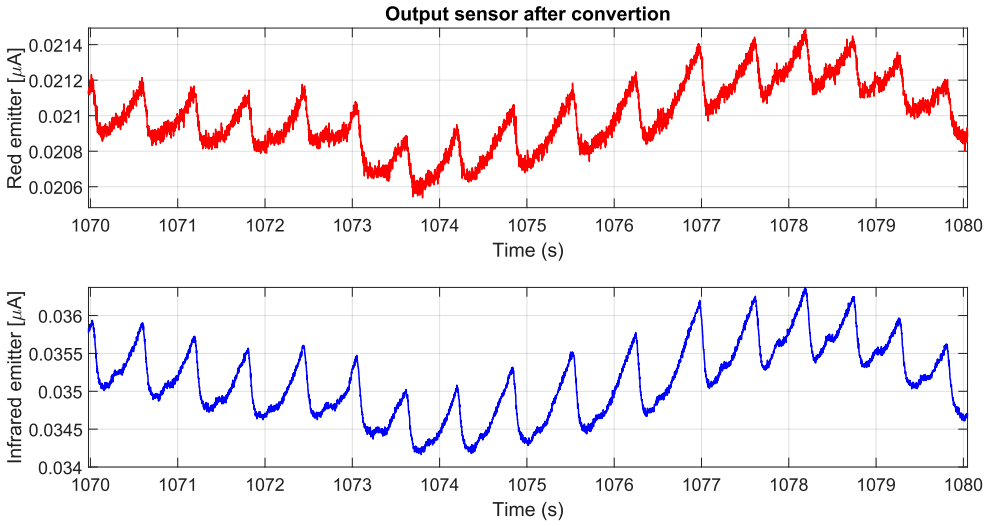

Figure 3.2: fNIRS sensor outputs (Red emitter and Infrared emitter) converted from digital values to current values

3.1.2 Start trigger

In the future, real-time implementation of this application is planned, with simultaneous recording of various physiological signals. To ensure accurate time alignment and a well-defined start for the acquisition of all data, it was chosen to introduce a trigger associated with a physiological event of particular interest to the study, such as cardiac activity. Specifically, the trigger was set on the second heartbeat of the test subject. This approach provides a precise reference point, enabling consistent and meaningful recording of physiological data, thus optimizing the overall quality of the information collected.

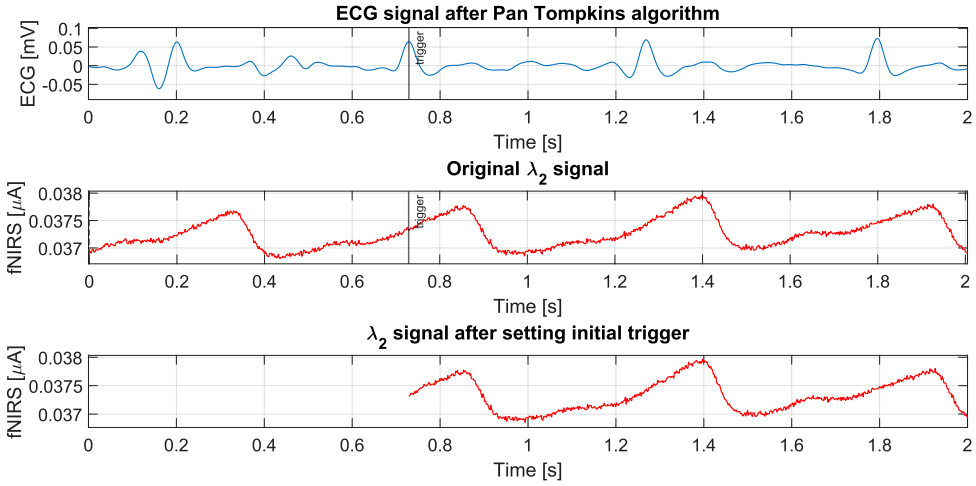

Figure 3.3: Trigger identification

To accurately detect QRS complexes in the electrocardiographic signals recorded by the Biosignalsplux sensor, the data converted to voltage values were processed through the Pan-Tompkins algorithm. This algorithm, proposed by Jiapu Pan and Willis J. Tompkins in 1985 [56] involves a series of filtering operations aimed at emphasizing the frequency content associated with rapid depolarization (R peak) and eliminating background noise.
The matrix *ECG_data* was then subjected to the following steps (shown in the Figure 3.4):

1. Second-order bandpass filter with a frequency range of 5-15 Hz;
2. Derivative filter: derivative, normalization concerning the maximum useful to go to highlight the QRS complex;
3. Squaring;
4. Moving window integration, to remove high frequency noise (0.150 seconds length)
5. Detection of peaks in the integrated ECG signal, using the built-in function of Matlab findpeaks, imposing that the distance between peaks is at least 200 ms. This limit is based on the physiological consideration of maximum heart rate.
6. Peaks control: the peaks identified in the previous step were verified using an adaptive double threshold and other decision rules; this is because they could be peaks caused by noise or the T-wave.

The output of the function provides the amplitude and index of the peaks relative to the R waves; the second identified index, corresponding to the second heartbeat, is selected as the trigger. The N samples before that index were eliminated for both matrices containing the samples acquired by the fNIRS sensor. In the Figure 3.3, the ECG signal of a subject is shown with the identification of the trigger at the second

Figure 3.4: Workflow Pan-Tompkins algorithm

heartbeat, along with the fNIRS signal associated with the infrared wavelength before and after removing the samples preceding the trigger.

3.1.3 Downsampling

The fNIRS signals, sampled at a frequency of 1000 Hz, underwent downsampling using a moving average filter with a frequency of 10 Hz. This downsampling operation was performed to improve subsequent filtering operations.
For each signal, a moving window approach was adopted, where a window of N samples was selected, equal to the ratio between the acquisition sampling frequency and the new sampling frequency. The central sample of each window was assigned the mean value of the signal within that specific window. This procedure was iterated over the entire length of the signal, including the last window, even if it consisted of a lower number of samples.
In the figure, the output signal associated with the infrared emitter is shown in blue, and the downsampled signal is represented in black, with new samples highlighted by blue markers.

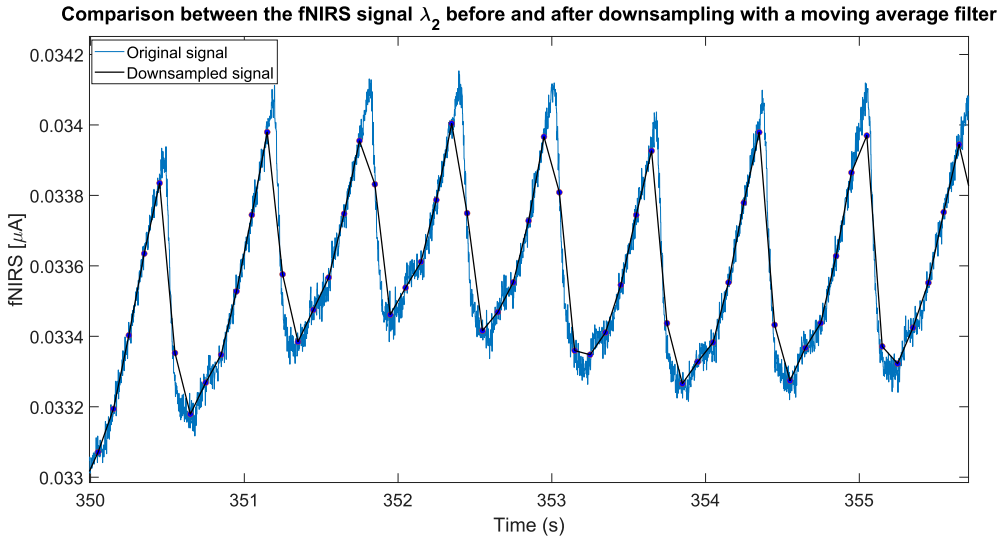

Figure 3.5: Signal before and after downsampling

3.1.4 Artifact removal: Low Pass Filter

The acquired fNIRS signals may contain artifacts from noise sources, primarily three:

- Instrumental noise, manifesting as a low-frequency drift;

- Artifacts due to movements;
- Physiological oscillations, such as cardiac activity.

The Matlab built-in function 'designfilt' was used to design a Butterworth low-pass filter suitable for removing high-frequency components not significant for the fNIRS signal. A cutoff frequency of 0.2 Hz was chosen, considering the typical frequencies of the heartbeat (1-1.5 Hz) and respiration (0.2-0.5 Hz) [57], with a passband ripple of 0.5 dB and a stopband attenuation of 80 dB. The filter mask is visualized in the Figure 3.6.

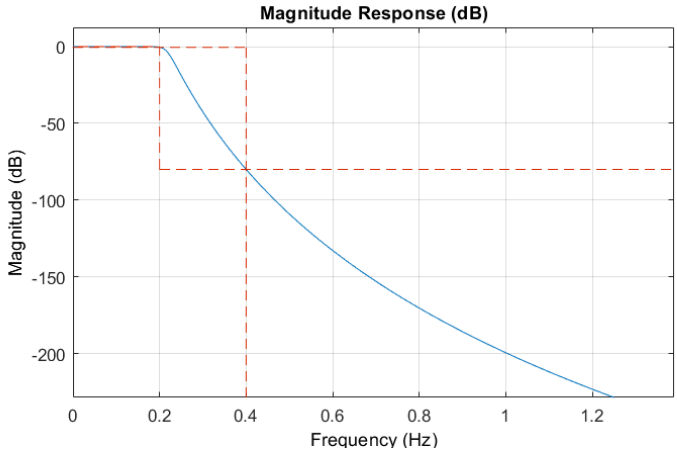

Figure 3.6: Low pass filter mask

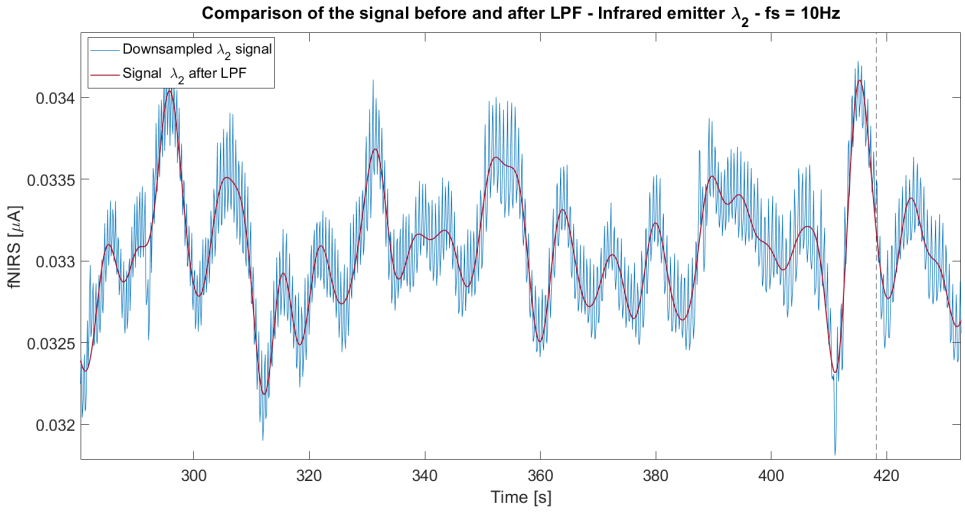

Figure 3.7: Filtered fNIRS signal with a Low Pass Filter (LPF)

Using this cutoff frequency, it was possible to remove any high-frequency noise associated with spike-like movements of the subjects.
In fact, to remove artifacts related to spike-type movements or experimental errors associated with sensor movement, it was observed that using a Savitzky-Golay filter,

which adapts a polynomial function to the data within the selected signal window and estimates the desired value based on the polynomial fit [58],[59], the signal did not show significant variations compared to the signal filtered with the Butterworth low-pass filter alone.
In the Figure3.7, it is possible to visualize the fNIRS signal for λ_2 wavelength before and after applying the low-pass filter (LPF).

3.1.5 Calculation of the variations in optical density

After removing the main artifacts that were corrupting the two signals recorded by the Biosignalsplux sensor at the two wavelengths λ_1 and λ_2, the conversion to concentrations of oxygenated and deoxygenated hemoglobin was performed (ΔHbO_2 and ΔHbR).
As introduced in the paragraph 2.8.2, to perform this conversion, the Modified Lambert-Beer law, reported in Equation 2.8, within which the variation in optical density is calculated.
The variations in optical density, also known as changes in absorbance, are calculated as differences between two time points, t_0 and t_1.
A crucial aspect of this conversion is the selection of the reference value, which is the light intensity associated with the moment t_0. To identify this value, six different methods were applied during the initial resting phase before the start of the Stroop test:

- Method 1: Mean value over the entire window, excluding the first and last 10 seconds of the signal;
- Method 2: Median value calculated on the same window used in Method 1;
- Method 3: Mean value calculated over a 60-second window preceding the start of Stroop 1;
- Method 4: Median value calculated on the same window used in Method 3;
- Method 5: Mean value calculated over a 60-second window centered at the midpoint of the REST1 phase;
- Method 6: Median value calculated on the same window used in Method 5.

In order to evaluate the best value to adopt, the results of the six methods were compared with method 1 used in the article through the calculation of the percentage deviation [60].
In Tables 3.8, the deviations for both wavelengths are reported for 16 subjects, with values exceeding 2% highlighted in red. Particular attention was focused on these latter participants, from which it emerged that the trend of the variations in optical density was the same for all six methods, as can be observed in the Figure 3.9. This is even more evident through the application of a high-pass filter that allows for the perfect overlap of the trends.
It was decided to adopt the light intensity value calculated with Method 1 as the reference.

RED EMITTER

Name_participant	Metodo 1 [%]	Metodo2 [%]	Metodo3 [%]	Metodo4 [%]	Metodo5 [%]	Metodo6 [%]
1	0.00	0.10	0.41	0.41	0.70	0.72
4	0.00	0.16	0.23	0.30	0.18	0.26
6	0.00	0.40	1.00	1.28	0.29	0.68
8	0.00	0.62	1.20	1.12	0.68	0.74
15	0.00	0.18	0.46	0.29	0.83	1.25
18	0.00	0.01	0.11	0.21	0.01	0.17
24	0.00	0.38	2.06	2.30	0.46	0.40
30	0.00	0.08	0.46	0.39	0.38	0.08
35	0.00	0.29	1.20	1.18	0.31	0.37
39	0.00	0.07	0.78	0.73	1.06	1.01
45	0.00	0.02	0.00	0.16	0.40	0.44
50	0.00	0.02	2.29	2.25	1.44	1.86
54	0.00	0.67	3.41	4.00	0.76	0.90
57	0.00	0.52	1.19	0.91	0.31	0.54
62	0.00	0.39	0.44	0.46	1.45	1.09
64	0.00	0.07	1.70	0.67	3.09	1.48

INFRARED EMITTER

Name_participant	Metodo 1 [%]	Metodo2 [%]	Metodo3 [%]	Metodo4 [%]	Metodo5 [%]	Metodo6 [%]
1	0.00	0.45	2.06	1.84	1.12	0.76
4	0.00	0.09	0.12	0.35	0.03	0.17
6	0.00	0.28	0.06	0.95	0.78	0.46
8	0.00	0.48	1.74	1.71	0.44	0.63
15	0.00	0.42	0.31	0.12	0.94	1.00
18	0.00	0.14	0.01	0.37	1.35	0.69
24	0.00	0.24	1.13	1.12	0.55	0.34
30	0.00	0.03	0.89	0.66	0.64	0.30
35	0.00	0.10	1.08	1.00	0.47	0.28
39	0.00	0.04	0.25	0.11	0.56	0.64
45	0.00	0.38	1.83	1.56	0.82	0.80
50	0.00	0.61	1.20	0.03	0.10	0.60
54	0.00	0.15	0.61	0.95	0.14	0.17
57	0.00	0.76	2.16	2.10	0.36	0.92
62	0.00	0.14	0.15	0.09	0.47	0.23
64	0.00	1.12	5.89	4.26	4.70	4.48

Figure 3.8: Percentage deviations relative to Method 1 for both wavelengths λ_1 (red emitter) and λ_2 (infrared emitter)

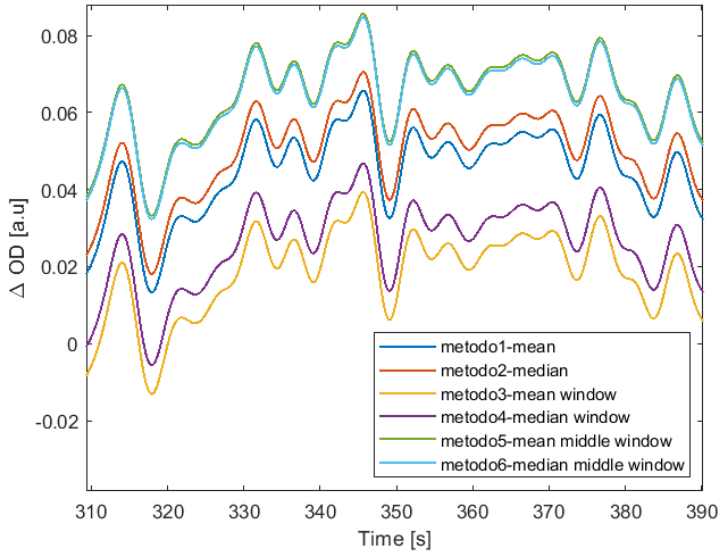

Figure 3.9: Comparison of the different variations in optical density obtained using the 6 methods

With the reference chosen, vectors for the two variations in optical density associated with the two emission wavelengths ($\lambda_1 = 660$nm and $\lambda_2 = 860$nm) of the fNIRS sensor were then calculated using the following formula.

$$\Delta \mathrm{OD}_{\lambda_1} = \log_{10}\left(\frac{I^{\lambda_1}_{\mathrm{rest}}}{I^{\lambda_1}_{\mathrm{task}}}\right) \tag{3.3}$$

$$\Delta \mathrm{OD}_{\lambda_2} = \log_{10}\left(\frac{I^{\lambda_2}_{\mathrm{rest}}}{I^{\lambda_2}_{\mathrm{task}}}\right) \tag{3.4}$$

3.1.6 Application of Modified Beer-Lambert Law

Successively, the concentrations of oxygenated and deoxygenated hemoglobin were calculated by solving the system of equations 2.9 and obtaining:

$$\Delta HbO_2 = \frac{\epsilon_1(\Delta \mathrm{OD}_{\lambda_2}/\mathrm{DPF}_2) - \epsilon_3(\Delta \mathrm{OD}_{\lambda_1}/\mathrm{DPF}_1)}{(\epsilon_1\epsilon_4 - \epsilon_3\epsilon_2)d} \tag{3.5}$$

$$\Delta HbR = \frac{\epsilon_4(\Delta \mathrm{OD}_{\lambda_1}/\mathrm{DPF}_1) - \epsilon_2(\Delta \mathrm{OD}_{\lambda_2}/\mathrm{DPF}_2)}{(\epsilon_1\epsilon_4 - \epsilon_3\epsilon_2)d} \tag{3.6}$$

For the values of molar extinction coefficients, literature values were utilized [61] associated with different wavelengths and the two distinct chromophores:

- ϵ_1 for HbR at wavelength λ_1 is 3.4408 mM^{-1} cm^{-1}
- ϵ_2 for HbO_2 at wavelength λ_1 is 0.3346 mM^{-1} cm^{-1}
- ϵ_3 for HbR at wavelength λ_2 is 0.7977 mM^{-1} cm^{-1}
- ϵ_4 for HbO_2 at wavelength λ_2 is 1.2071 mM^{-1} cm^{-1}

The value of the source-detector distance (d) for the used sensor, as provided by the datasheet, is equal to 2 cm.
The Differential Pathlength Factor (DPF), which accounts for the scattering that occurs within the subject's scalp, was derived using the formula proposed by Scholkmann et al.[62], considering the subjects' different ages and the two emission wavelengths of the sensor.

$$DPF(\lambda, A) = \alpha + \beta A^{\lambda} + \delta\lambda^3 + \epsilon\lambda^2 + \zeta\lambda \tag{3.7}$$

Where: $\alpha = 223.3$, $\beta = 0.05624$, $\gamma = 0.8493$, $\delta = -5.723 \times 10^{-7}$, $\epsilon = 0.001245$, and $\zeta = -0.9025$.
In the Figure 3.10, the results are presented in terms of the variation in concentrations of oxygenated and deoxygenated hemoglobin following the application of the law. This represented the output of branch labeled 1 of the pipeline.

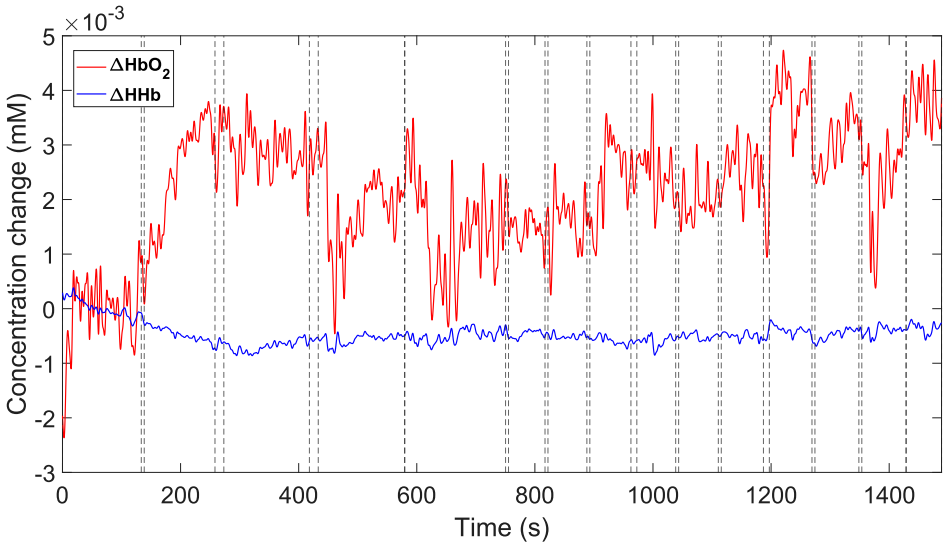

Figure 3.10: Signal after MBLL application

3.1.7 High-pass filter

As anticipated and explained in Section 3.1, a high-pass filter was applied to the two vectors related to the changes in the concentration of HbO_2 and HbR, only for some of the extracted features (path 2 of the pipeline). This filter was designed to eliminate instrumental noise, particularly the low-frequency drift. The choice of filter specifications was based on parameters commonly used in the literature [63][60]. Using the built-in Matlab function 'designfilt', a Butterworth type IIR high-pass filter was designed with the following specifications:

- Cutoff frequency set to 0.01Hz
- StopbandFrequency set to 0.006 Hz
- Ripple in the passband of 0.5dB
- Attenuation in the stopband of 80dB

This configuration, with a filter order of 21, proved effective in removing unwanted low-frequency components, thereby improving the quality of the processed signal. In the Figure 3.11, the concentration trends before and after the application of this filter are shown.

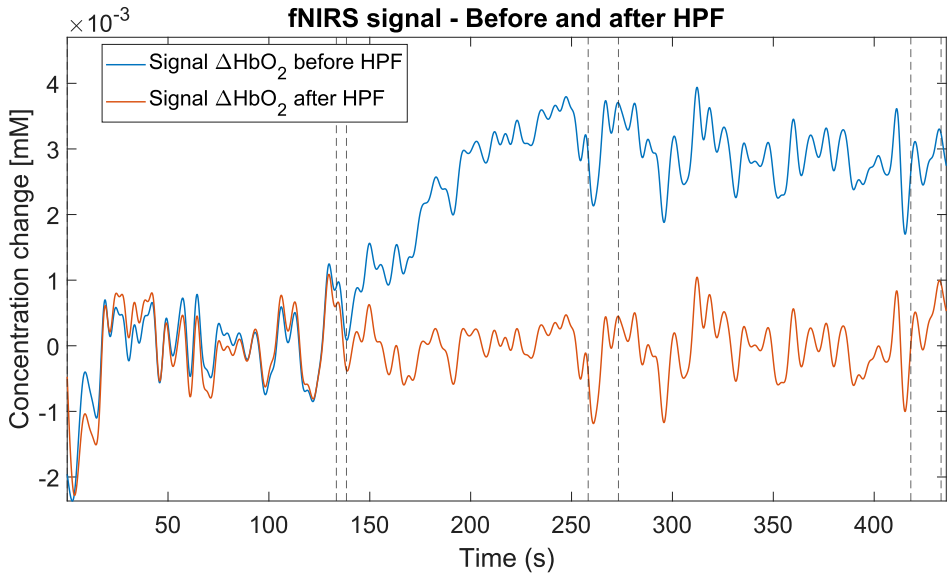

Figure 3.11: Comparision of the signal relating to ΔHbO_2 before and after the application of the Butterworth HPF

In Figure 3.12, both hemoglobin variations after applying the high-pass filter have been reported; they represented the output of the pipeline labeled 2.

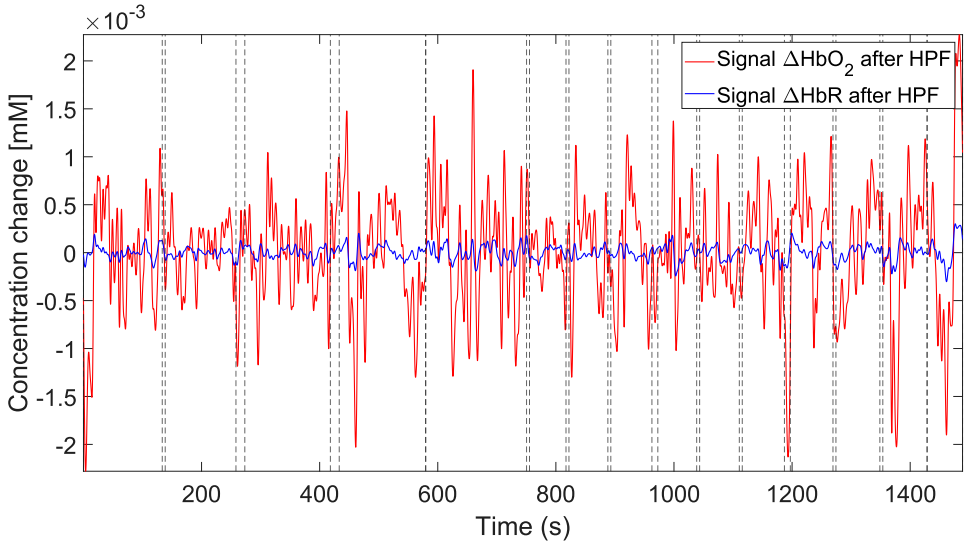

Figure 3.12: Signals output of branch labeled 2 in the pipeline

3.2 Feature extraction

Features extracted from signals ΔHbO_2 and ΔHbR 1	**Features extracted from signals ΔHbO_2 and ΔHbR filtered with HPF** 2
Statistical	**Statistical**
· Mean value	· Max value · Min value · Variance · Standard deviation · Kurtosis · Skewness
Temporal	**Temporal**
· Slope · Entropy · Area under the curve · Total energy	· Polarity · Mean of differences · Zero crossing rate · Peak to peak distance
	Spectral
	· Maximum frequency · Power bandwidth · Median frequency · Spectral entropy

Table 3.1: Features divided according to the type of signal on which they were calculated

Through an analysis of the literature Section 2.9, 19 features have been identified. These features were extracted for both the signal representing the variation in the concentration of oxygenated hemoglobin (ΔHbO_2) and the signal related to the variation in the concentration of deoxygenated hemoglobin (ΔHbR), resulting in a total of 38 features calculated for each phase of the test (15) and each participant (62). In Table 3.1, these features have been divided into two groups based on the signal from which they are extracted, following the description in Section 3.1.
In the following subsections, the features extracted through pathway 1 of the pipeline, corresponding to column 1 of the table, will be detailed first. Subsequently, the features extracted through pathway 2, corresponding to column 2 of the table, will be presented.

3.2.1 Features extracted from signals ΔHbO_2 and ΔHbR

Statistical features

Mean value: average signal value, calculated using the built-in Matlab function mean.

Temporal features

Slope: represents the signal slope and is calculated as the angular coefficient of the linear regression line of the signal portion associated with the i-th phase. This linear regression was obtained using the built-in Matlab function polyfit.

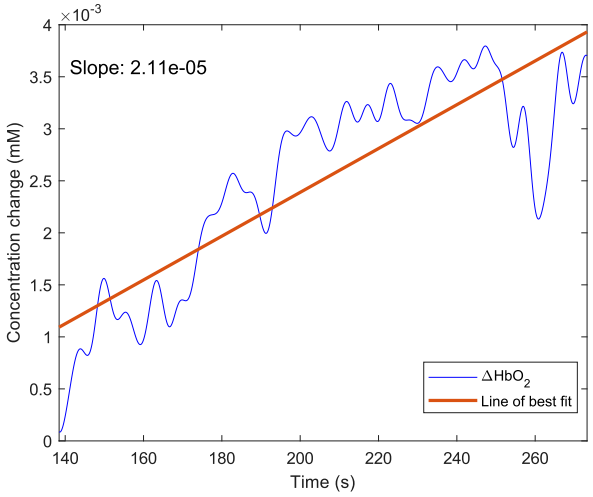

Figure 3.13: Slope feature for Stroop 1 phase

Entropy: calculated using the Shannon entropy reported in equation (3.8), it serves to assess the signal complexity in the time domain.

$$Entropy = -\sum_{i} P_i \cdot \log_2(P_i) \tag{3.8}$$

In the formula, P represents the probabilities associated with different signal values in the time domain.
To calculate this feature, the steps presented in the flowchart in Figure 3.14 were followed.

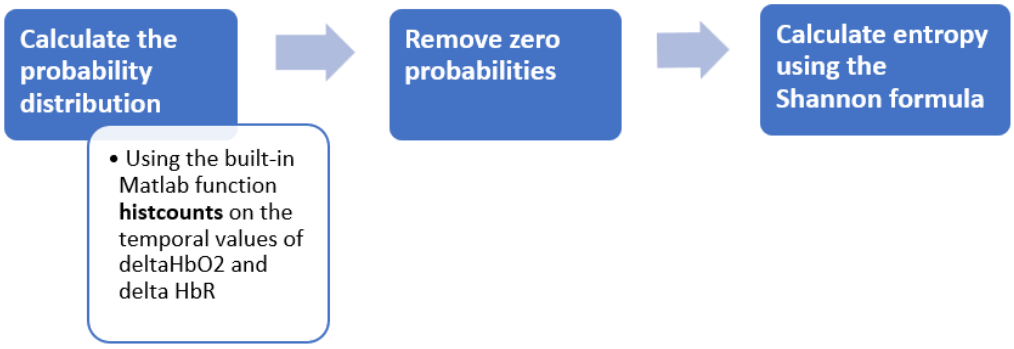

Figure 3.14: Step to calculate the feature entropy

Total energy: represents the amount of energy contained in the signal during the considered time interval. Since different phases of the test have different durations, the calculation of total energy is time-relative to allow meaningful comparisons.
The formula for calculating total energy is defined as:

$$\text{Total energy} = \frac{\sum_{i=1}^{N} x_i^2}{T} \tag{3.9}$$

where N represents the number of samples, T is the duration of the examined phase, and x_i is the value of the i-th signal sample.

Area under the curve: the area under the signal curve related to the concentration of oxygenated or deoxygenated hemoglobin using the trapezoidal rule. Again, as with the total energy feature, to allow a meaningful comparison of the value associated with different phases, it was necessary to divide by the duration of the phase.
The formula used is as follows:

$$\text{Area under the curve} = \frac{1}{2 \cdot T} \sum_{i=1}^{N-1} (x_i + x_{i+1}) \cdot (t_{i+1} - t_i) \tag{3.10}$$

where N represents the number of samples, T is the duration of the examined phase, and x_i and t_i are, respectively, the value and time associated with the i-th sample.

3.2.2 Features extracted from signals ΔHbO_2 and ΔHbR filtered with HPF

Statistical features

Max value: the maximum absolute value of the signal within the analyzed phase, obtained using the built-in Matlab function max;

Min value: the minimum absolute value of the signal within the analysis phase, utilizing the built-in Matlab function min;

Variance: the variance of the signal, determined through the utilization of Matlab's inherent var function;

Standard deviation: the standard deviation of the signal, computed using the built-in Matlab function std;

Kurtosis: kurtosis measures the greater or lesser flattening of the data distribution compared to the normal distribution, calculated using the built-in Matlab function kurtosis;

Skewness: skewness provides an indicator of the asymmetry of the data distribution, and for the calculation, the built-in Matlab function skewness was used;

Temporal features

Mean of differences: the average of signal derivatives, was calculated using the built-in Matlab function to compute differences, and subsequently, the associated mean value was calculated. A low value may indicate greater temporal stability of the fNIRS signal (few significant variations between successive samples), while a higher value might suggest faster variations, potentially associated with rapid changes in hemodynamic response, which could be linked to specific stimuli occurring during the test.

Polarity: determined by extracting the maximum and minimum absolute values from the signal, then calculating the absolute ratio between the two.

$$\text{Polarity} = |\frac{\max(x)}{\min(x)}| \tag{3.11}$$

It represents the magnitude of the amplitude variation between the maximum and minimum concentration values of hemoglobin, regardless of the direction of this variation.
If this ratio is close to 1, it means that the maximum and minimum values are close to each other, indicating a relatively low amplitude variation. On the contrary, if the ratio is much greater than 1, it suggests a significant difference between the maximum and minimum values in the phase, indicating a more pronounced amplitude variation.

Zero crossing rate: represents the number of zero crossings in the signal. This feature is particularly useful for assessing changes in sign in the signal, providing a measure of dynamism and temporal variations. The calculation involves counting every time a sign change occurs between successive samples (positive to negative or conversely) in the i-th phase, and dividing the total number by the overall number of samples comprising the phase. This approach provides a meaningful metric of how frequently the signal changes sign during the considered period.

Peak to peak distance: represents the maximum distance between a local maximum and the subsequent local minimum.
For this feature, it was decided to further filter the signal to obtain a smoother signal profile.
The signal related to the concentration of oxygenated and deoxygenated hemoglobin underwent a double-pass filtering using a Butterworth low-pass filter. This filter was implemented using Matlab's Butter function, with a cutoff frequency of 0.08 Hz and a filter order of 5. This frequency was chosen by observing the power spectrum of the signals in various phases of the test, and it was noticed that the main peak of the power spectral density (PSD) is almost always below this frequency.
In the Figure 3.15, an example of the power spectrum associated with the signal related to the variation in concentration of oxygenated hemoglobin is shown.
After filtering the signal, the first derivative was calculated for each phase, allowing the identification of local maxima and minima. In cases where there are multiple local maxima and minima, the peak-to-peak distance was calculated for each successive pair of local maxima and minima, and the feature was assigned the maximum value thus identified.
In the Figure 3.16, it is possible to visualize the signal related to the variation in concentration of oxygenated hemoglobin, both filtered and unfiltered, along with its associated local maxima and minima.

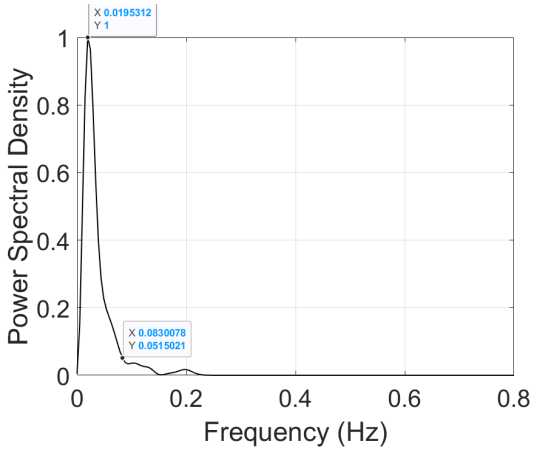

Figure 3.15: Power spectral density

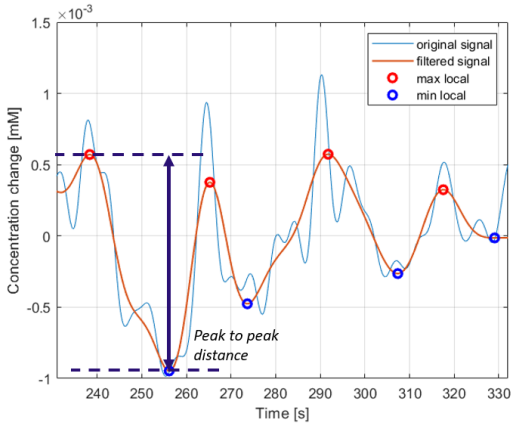

Figure 3.16: Feature peak to peak distance

Spectral features

Maximum frequency: represents the maximum frequency present in the power spectrum of the signal. The power spectrum was calculated using the Pwelch method on the signal without the mean value, applying Hamming windows with 512 points and a 50% overlap.

Power bandwidth: provides an indication of the frequency band where the majority of the signal power is concentrated, with the bandwidth representing the range of frequencies covering 95% of the total power. The calculation of the bandwidth involves the following steps:

1. Power Spectrum calculation: Using the Pwelch method on the signal without the mean value, applying Hamming windows with 512 points with a 50% overlap;
2. Cumulative power calculation in the power spectrum;
3. Lower Limit Determination (f_{lower}): identifying the frequency of the lower limit, representing the frequency below which 95% of the cumulative power is located;
4. Inverse cumulative power calculation;
5. Upper Limit Determination (f_{upper}): identifying the frequency of the upper limit, representing the frequency above which 95% of the cumulative power is located;
6. Bandwidth calculation: the bandwidth of the power spectrum is calculated as the absolute difference between f_{upper} and f_{lower}:

$$\text{Power Bandwidth} = |f_{\text{upper}} - f_{\text{lower}}|$$

Median frequency: represents the frequency below which 50% of the total signal energy is located. This is obtained by analyzing the spectral distribution resulting from the Fourier transform.

Spectal entropy: measures the complexity of the fNIRS signal in the frequency domain. The calculation involves the following 4 steps:

1. Calculate the power spectrum;
2. Normalize the power spectrum to obtain probability distributions;
3. Remove zero probabilities;
4. Calculate entropy using the Shannon formula:

$$\text{Spectral entropy} = -\sum_i P_i \cdot \log_2(P_i) \tag{3.12}$$

Chapter 4

Results

In this chapter, the results obtained through statistical analysis are presented.
Before conducting these analysis, it was necessary to further manipulate the data by normalizing them and dividing them into four classes based on the responses provided by participants in the Subjective Assessment Questionnaire (SAQ).
In particular, various normalization methods were compared to select the most suitable one in terms of standard deviations.
Finally, in the chapter, it is detailed how non-parametric statistical tests, specifically the Kruskal-Wallis and Mann-Whitney tests, were employed.

4.1 Data normalization

After extracting the 38 features related to the recorded fNIRS signal for each of the 62 participants, they were divided into four datasets:

1) Values of the features extracted during the three phases characterizing the Stroop task, along with the values from the features extracted during the rest1 phase.

2) Values of the features extracted during the three phases characterizing the Visual N-back task, along with the values from the features extracted during the rest1 phase.

3) Values of the features associated with the three phases characterizing the Auditory N-back task, along with the values from the features extracted during the rest1 phase.

4) Values of the features associated with the three phases characterizing the Dual N-back task, along with the values from the features extracted during the rest1 phase.

It was decided to consider the data from dataset 1 for studying stress, while the data from datasets 2, 3, and 4 were analyzed for workload since, as explained earlier in sections 2.4.1 and 2.4.2 and in the literature, the Stroop test is commonly used to induce stress, while the N-back test is employed to induce cognitive load.

For each feature and each dataset, a matrix NxM was obtained, with N (62) representing the number of rows equal to the number of test participants, and M (4) representing the number of columns related to the rest phase and the three cognitive test phases (Stroop, Visual N-back, Auditory N-back, or Dual N-back). Subsequently, for each of these matrices, participant-wise normalization was performed.
To determine the most suitable normalization technique, a workflow illustrated in Figure 4.1 was developed and followed. For each matrix and each participant, four

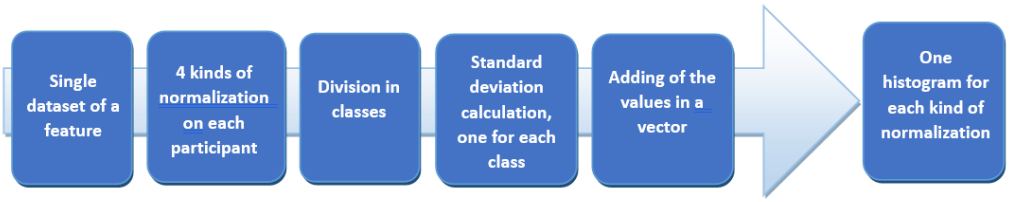

Figure 4.1: Workflow for choosing the type of normalization to adopt

normalization techniques were examined: mean scaling, z-score standardization, min-max scaling, and Euclidean normalization. These normalizations were introduced earlier in Section 2.12. The primary objective of this variety of normalizations was to identify which one allowed obtaining a lower standard deviation of the data. A lower standard deviation suggests greater consistency and stability in the data, providing a solid foundation for subsequent interpretations and statistical analyses.
After applying the four normalizations, it was necessary to assign a label to the features extracted from different phases of the test in order to categorize them into classes. This is because it is not guaranteed that two individuals perceived the same level of stress or cognitive load when facing the same phase. Additionally, it is not assured that level 2 of the Stroop for a specific subject was more stressful than phase one of the Stroop.
To overcome this challenge, participants in the test were subjected, at the end of the data acquisition, to a subjective questionnaire 2.11.2 to assess the level of perceived stress and load in different phases of the Biload Test.
Based on these responses, the features were divided into 3 classes:

- **Class 1**: Low level of stress or cognitive load;
- **Class 2**: Medium level of stress or cognitive load;
- **Class 3**: High level of stress or cognitive load.

The fourth class, Class 0, was associated with the values of the features extracted during the rest phase where the subject did not perform any cognitive tasks (REST1).
To evaluate which of the 4 normalizations was the most suitable, the standard deviation values for the 4 classes were calculated for each normalization and stored in a vector.
This process was repeated for each type of feature and for each dataset, aiming to obtain a single vector for each normalization containing the standard deviations associated with the features.

Subsequently, histograms were created to visualize the standard deviations of the four normalization techniques. Stress analysis focused solely on Dataset 1, while workload analysis considered the three datasets related to N-back tasks.

4.1.1 Analysis of results: choice of normalization method

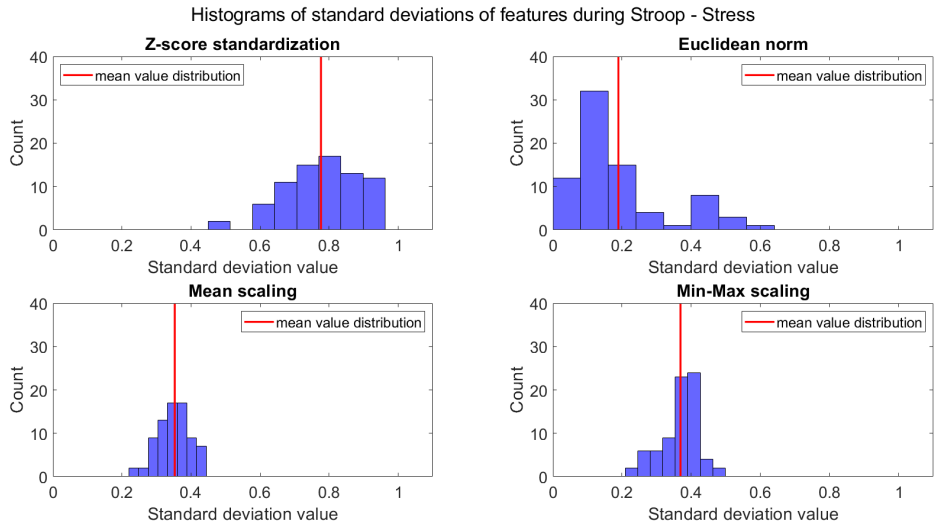

Figure 4.2: Distributions of standard deviations for features in the Stress dataset

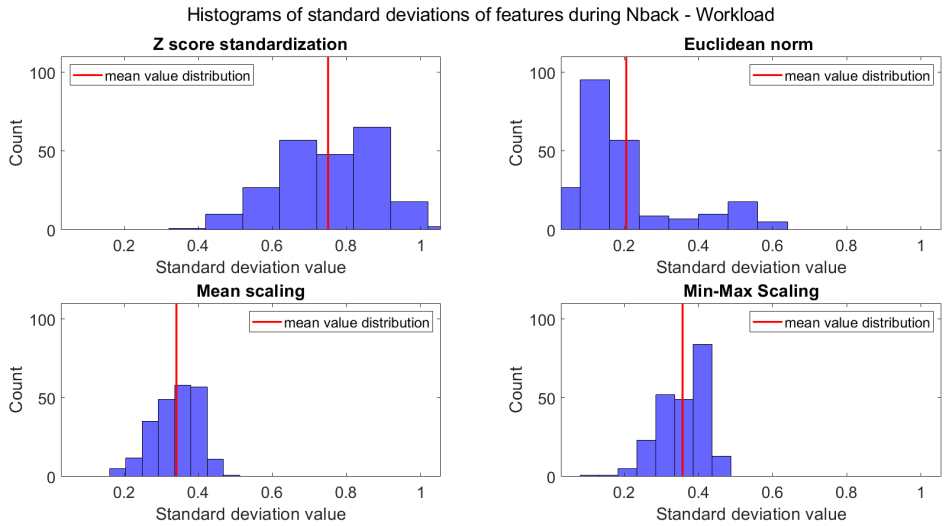

Figure 4.3: Distributions of standard deviations for features in the Workload datasets (Visual Nback, Auditory Nback and Dual Nback)

In Figures 4.2 and 4.3, histograms related to the four types of normalizations used for stress and workload are presented, respectively. For stress, the dataset associated with the Stroop test was used, while for workload, data from all three datasets of the N-back test were utilized.

From the analysis of the graphs, it emerges that, both for the stress dataset and for the datasets representative of workload, Euclidean normalization proved to be the best in terms of data standard deviations. This is highlighted by the fact that the distribution of this normalization has a mean value (represented by the red line in the plot) shifted towards lower standard deviation values. In particular, it is observed that a greater number of standard deviations have values below 0.2, as indicated by the count of the highest bin in this region.
Following this observation, the decision was made to apply the same normalization methodology, based on the **Euclidean norm**, to all four datasets, using the Formula 2.10 and 2.11.

4.2 Statistical Analysis

The key point of this study is represented by the statistical test adopted on the features extracted from the fNIRS signal. The objective is to determine whether there are characteristics among them that prove to be discriminative in detecting variations in stress or cognitive load, or in identifying the presence or absence of stress or cognitive load.

After dividing the normalized features into four datasets based on class membership,

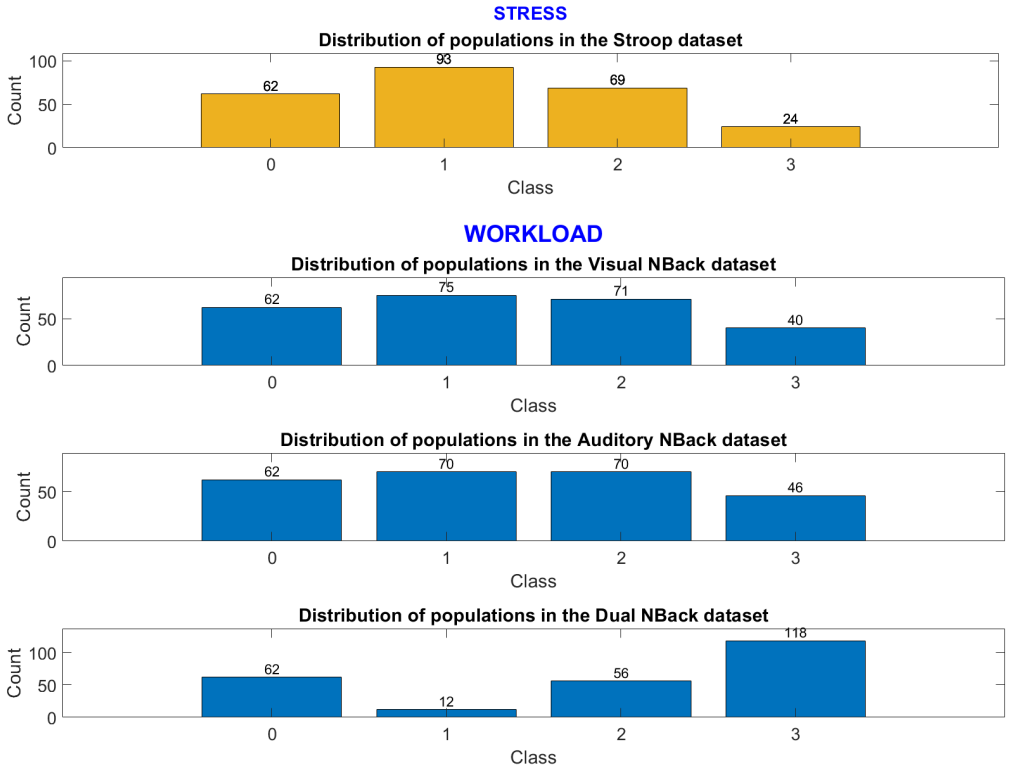

Figure 4.4: Population distributions in various datasets: Stroop dataset for analyzing stress in orange while in blue the Visual Nback, Auditory Nback, and Dual Nback datasets for analyzing workload

an analysis of class sizes was conducted. The goal was to ensure that there were no

significant imbalances before proceeding with the statistical test. This verification was performed by creating graphical representations of population distribution.
in the Dual N-back dataset, Class 1 is of an order of magnitude different from Class 3. Despite this imbalance, it was considered acceptable because the population of Class 1 was sufficiently substantial to ensure the effectiveness of the subsequent statistical analysis. No additional classes needed to be included for any dataset, allowing for the statistical test to proceed using all 4 classes in all datasets.
Given the non-normal nature of the data associated with features extracted from fNIRS signals, the choice was made to use the Kruskal-Wallis statistical test. As previously discussed in the Section 2.13.1, this non-parametric test assesses differences in the ranks of distributions among three or more independent groups. The objective is to determine if there are statistically significant differences among these groups.
The Figure 4.5 illustrates the steps taken to perform statistical analysis for each feature.

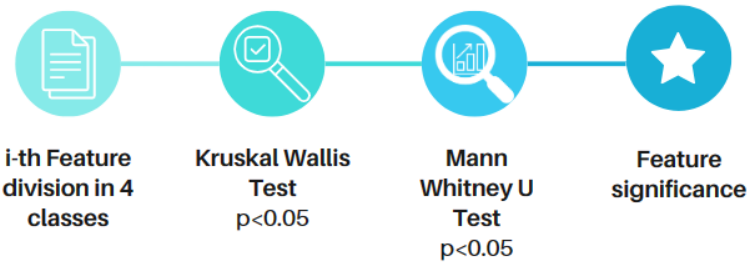

Figure 4.5: Steps of the statistical approach

For each dataset and for all 38 features, the Kruskal-Wallis test was performed using the kruskal function from the scipy.stats library in Python. In the execution phase, the vectors of the four classes associated with the i-th feature were inputted to this function; these vectors represent the four independent groups under study, each characterized by a non-normal distribution. The function outputted the value of the H statistic and the associated p-value, crucial for assessing any significant differences among the four classes.
With a significance level set at 0.05, for each dataset, features were identified that returned a p-value below this threshold. The Kruskal-Wallis test returned a positive result for these features, indicating the presence of at least one significant difference among the four groups.
To compare the various groups and determine which of them differed, it was necessary to perform an additional statistical test on the features that turned out to be significant according to the Kruskal-Wallis test. The Mann-Whitney test (Section: 2.13.2) was used to conduct this paired analysis. This test was performed for the 6 combinations of possible pairs with 4 groups: 0 vs 1, 0 vs 2, 0 vs 3, 1 vs 2, 1 vs 3, and 2 vs 3.
Using a counter, the number of pairs for which the Mann-Whitney test identified a statistically significant difference between the two populations ($p < alpha$) was enumerated. In this case as well, a significance level of alpha equal to 0.05 was chosen.

Subsequently, the granularity of differentiation was reduced to examine whether it was possible to discriminate a binary condition, stress/no stress, or cognitive load/no cognitive load. This was achieved by repeating the Kruskal-Wallis test on all features and for all 4 datasets.
For features that showed a p-value < 0.05, a more in-depth analysis was conducted using the Mann-Whitney test, exclusively on pairs 0 vs 1, 0 vs 2, and 0 vs 3. This approach allowed for a more targeted assessment of the presence of specific differences in a dual condition.
In this case as well, using a counter, the number of pairs that yielded a positive result in the Mann-Whitney test for that specific feature and dataset were counted.

4.2.1 Analysis of results

In Table 4.1, the results of the first statistical test using only the threshold of p < alpha are reported.

	STRESS	WORKLOAD		
	STROOP	NB_V	NB_A	NB_AV
K test significance	30	29	30	30
Feature significance (>1)	30	29	28	28
Feature significance (>2)	24	27	26	26
Feature significance (>3)	14	12	7	7
Feature significance (>4)	8	11	2	2
Feature significance (>5)	3	4	0	0

Table 4.1: Statistical test results with $p < 0.05$ for each dataset: Stroop, Visual Nback (NB_V), Auditory Nback (NB_A), and Dual Nback (NB_AV)

In the first row of the table, the number of features that, for each dataset (Stroop, Visual Nback, Auditory Nback, and Dual Nback), produced a positive result in the Kruskal-Wallis test has been reported. These constitute approximately 79% of the features extracted from the fNIRS signal for all four datasets.
Subsequently, in the following rows, the results of the Mann-Whitney test are presented. Specifically, the counter used to measure the number of significant pairs allowed us to identify how many features had more than one significant pair (feature significance > 1), more than 2 significant pairs (feature significance > 2), more than 3 significant pairs (feature significance > 3), more than 4 significant pairs (feature significance > 4), and finally, the features that showed a statistical difference in all 6 combinations of populations.
It is possible to notice that, by increasing the granularity of the analysis (Feature significance>3), that is, investigating whether there are features capable of detecting differences in terms of perceived cognitive load or perceived stress, there is a reduction of 50% in the number of features compared to the total number of features that produced a positive result in the Kruskal-Wallis test.
Of particular importance is the last row of the table, especially for the Stroop dataset and the Visual Nback dataset.

In the Stroop dataset, the 3 features that showed significant differences in terms of data distribution for all 6 combinations are: the mean value, the area under the curve, and the total energy related to the variation in deoxygenated hemoglobin concentration.
In the case of the Visual Nback dataset, the 4 features are: the mean value of both the signal associated with the variation in oxygenated hemoglobin and the signal associated with the variation in deoxygenated hemoglobin, the total energy, and the area under the curve related to the signal associated with the variation in oxygenated hemoglobin concentration.
In Table 4.2, instead, the results related to the binary analysis are reported.

	STRESS	WORKLOAD		
	STROOP	NB_V	NB_A	NB_AV
K test significance	30	29	30	30
Feature significance (>0)	29	29	30	30
Feature significance (>1)	24	27	25	25
Feature significance (>2)	20	25	23	23

Table 4.2: Statistical test results for binary analysis with $p < 0.05$ for each dataset

In this case, as well, the first row reports the number of features that the Kruskal-Wallis test identified as significant with the threshold set on the p-value. It is important to note that these features are the same as those reported in the previous table, as there were no changes in how the Kruskal-Wallis test was conducted in the binary analysis. The main variation concerns the number of pairs examined using the Mann-Whitney test.
Thanks to the counter used to measure the number of significant pairs, it was possible to identify the features that had at least one significant pair (feature significance >0), more than one significant pair (feature significance >1), and more than two significant pairs (feature significance >2).
In contrast to the Table 4.1 reporting the results of the first test, in this case, the row with feature significance >0 is present. This row differs from the first one because some features may have appeared significant in the Kruskal-Wallis test due to statistical differences between pairs, such as 1 vs 2, which are not analyzed in the dual case.
Indeed, it can be observed that in the case of the Stroop dataset, one less feature was identified compared to the number of features deemed significant in the Kruskal-Wallis test.
The 52.6% of the extracted features allow discriminating a dual condition for the Stroop dataset. In the case of the Visual Nback dataset, the highest percentage is observed, amounting to 65.8%, while for the Auditory Nback and Dual Nback datasets, this percentage is 60.5%. It is important to note that these percentages refer to features for which the Mann-Whitney test has detected statistical significance in all performed paired analyses, indicating differences in the distributions of the

considered groups (Feature significance >2).
These features have been examined and are listed in the table in Figure 4.6. The features common to the four datasets, highlighted in green, constitute 50% of the 38 extracted features. The features extracted from the signal associated with the variation in the concentration of oxygenated hemoglobin (ΔHbO_2) are listed in the upper part, while in the lower part, there are features related to the signal of the variation in the concentration of deoxygenated hemoglobin (ΔHbR).

	STROOP	NBACK V	NBACK A	NBACK AV
ΔHbO2	Min value	Min value	Min value	Min value
	Max value	Max value	Max value	Max value
	Mean	Mean	Mean	Mean
	Variance	Variance	Variance	Variance
	Standard deviation	Standard deviation	Standard deviation	Standard deviation
	Area under the curve	Area under the curve	Area under the curve	Area under the curve
	Total energy	Total energy	Total energy	Total energy
	Entropy	Entropy	Entropy	Entropy
	Peak to peak	Peak to peak	Peak to peak	Peak to peak
	Mean difference	Max frequency	Max frequency	Max frequency
		Median frequency	Median frequency	Median frequency
		Kurtosis		
		Spectral entropy		
ΔHbR	Min value	Min value	Min value	Min value
	Max value	Max value	Max value	Max value
	Mean	Mean	Mean	Mean
	Variance	Variance	Variance	Variance
	Standard deviation	Standard deviation	Standard deviation	Standard deviation
	Area under the curve	Area under the curve	Area under the curve	Area under the curve
	Total energy	Total energy	Total energy	Total energy
	Kurtosis	Kurtosis	Kurtosis	Kurtosis
	Peak to peak	Peak to peak	Peak to peak	Peak to peak
	Median frequency	Median frequency	Median frequency	Median frequency
		Entropy	Entropy	Entropy
		Spectral entropy	Power bandwidth	Power bandwidth

Figure 4.6: Significant features for dual analysis for each dataset

4.3 Kruskal-Wallis Test with threshold H and p value

Observing the results of the features that were found to be significant in dual classification, it was noted that only some of them show strong and significant deviations across the four conditions. In order to obtain a more restrictive and relevant subset of features, a double threshold was introduced: in addition to the threshold on the p-value, a threshold on the H statistic of the Kruskal-Wallis test was included.
This threshold was chosen from the direct observation of the trends in the distributions of features for each class. In particular, the features that the Kruskal-Wallis statistical

test had found significant with the condition p<0.05 were analyzed. It was noticed that in some cases, for certain features, the deviation between the distributions of the 4 classes was not as clear-cut, as shown, for example, in Figure 4.7 for the Kurtosis and Peak to Peak features compared to the deviation between the distributions of the Mean feature.
Indeed, as reported in Table 4.3, the Mean feature returns a higher H value, indicative of a significant deviation from the overall mean value of the distributions of the four groups.

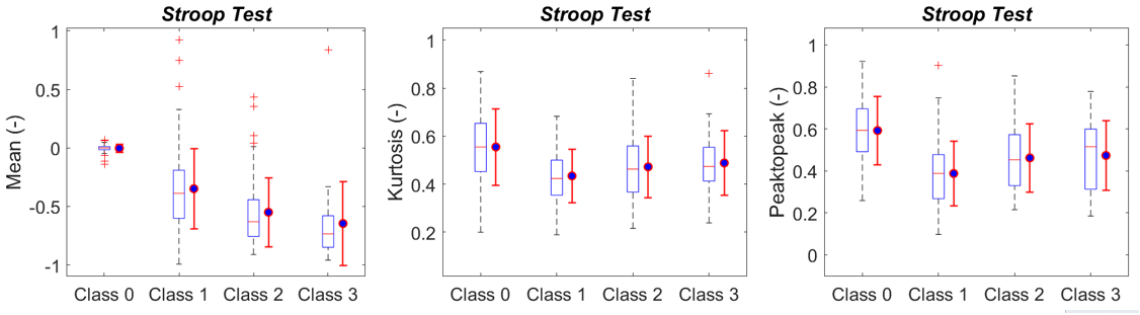

Figure 4.7: Trends in the distributions of the various classes of the following features extracted from the Stroop dataset: mean, kurtosis, and peak to peak

Name Feature	H(3)	p-value
Mean ΔHbR	113	2.5×10^{-24}
Peak to peak ΔHbO_2	48.2	1.9×10^{-10}
Kurtosis ΔHbR	26.1	9×10^{-6}

Table 4.3: Output of the Kruskal-Wallis test for the features mean, peak to peak, and kurtosis

Therefore, it was decided to impose a threshold of 50 to exclude those cases, such as kurtosis and peak to peak features, that, although significant for dual classification, did not exhibit a high deviation from the overall mean value of the distributions.
Thus, the test was repeated both in binary mode and with greater granularity, following the same procedure presented in Section 4.2, but introducing the dual condition for the Kruskal-Wallis test (p<alpha and H>50). In this way, the Mann-Whitney test was performed only for features that satisfied both conditions.

4.3.1 Analysis of statistical test results with threshold on H and p value

In Table 4.4, the number of features that showed significant results for both the Kruskal-Wallis and Mann-Whitney tests is reported for each dataset. As in the case of Table 4.1, the first row refers to the number of features that tested positively in the Kruskal-Wallis test with conditions on the H statistic and p-value. Comparing

Table 4.2 and Table 4.4, obtained using only the p-value condition, the following observations can be made:

- a 50% reduction in the number of significant features for the Stroop dataset;
- a 34.5% reduction in the number of significant features in the other three datasets;
- an equal number of significant features showing a feature significance >5.

	STRESS	WORKLOAD		
	STROOP	NB_V	NB_A	NB_AV
K test significance	15	19	19	19
Feature significance (>1)	15	19	19	19
Feature significance (>2)	15	19	19	19
Feature significance (>3)	10	10	5	5
Feature significance (>4)	7	9	2	2
Feature significance (>5)	3	4	0	0

Table 4.4: Statistical test results with p < 0.05 and H>50 for each dataset: Stroop, Visual Nback (NB_V), Auditory Nback (NB_A), and Dual Nback (NB_AV)

Furthermore, as in the test performed with the only constraint of significance imposed on the p-value, it can be observed that, as the sought level of differences increases (starting from a feature significance>3) there is a reduction in the number of features compared to the previous row. In particular, for the Auditory Nback and Dual Nback datasets, this reduction is greater than 50%.
Of extreme importance is the last row of the table, which, as previously mentioned, reports the same values as Table 4.1, associated with the same features.
This demonstrates that these features are highly significant and can be discriminative in studying variations in perceived stress levels or cognitive workload.
Table 4.5 reports the results associated with the binary analysis performed with the double condition.

	STRESS	WORKLOAD		
	STROOP	NB_V	NB_A	NB_AV
K test significance	15	19	19	19
Feature significance (>0)	15	19	19	19
Feature significance (>1)	15	19	19	19
Feature significance (>2)	15	19	19	19

Table 4.5: Statistical test results for binary analysis with double condition (p < 0.05 and H>50) for each dataset

It can be observed that all the features significant for the Kruskal Wallis test under the dual condition (p<0.05 and H>50) showed a statistically significant difference in

all three pairs of populations analyzed. This means that the threshold put on the H statistic saves the most significant features, with a sharper difference between the rest state and altered states. These features allow for the discrimination of a binary condition: stress/rest or cognitive load/rest.
The features that are significant for discriminating these two conditions and that are common to all four datasets are 15, corresponding to 39% of the extracted features. These are highlighted in green in the table shown in Figure 4.8.

	STROOP	NBACK V	NBACK A	NBACK AV
ΔHbO2	Min value	Min value	Min value	Min value
	Max value	Max value	Max value	Max value
	Mean	Mean	Mean	Mean
	Variance	Variance	Variance	Variance
	Standard deviation	Standard deviation	Standard deviation	Standard deviation
	Area under the curve	Area under the curve	Area under the curve	Area under the curve
	Total energy	Total energy	Total energy	Total energy
	Entropy	Entropy	Entropy	Entropy
	Peak to peak	Peak to peak	Peak to peak	Peak to peak
	Mean difference	Max frequency	Max frequency	Max frequency
		Median frequency	Median frequency	Median frequency
		Kurtosis		
		Spectral entropy		
ΔHbR	Min value	Min value	Min value	Min value
	Max value	Max value	Max value	Max value
	Mean	Mean	Mean	Mean
	Variance	Variance	Variance	Variance
	Standard deviation	Standard deviation	Standard deviation	Standard deviation
	Area under the curve	Area under the curve	Area under the curve	Area under the curve
	Total energy	Total energy	Total energy	Total energy
	Peak to peak	Peak to peak	Peak to peak	Peak to peak
	kurtosis	Kurtosis	Kurtosis	Kurtosis
	median frequency	Median frequency	Median frequency	Median frequency
		Entropy	Entropy	Entropy
		Spectral entropy	Power bandwidth	Power bandwidth

Figure 4.8: Significant features for binary analysis for each dataset with the dual condition ($p<0.05$ and $H>50$)

In this table, the significant features for each dataset obtained from the binary analysis with the dual condition for the Kruskal-Wallis test are listed. The features previously identified as significant only with the p-value threshold and excluded from the test with the dual condition are highlighted in red.

4.4 Resume of statistical analysis results

In conclusion, it can be stated that 15 out of the 38 features extracted from ΔHbO_2 and ΔHbR allow for binary classification of the two altered states and are common to all four datasets. It was observed that the significant features for both signals ΔHbO_2 and ΔHbR are similar, except for the "peak to peak" feature, which was

found to be significant only for the variation in deoxygenated hemoglobin concentration. Additionally, among these 15 features, none is of a spectral nature.
Another observation is that the imposition of the threshold on the H statistic effectively allowed the selection of features that simultaneously showed very high sensitivity to stress and cognitive load variations. Therefore, they could enable a binary classification between the rest state and the altered state, which could be both stressed and with high Mental Workload (MWL).
Finally, it could be seen that obtaining a greater granularity of results is more difficult.

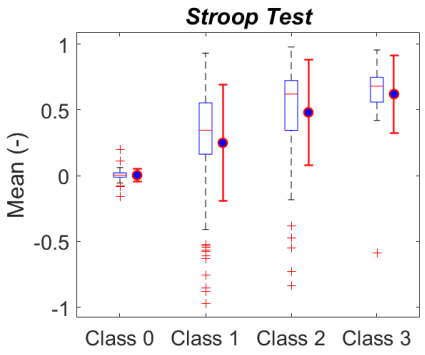

Figure 4.9: Mean feature extracted from the ΔHbO_2 during Stroop Test

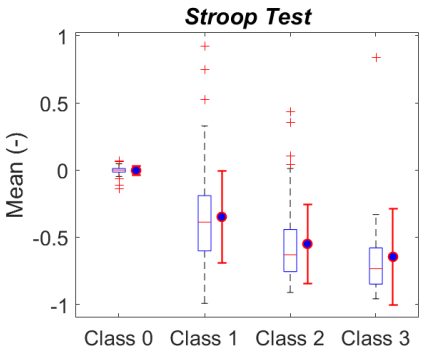

Figure 4.10: Mean feature extracted from the ΔHbR during Stroop Test

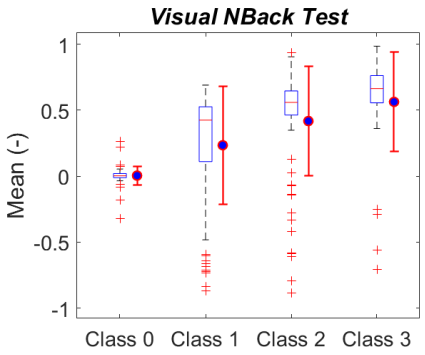

Figure 4.11: Mean feature extracted from the ΔHbO_2 during Visual Nback Test

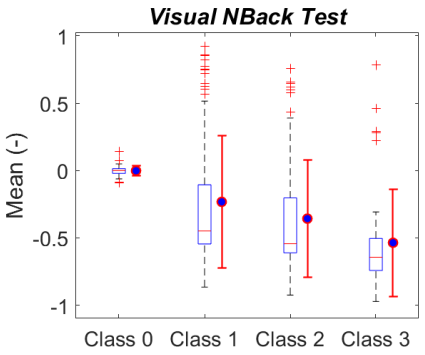

Figure 4.12: Mean feature extracted from the ΔHbR during Visual Nback Test

From the analysis of the trends in the distributions of the significant features in various classes, interesting patterns were observed.
Firstly, for both types of tests, the feature associated with the mean value of both the signal related to the change in concentration of oxygenated hemoglobin and the signal related to the change in concentration of deoxygenated hemoglobin was found to be significant for binary analysis. This significance was identified for all four datasets, and especially for the n-back video dataset, these two features were discriminant in detecting statistically significant differences in all six paired analyses. Indeed, by observing the trends shown in the Figure 4.11 and Figure 4.12, it is

possible to notice, as reported in the literature, an increase in the mean value of the variation in oxygenated hemoglobin concentration during the test, while simultaneously observing a decrease in the mean value of deoxygenated hemoglobin concentration. In both cases, there is a gradual increase or decrease among the various levels of perceived cognitive load/stress, with a more pronounced variation in the transition from a resting state to a state where the subject perceives a certain level of cognitive load. This last observation is also valid for the other three datasets. It was also noted that for both types of signals, the features standard deviation and variance were significant for discriminating a binary condition. As observed from the respective graphs shown in Figure 4.13 and in Figure 4.14, these features highlight a reduction in the variability of fNIRS signals following a cognitive task inducing stress. This reduction is also observable in the datasets related to cognitive load.

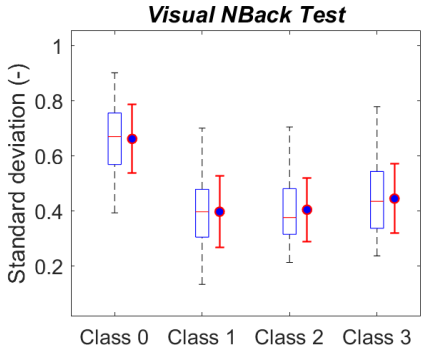

Figure 4.13: Standard deviation feature

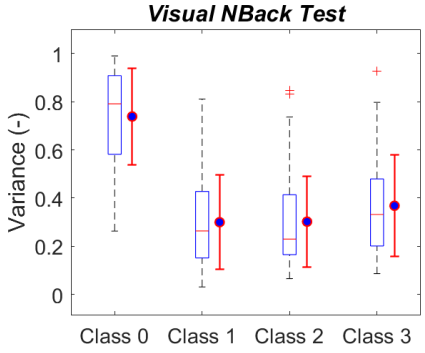

Figure 4.14: Variance feature

Regarding total energy and the area under the curve, a progressive increase has been observed with the increase in the level of stress, highlighting a significant difference in all pairs, in the case of the ΔHbR signal (Figure 4.15 and Figure 4.16). This same observation can be made for ΔHbO_2 only in the case of the Visual Nback dataset, where the different perceived levels of cognitive load are studied. In the other datasets, both of these features are significant for dual analysis, showing an increase from the comparison between class 0, representative of the resting phase, and the other classes.
Finally, the absolute minimum value for both oxygenated and deoxygenated hemoglobin

increases from the resting state to when the subject is performing a cognitive task, while the absolute maximum value decreases.

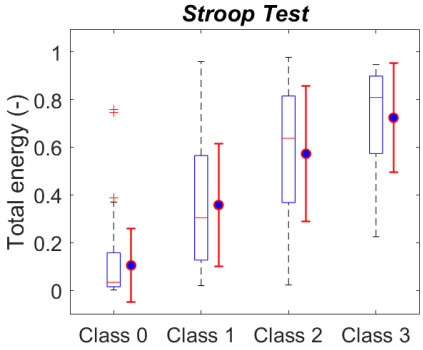

Figure 4.15: Total energy feature extracted from the ΔHbR during Stroop Test

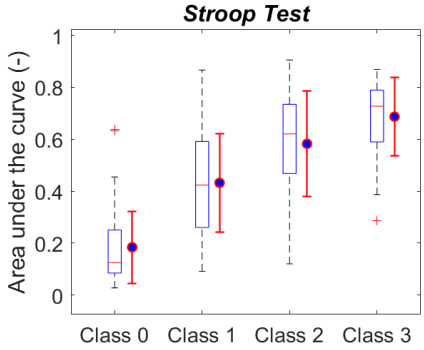

Figure 4.16: Area under the curve feature extracted from the ΔHbR during Stroop Test

In Appendix A, the trends of the distributions of features extracted from the signal associated with the variation in concentration of oxygenated hemoglobin (ΔHbO_2) are reported for each dataset. In Appendix B, those related to the features extracted from the signal associated with the variation in concentration of deoxygenated hemoglobin (ΔHbR) are reported.

Chapter 5

Conclusions

Human-Machine Interaction (HMI) systems involve communication between machines and humans to perform specific functions. It is common for this interaction to generate an increase in stress and cognitive load in the user, which the HMI system must be able to detect, measure, and report in real-time.
In the context of this study, the choice to analyze the fNIRS signal was motivated by its promising potential as an indicator of brain activity, particularly for assessing stress and cognitive load. This decision was driven by the limited number of papers exploring the correlation between the fNIRS signal, stress, and cognitive load. Additionally, the ease of integrating devices that allow the acquisition of the fNIRS signal into Human-Machine Interface (HMI) systems has added an incentive to fully explore and understand the role of this signal under these two cognitive conditions.
This study aimed to investigate the relationship between the fNIRS signal, stress, and cognitive load, reaching all the objectives listed in Section 1.1.
At first, through a state-of-the-art analysis, the most significant fNIRS signal features to evaluate stress and mental workload variations were identified. A total of 19 features were selected, comprising 8 temporal, 7 statistical, and 4 spectral features to be extracted from the two signals (ΔHbO_2 and ΔHbR), resulting in a cumulative total of 38 features.
Subsequently, the design and implementation of tests aimed at detecting variations in stress or in mental workload were undertaken to collect a substantial dataset.
The Biload Test was conducted, divided into two parts: the Stroop test and the n-back test, involving 64 participants. The signals were acquired using the Biosignalsplux sensor during the execution of these cognitive tasks designed to induce stress and cognitive load in the participants.
The acquired data underwent a preprocessing procedure. The followed pipeline, based on studies in the literature that examine the fNIRS signal, involved a series of steps aimed at obtaining the variation in the concentration of oxygenated hemoglobin (ΔHbO_2) and deoxygenated hemoglobin (ΔHbR) from the two signals output by the sensor.
The Biosignalsplux sensor provided two digital signals, one from the infrared wavelength (860 nm) and the other from the red wavelength (660 nm). The first step performed was to convert the digital values of the two outputs into current values using the transfer function provided by the sensor's datasheet.
Subsequently, utilizing the simultaneous acquisition of the ECG signal, it was possible

to set a physiological trigger at the second heartbeat. The identification of the R-wave was performed using the Pan-Tompkins algorithm. This step was included to enable, in a potential future application, accurate temporal alignment and a well-defined start for the acquisition of all signals. After identifying the trigger, the preceding samples were removed.
It was necessary to downsample the signal to 10 Hz using a moving average filter.
The downsampled signals underwent dual-pass filtering using a 15th-order Butterworth low-pass filter with a cutoff frequency of 0.2 Hz. This filter was employed to remove high-frequency artifacts, including cardiac activity, respiration, and 50 Hz interference.
Subsequently, the optical density variations associated with the two wavelengths were calculated, using the mean value of the signal during the resting period as a reference. This step was crucial to applying the Modified Beer-Lambert law, allowing the calculation of changes in the concentration of oxygenated and deoxygenated hemoglobin (ΔHbO_2 and ΔHbR) from optical density variations.
These concentrations are relative to the brain region where the sensor is placed and are influenced by the pathlength factor (DPF), which takes into account the scattering that photons undergo when passing through the brain tissue.
After obtaining the signal associated with the variation in the concentration of oxygenated and deoxygenated hemoglobin, a high-pass Butterworth filter with a cutoff frequency of 0.01 Hz and order 21 was applied. This filter aimed to remove instrumental noise, which appears as a low-frequency drift.
For the 15 phases characterizing the test, the previously identified 19 features were extracted for both signals (ΔHbO_2 and ΔHbR). Out of these 19, five features (mean, total energy, area under the curve, slope, and entropy) were extracted from the signals related to the variation in the concentration of oxygenated and deoxygenated hemoglobin without the application of the high-pass filter. The use of this filter removes the mean value of the signal, and it would not have been meaningful to analyze the trend of such temporal features.
To achieve the last and most important goal, which is to assess the correlation between stress, cognitive load, and features related to the fNIRS signal, a statistical analysis was conducted.
The test is divided into two parts: in the first part, a more in-depth analysis is performed to determine whether there exists a set of features capable of discriminating various levels of stress or perceived cognitive load in the subject; in the second part, a binary analysis is conducted to identify a set of features that can distinguish a condition of stress from a resting state or a situation of cognitive load from a resting state.
To perform this statistical analysis, the features extracted from each participant's signal were divided into four distinct datasets (Stroop, Visual Nback, Auditory Nback, and Dual Nback) and four classes. The classification was made possible thanks to the responses provided by participants in a subjective questionnaire, where they were asked to quantify, on a scale from 1 to 3, the perceived stress or cognitive load in different phases of the test.
Each part of the statistical test is structured on two levels. Initially, for each feature and within each dataset, the Kruskal-Wallis test ($p<0.05$) was performed to identify features that showed a significant variation in the distribution of data in at least

one of the classes. Subsequently, for these identified features, a further analysis was conducted using the Mann-Whitney test. These paired analyses helped determine which class pairs exhibited a significant difference in data distributions. This approach allowed the identification of the most significant features not only for binary classification but also for a more in-depth classification involving different levels of perceived stress or cognitive load.
This test highlighted how 66% of the extracted features allow for a binary classification between the relaxation state and altered state in at least one type of dataset. Instead, 50% of the 38 features extracted allow for this type of classification across all four datasets.
From the analysis of these results, the need to repeat the statistical test emerged, imposing a double condition of significance in the Kruskal-Wallis test, both on the p-value and the H statistic. This approach allowed the identification of a more restrictive and significant subset of features considered important for discriminating between the two cognitive conditions, whether the subject is in a state of stress or cognitive load compared to rest.
Important are the results obtained in the binary classification, where it was observed that the number of features common to the four datasets, which allows discriminating a situation of stress or cognitive load from a state of rest, turns out to be 15, approximately 40% of the extracted features.
From the analysis of the distributions of significant features, it emerged that both the variation in the concentration of oxygenated hemoglobin and in the concentration of deoxygenated hemoglobin show a reduction in variability (reduction in both the variance and standard deviation features) during the transition from a resting state to a state where the subject has perceived stress or cognitive load.
Additionally, an increase in the total energy and area under the curve features was observed for both signals and across all datasets.
Particularly relevant is the result obtained regarding the mean value, which aligns with what is reported in the literature. During a cognitive task, an increased demand for oxygen in the brain regions involved in the task is expected. Indeed, there is an increase in the mean value of oxygenated hemoglobin concentration and, correspondingly, a decrease in the mean value of deoxygenated hemoglobin concentration.
Finally, the overall statistical result, with or without any threshold on the H statistic value, suggests that distinguishing different levels of stress or cognitive load perfectly from the analysis of features extracted from the fNIRS signal is very difficult.

5.1 Future work

In light of the results obtained in this thesis work on the use of the fNIRS signal in the analysis of stress and cognitive load, an important perspective emerges that could revolutionize how these two conditions are recognized and managed.
One could consider integrating the set of significant features of the fNIRS signal with results from other physiological signals that are responsive to these two different conditions. This would allow for a comprehensive and accurate understanding of the dynamics related to stress and cognitive load.
This leads to another important perspective, the possibility of developing an advanced

predictive model capable of discriminating with high accuracy between states of stress and cognitive load compared to a resting state. The use of machine learning algorithms could facilitate a timely and reliable prediction of the subject's cognitive conditions, enabling more sophisticated and personalized monitoring.
One could consider developing a wearable device capable of monitoring and managing stress and cognitive load in real time. To achieve this, the device could utilize only the features from various physiological signals that have demonstrated a significant correlation with the variations in these two conditions.
This represents a fundamental step towards the practical application of these discoveries. These devices, designed for various contexts, from medicine to industry, could provide active support by intervening to maintain users in optimal cognitive conditions.
Ultimately, the broader impact of this research is reflected in the potential to create safer Human-Machine Interface (HMI) systems, with a significant reduction in the risk of hazardous situations. The dynamic adaptation of such systems to users' cognitive conditions, based on the results of this research, could be a crucial element for safety in various critical contexts, from aviation to other industrial sectors.

Appendix A

The boxplot of features extracted from the ΔHbO_2 signal

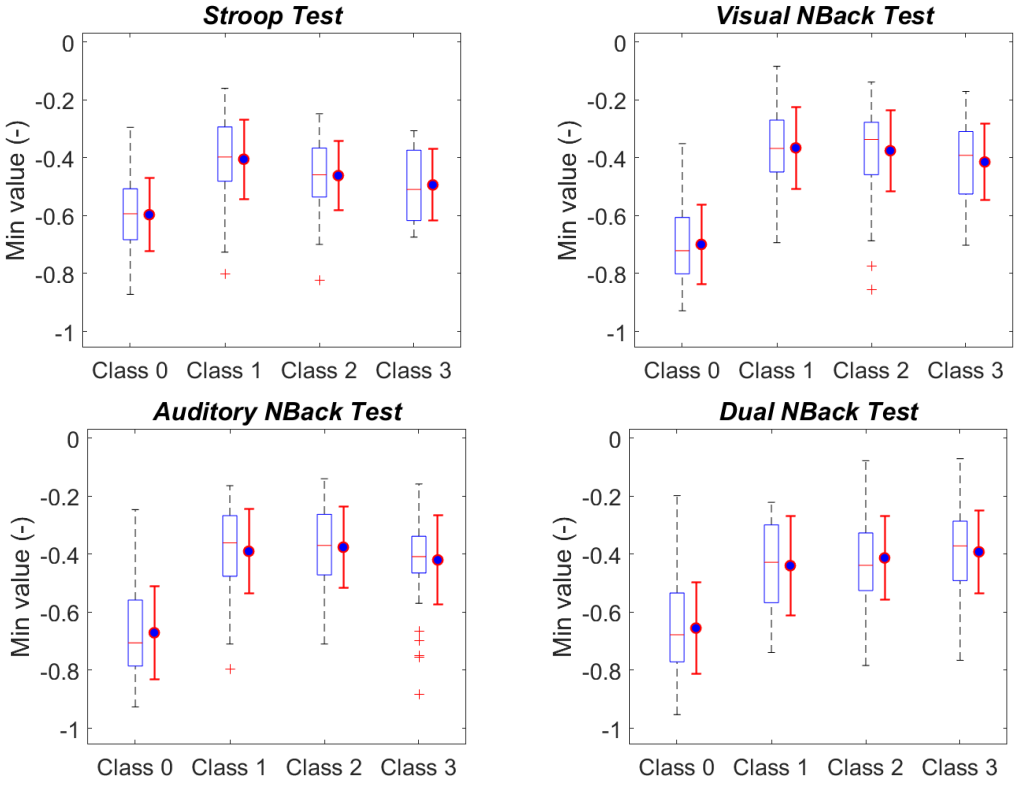

Figure A.1: Min value feature

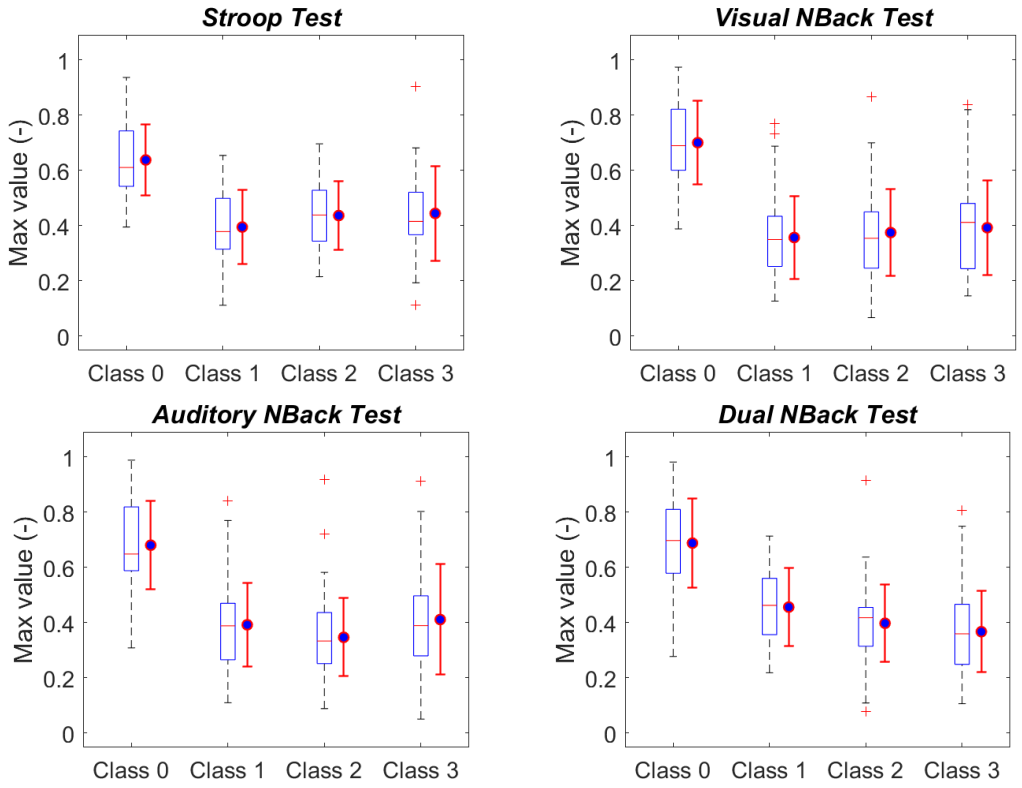

Figure A.2: Max value feature

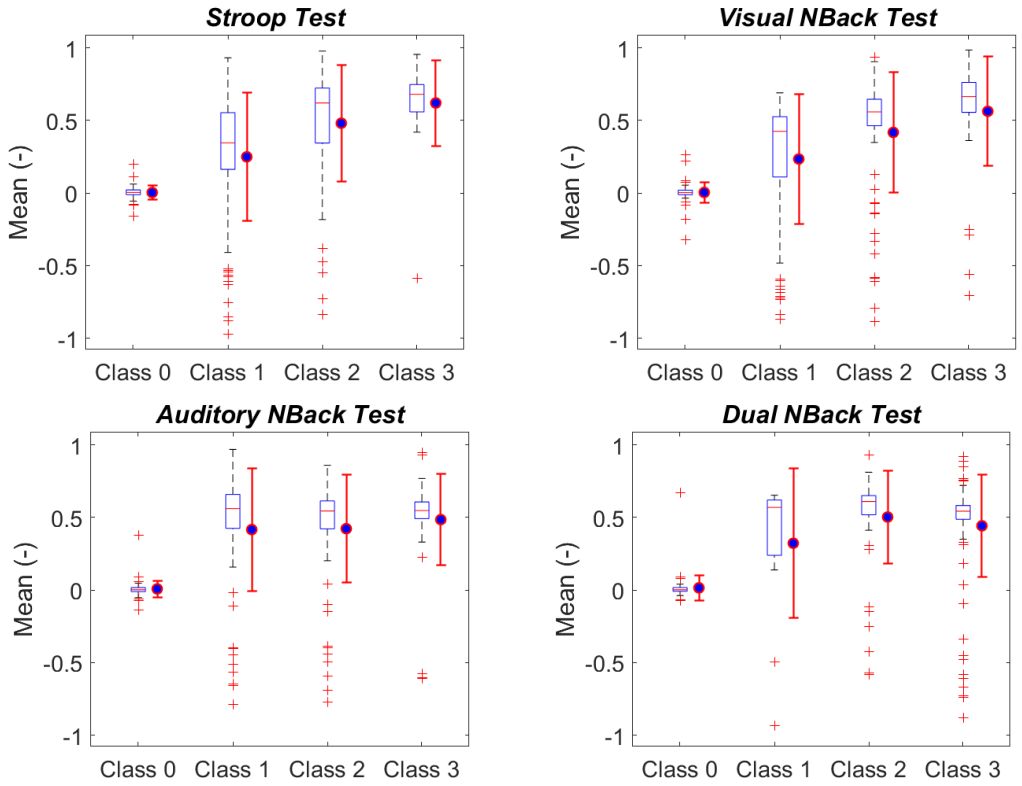

Figure A.3: Mean value feature

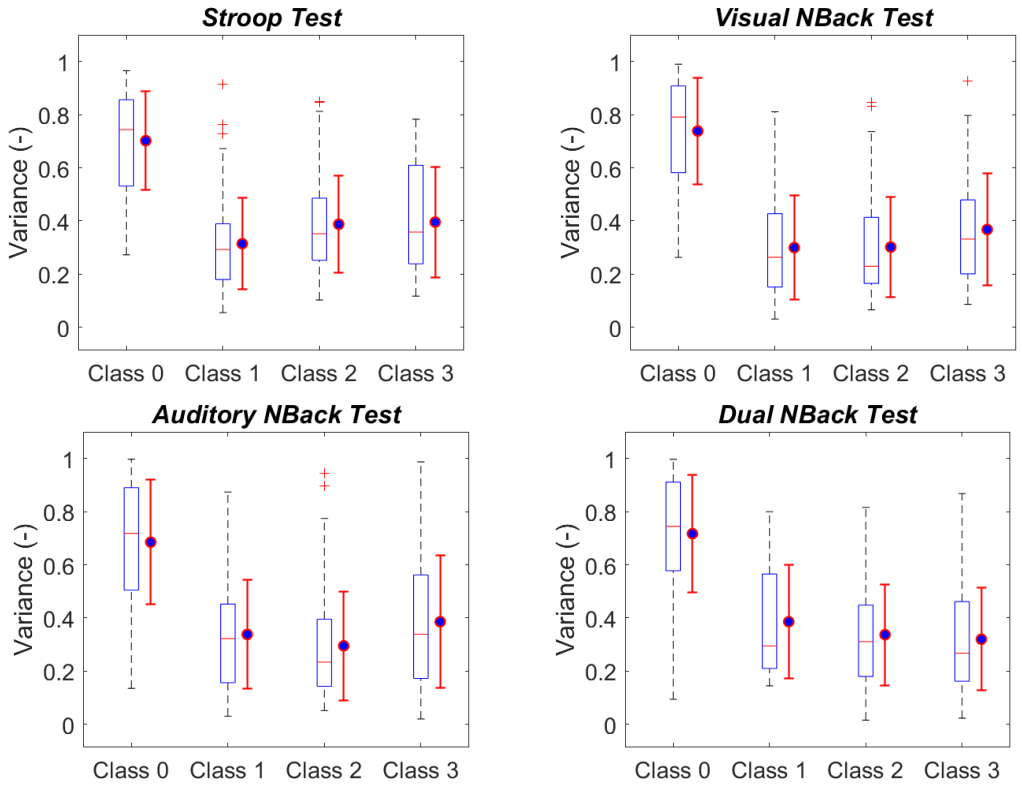

Figure A.4: Variance feature

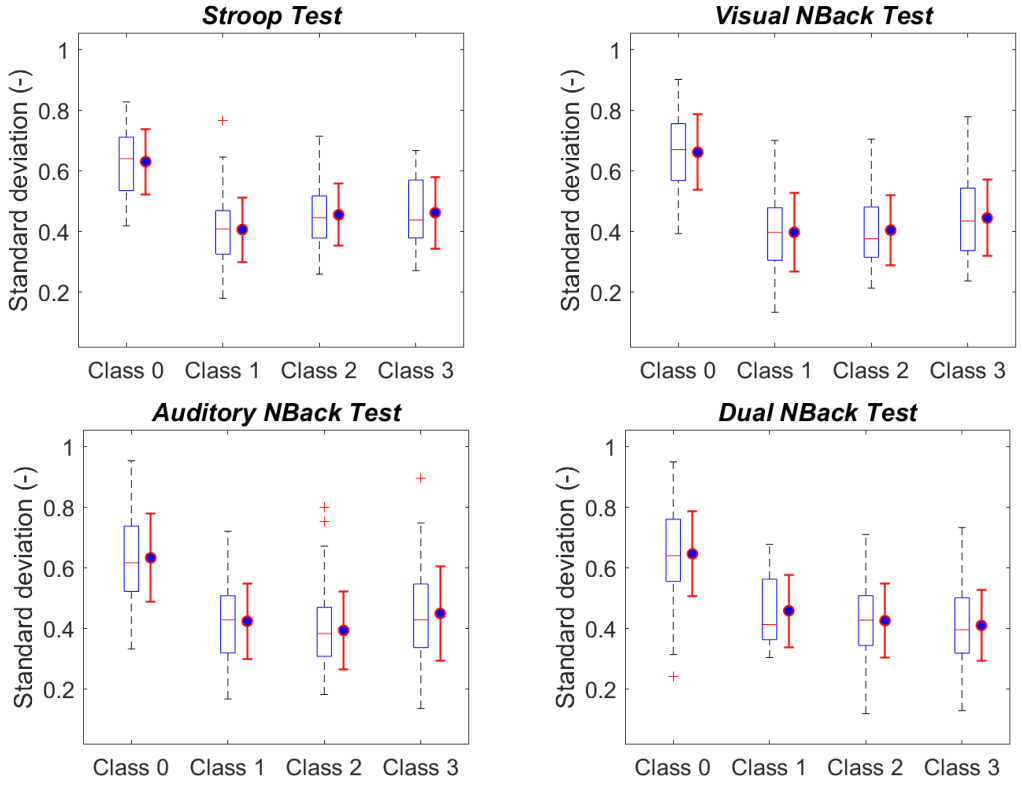

Figure A.5: Standard deviation feature

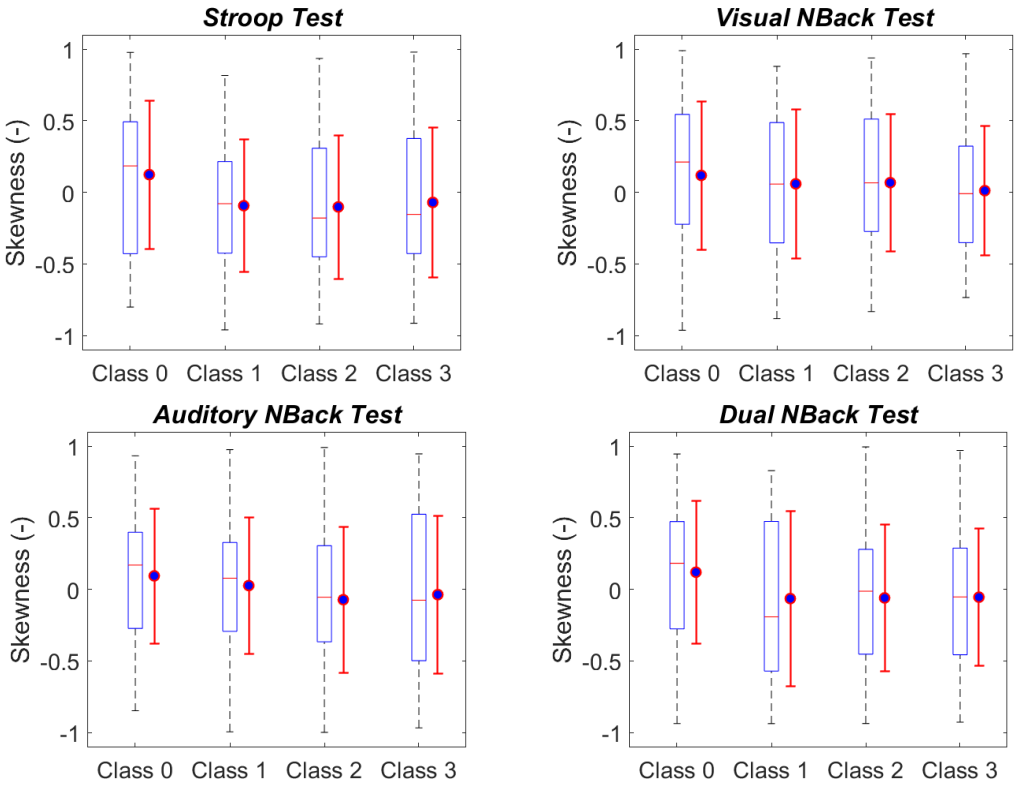

Figure A.6: Skewness feature

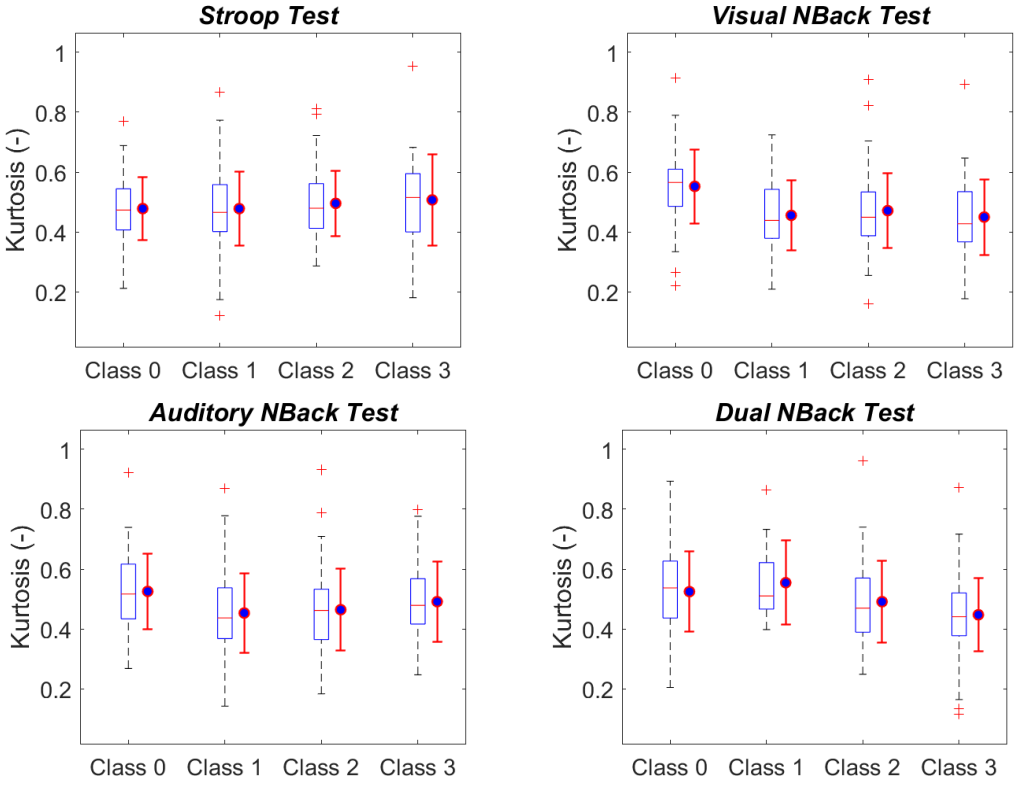

Figure A.7: Kurtosis feature

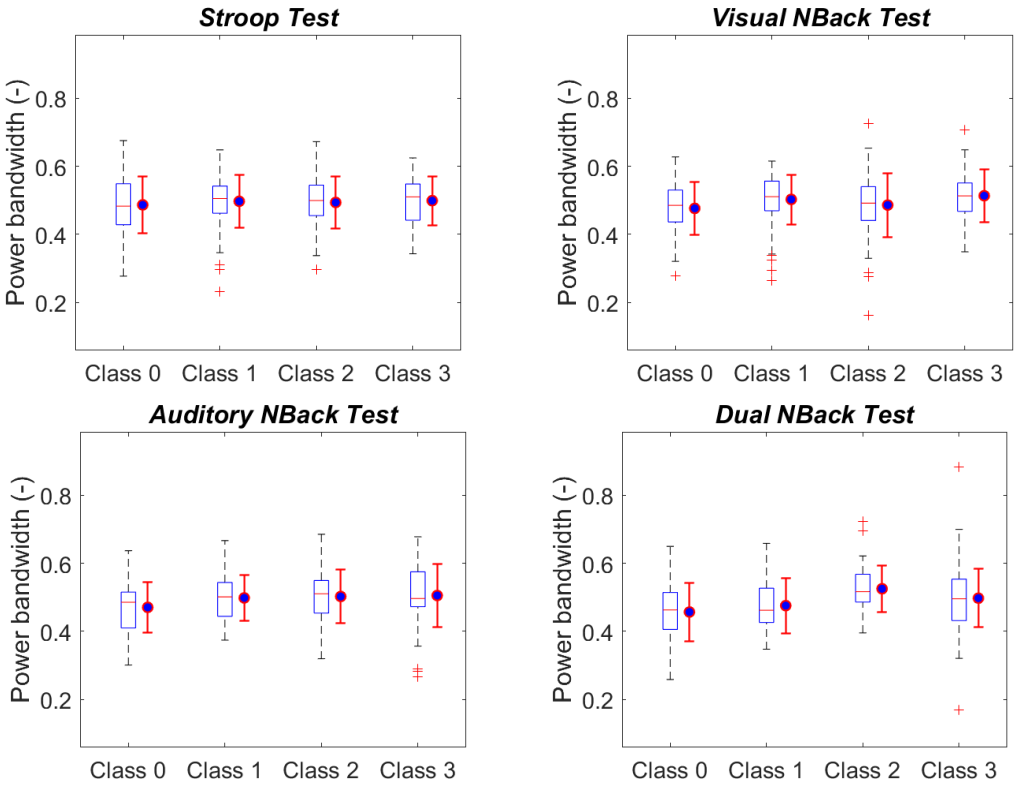

Figure A.8: Power bandwidth feature

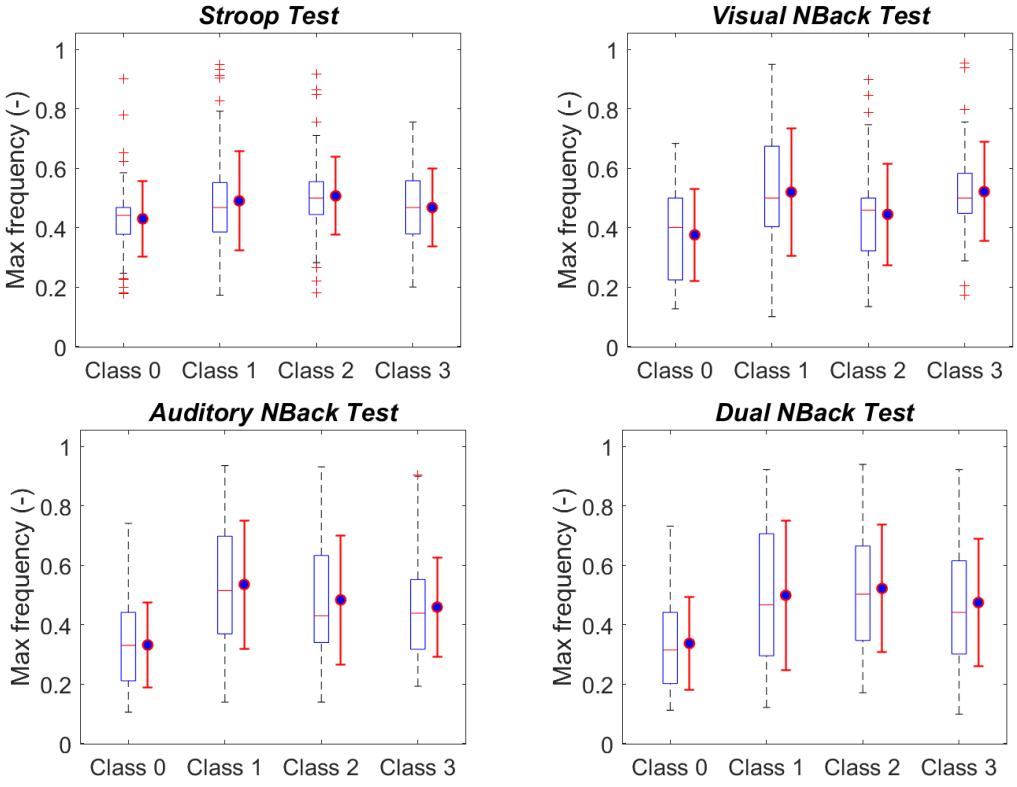

Figure A.9: Max frequency feature

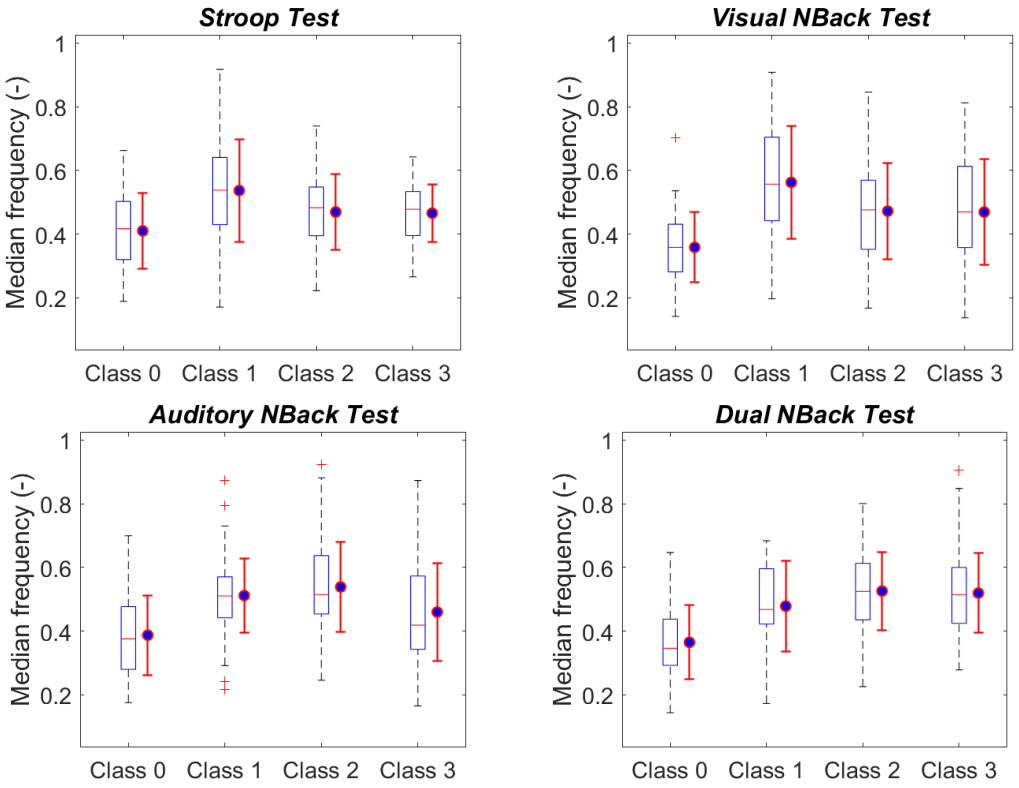

Figure A.10: Median frequency feature

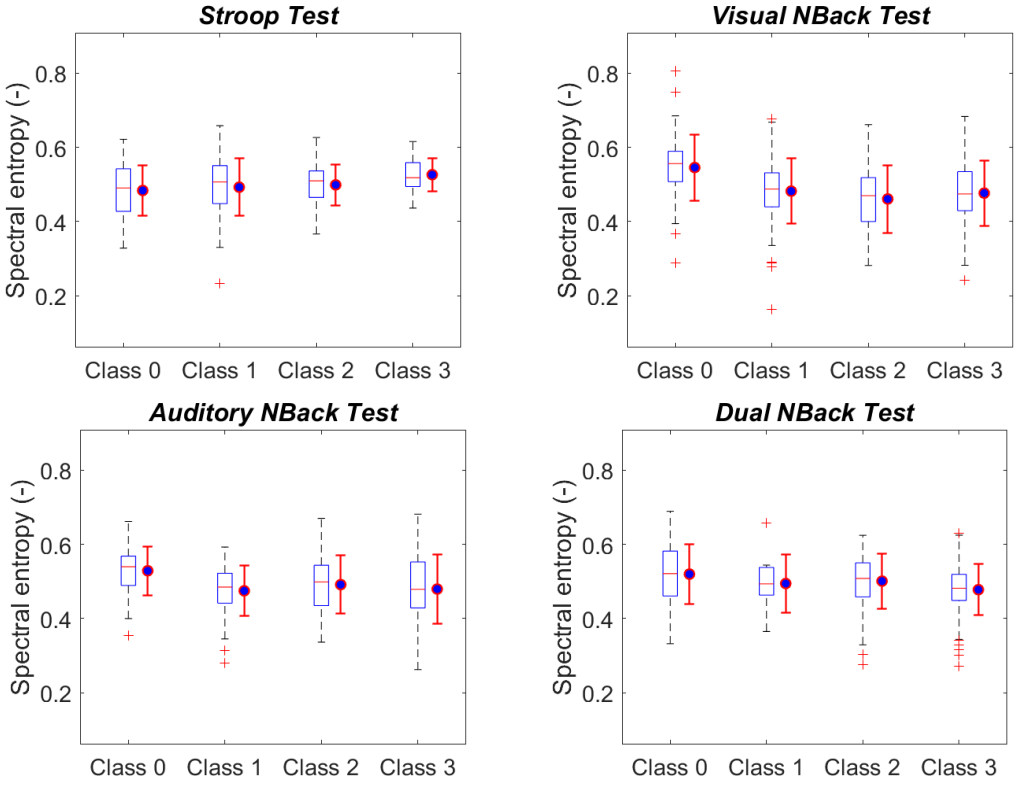

Figure A.11: Spectral entropy feature

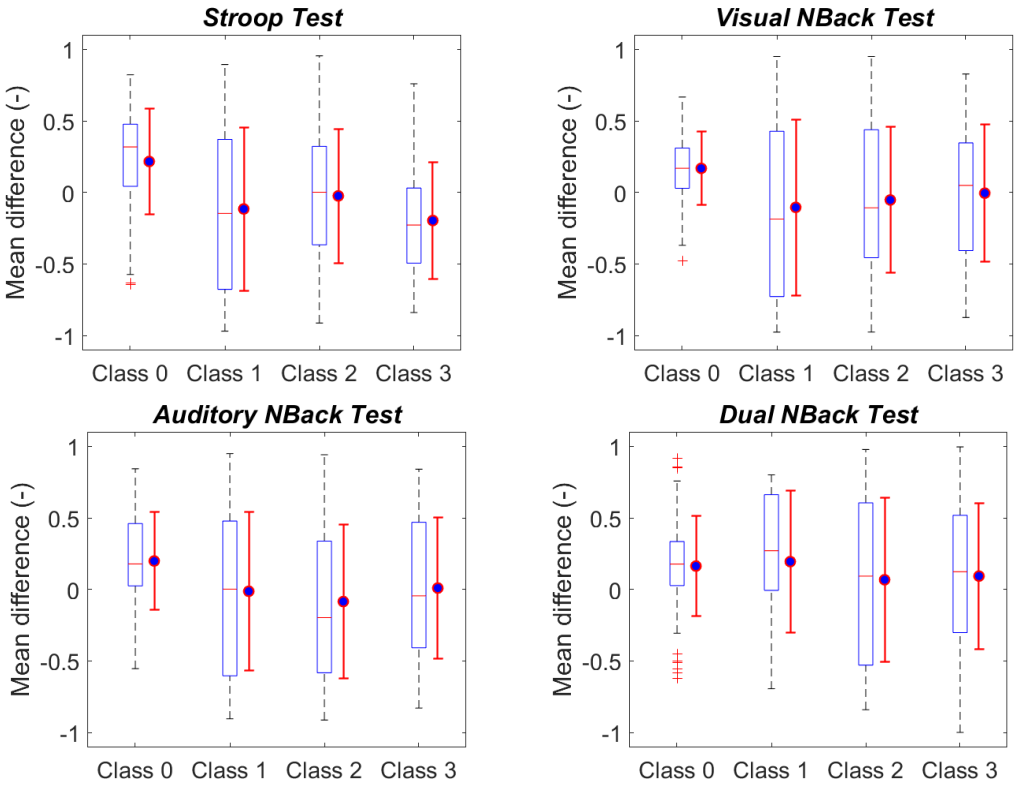

Figure A.12: Mean difference feature

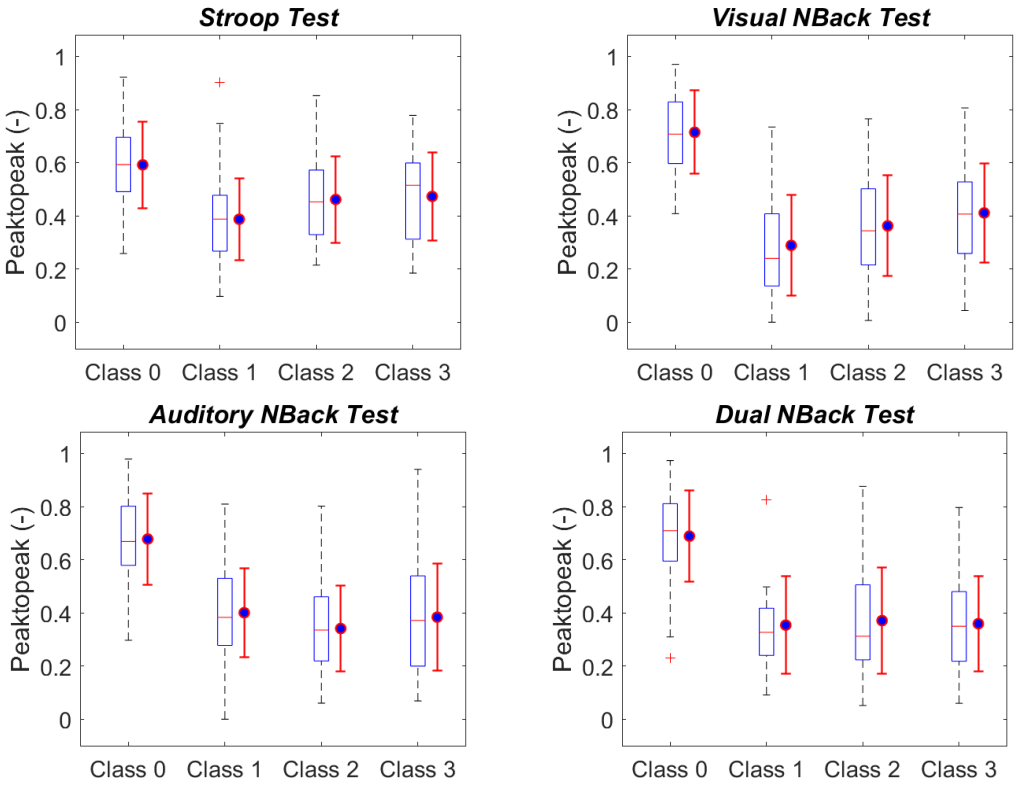

Figure A.13: Peak to Peak feature

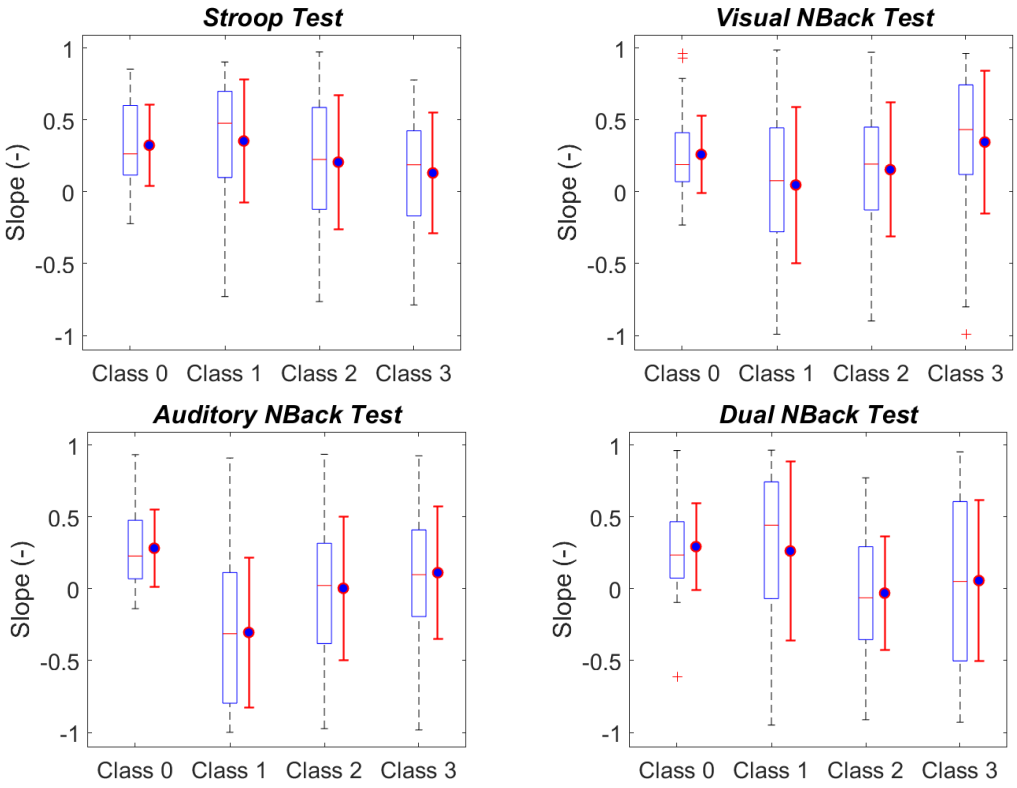

Figure A.14: Slope feature

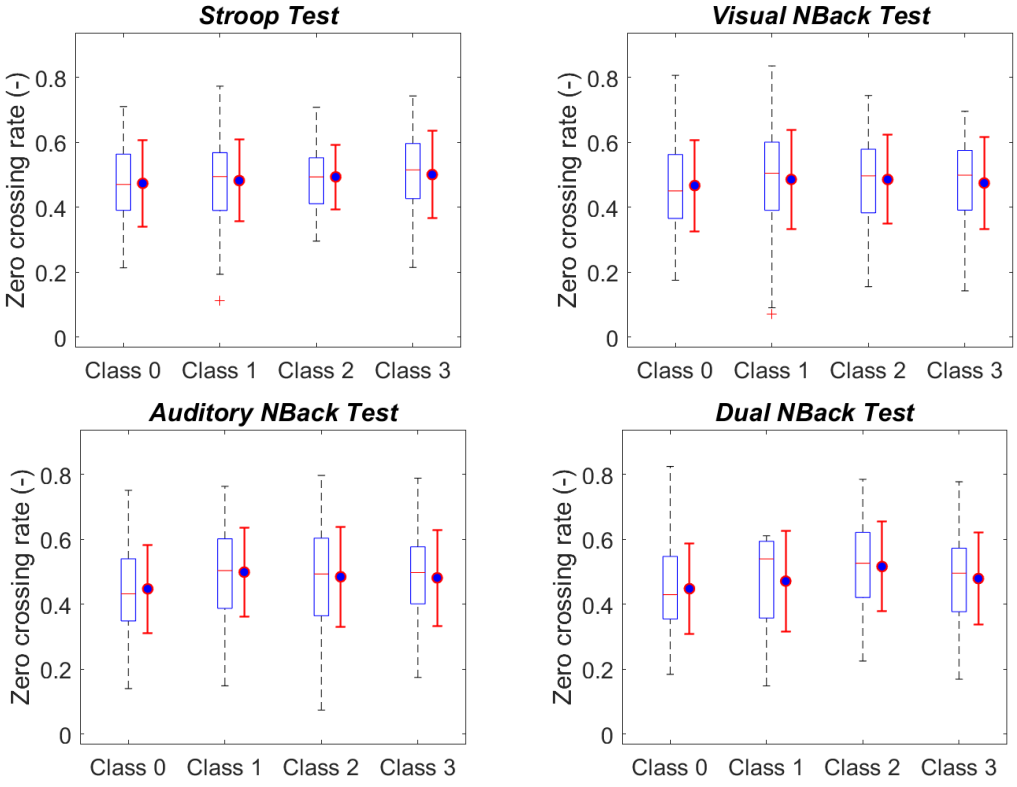

Figure A.15: Zero crossing rate feature

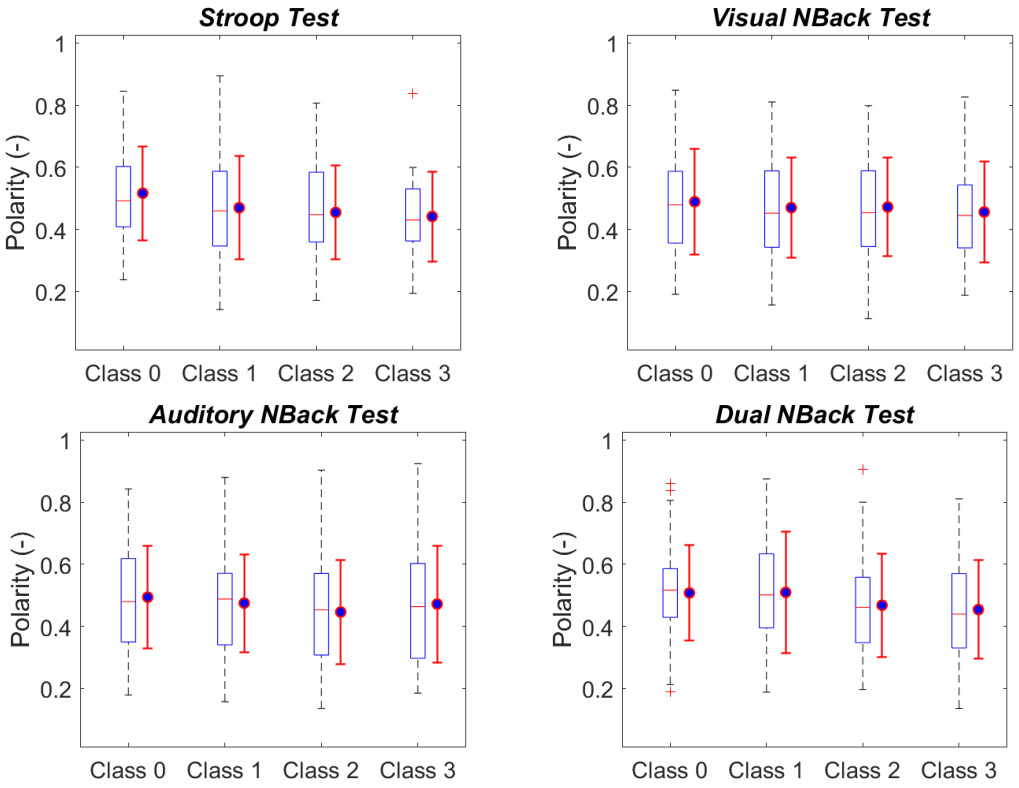

Figure A.16: Polarity feature

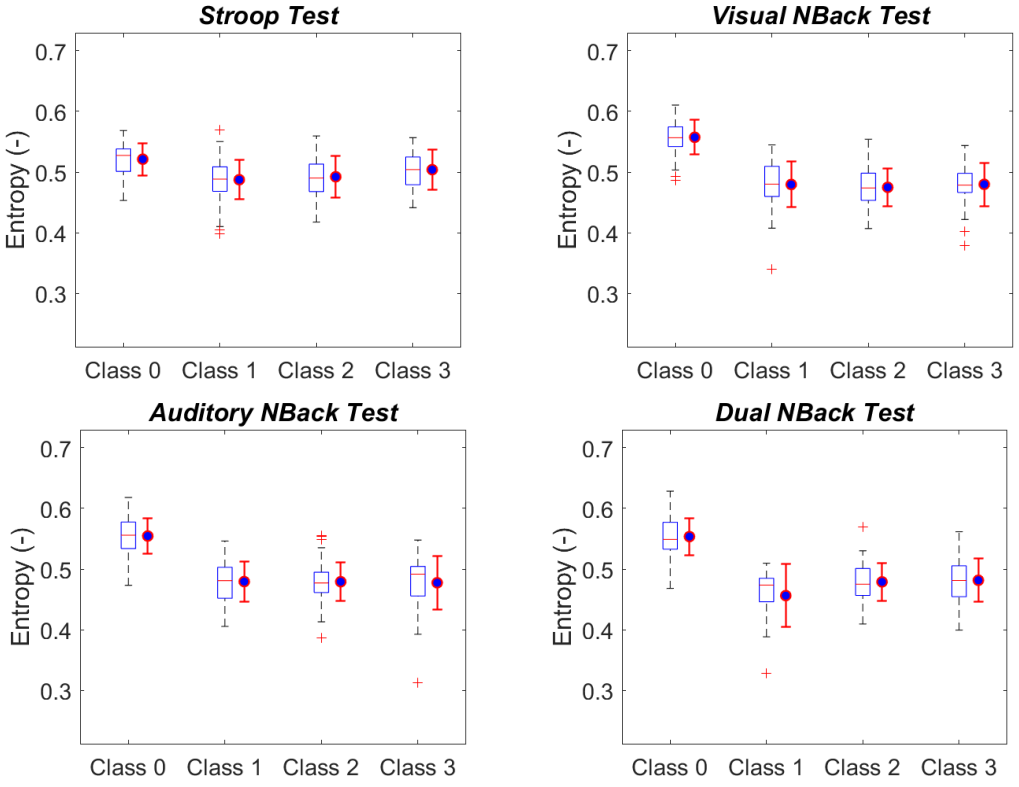

Figure A.17: Entropy feature

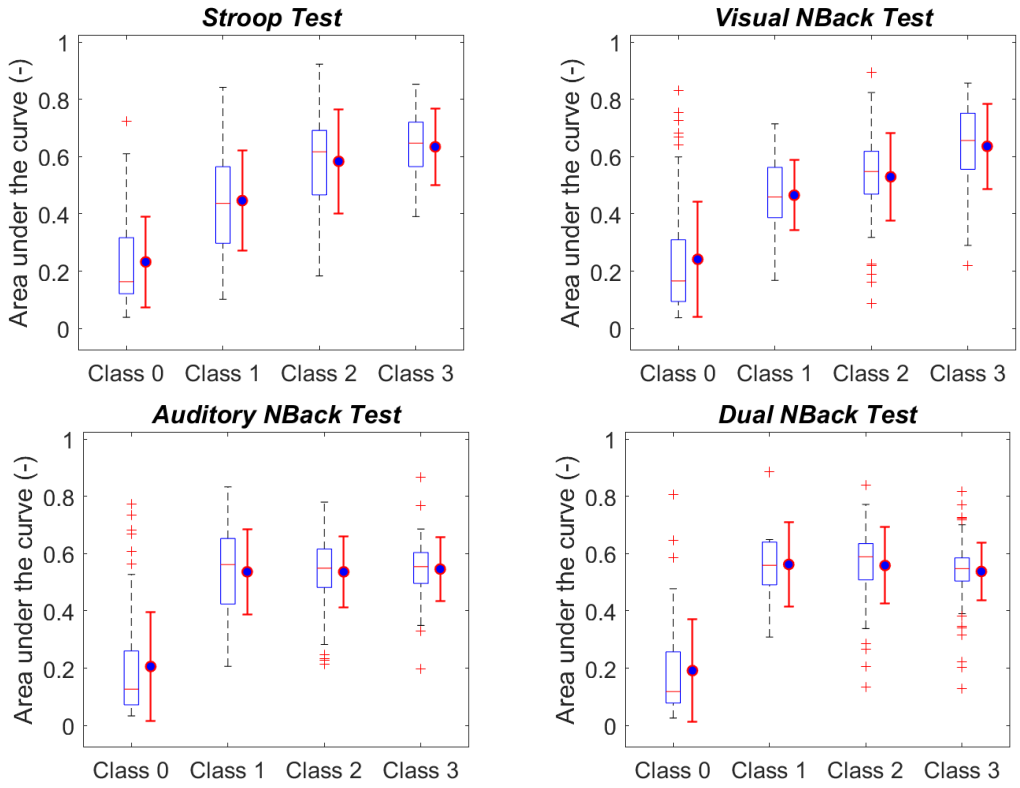

Figure A.18: Area under the curve feature

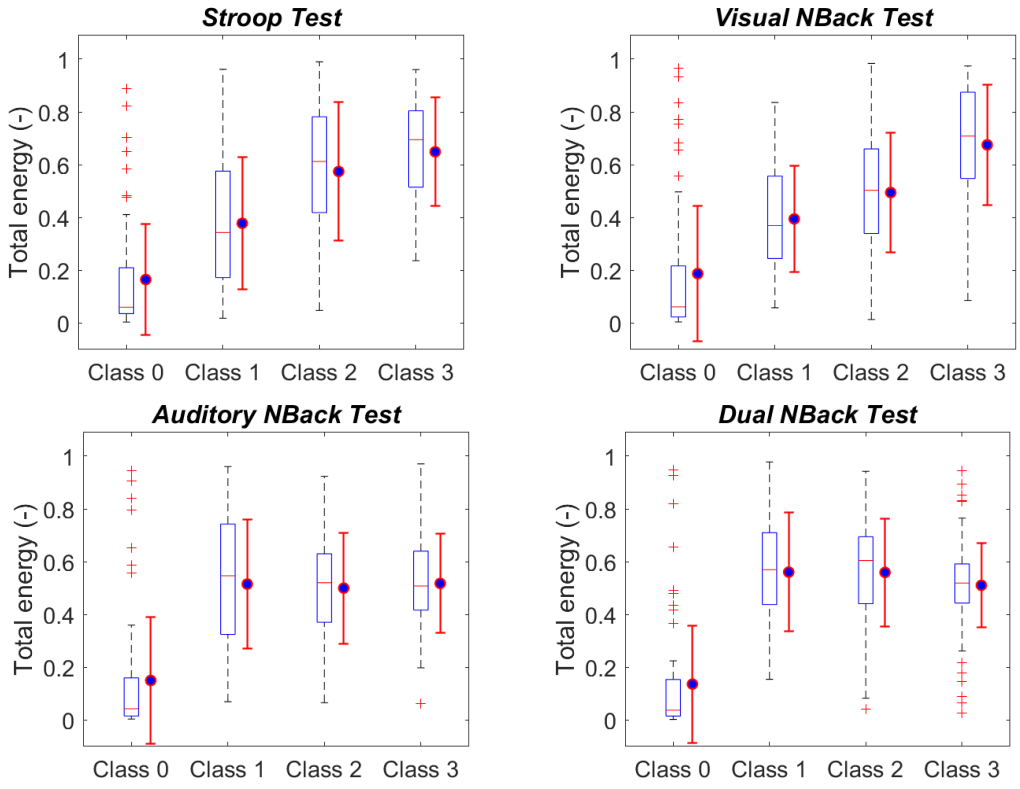

Figure A.19: Total energy feature

Appendix B

The boxplot of features extracted from the ΔHbR signal

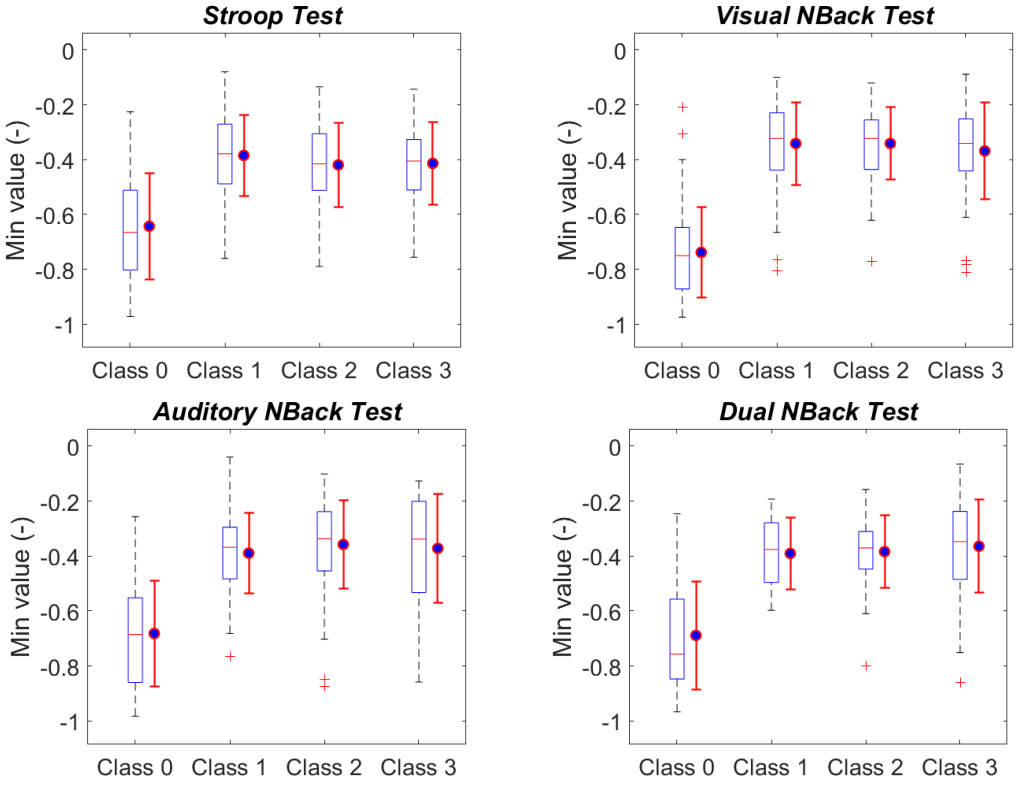

Figure B.1: Min value feature

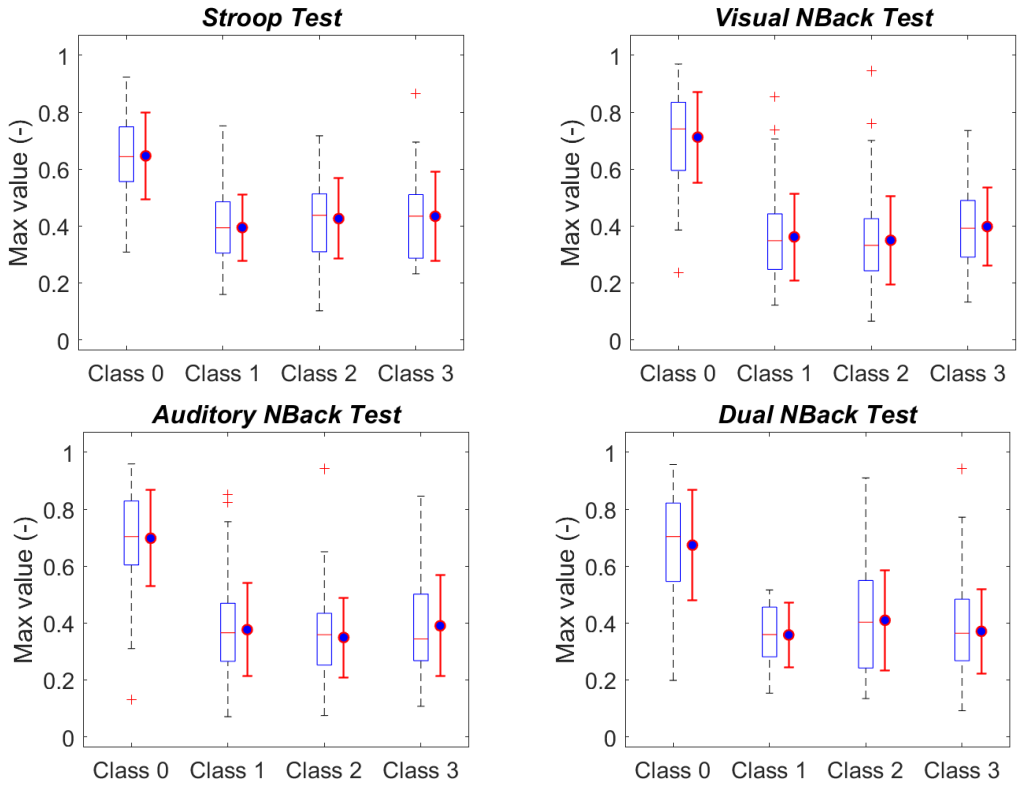

Figure B.2: Max value feature

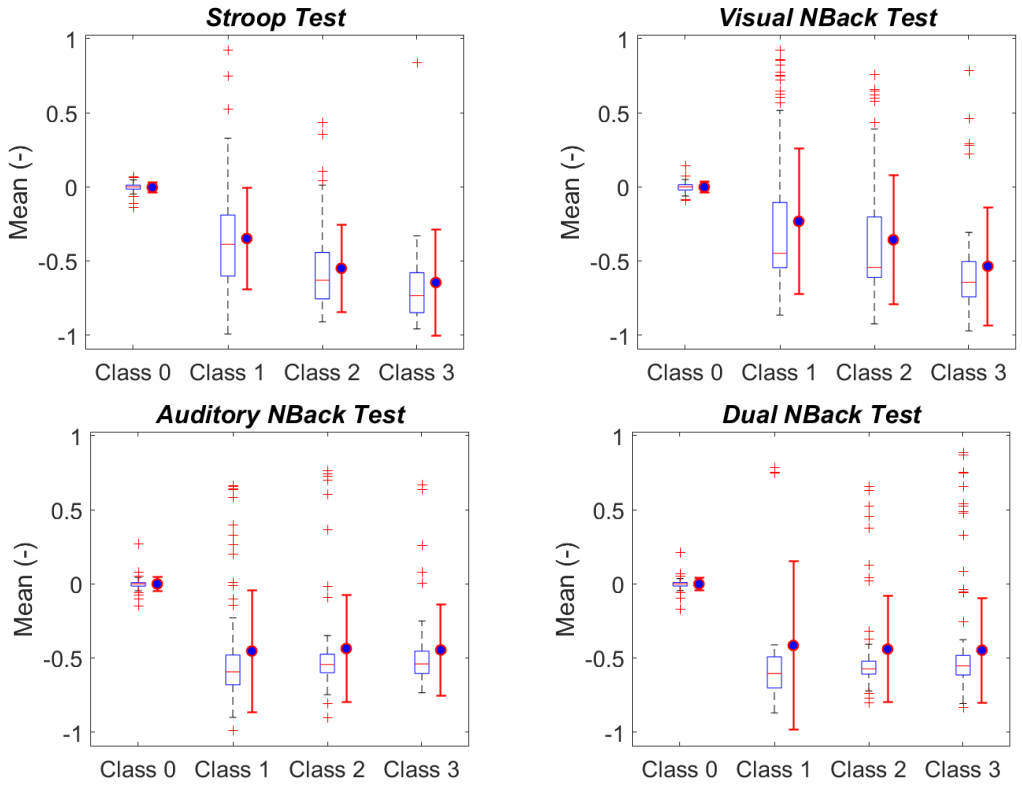

Figure B.3: Mean feature

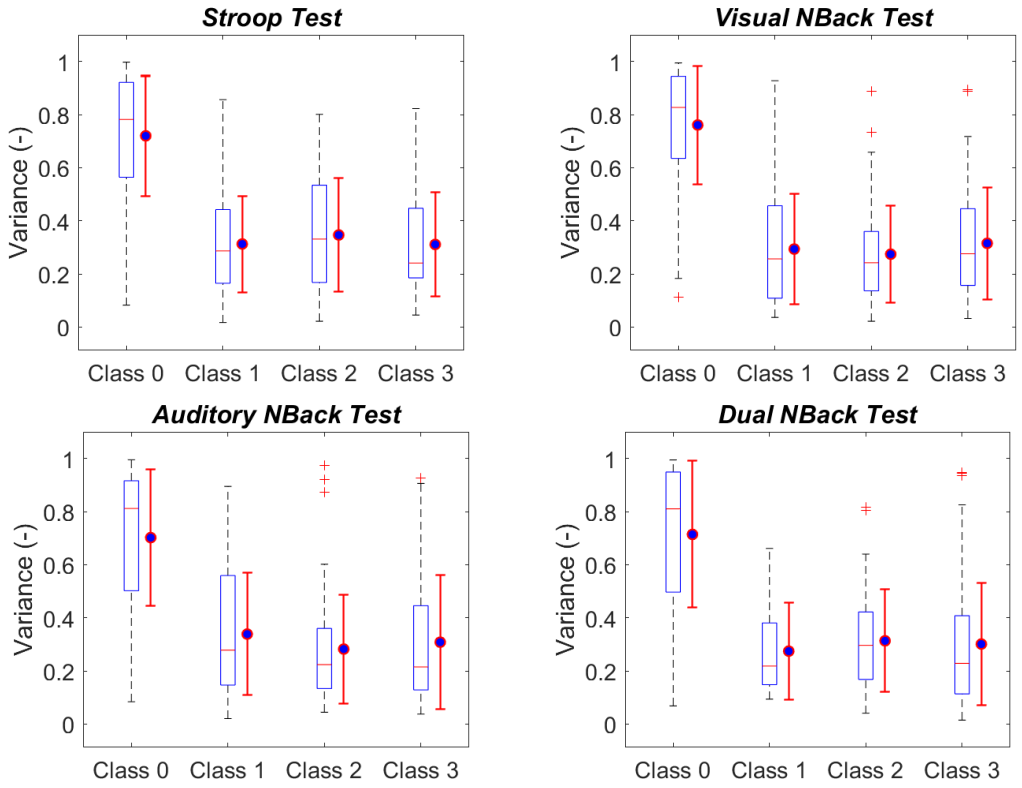

Figure B.4: Variance feature

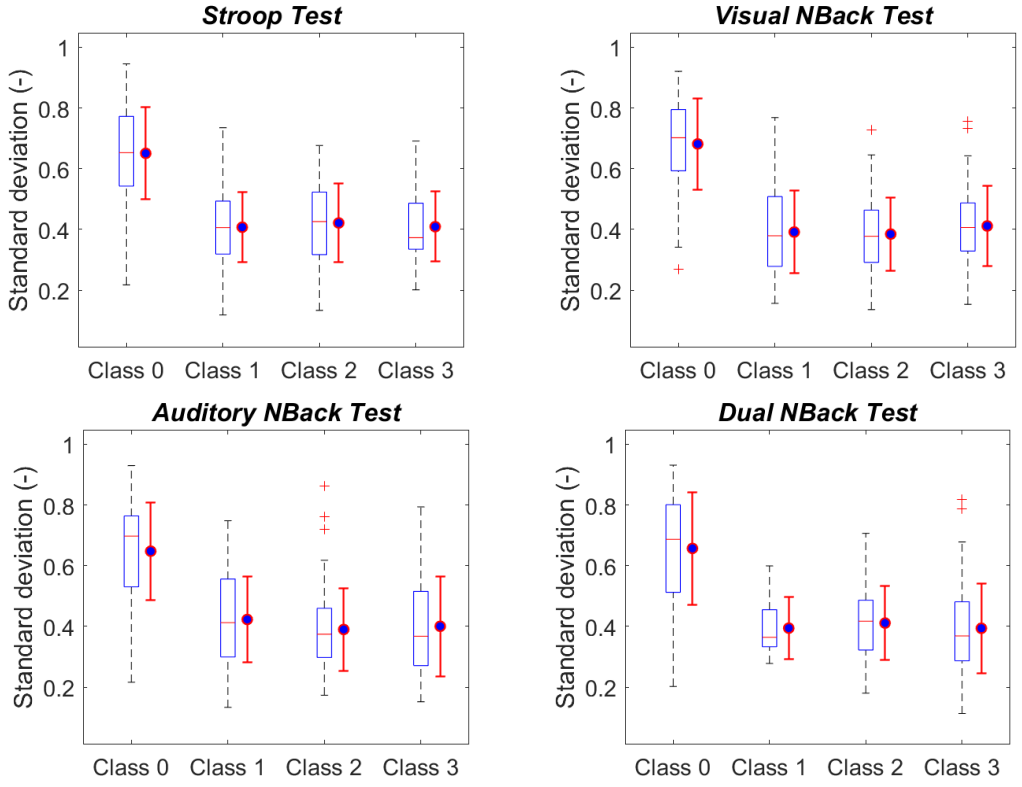

Figure B.5: Standard deviation feature

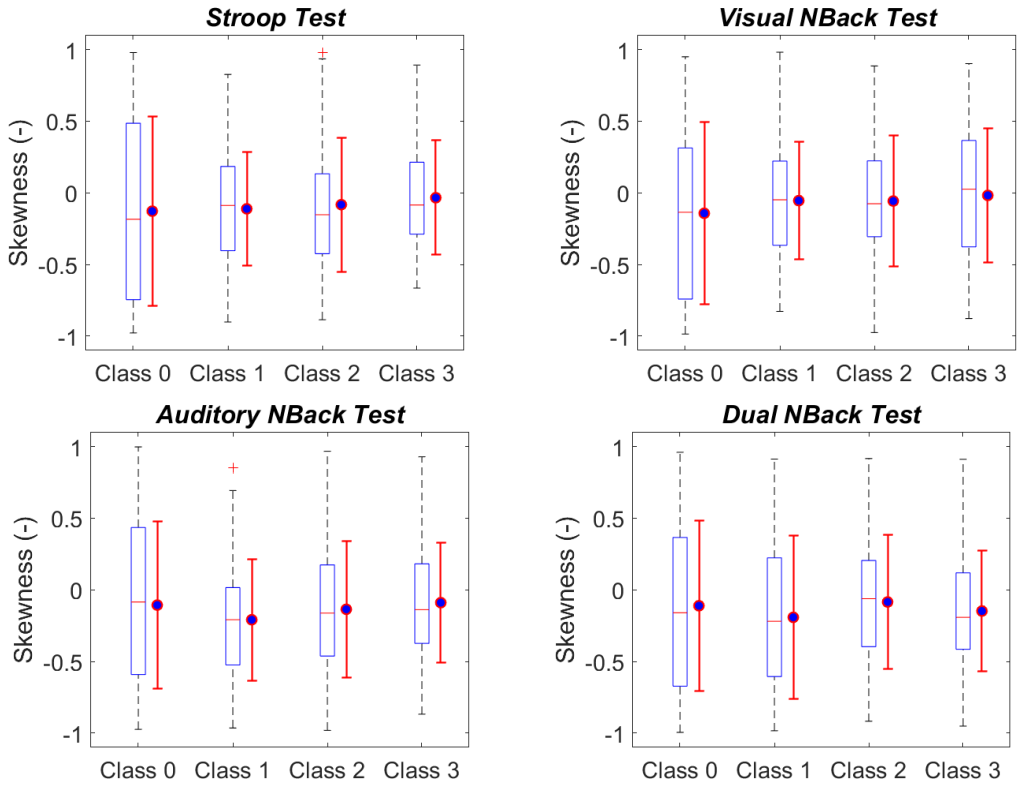

Figure B.6: Skewness feature

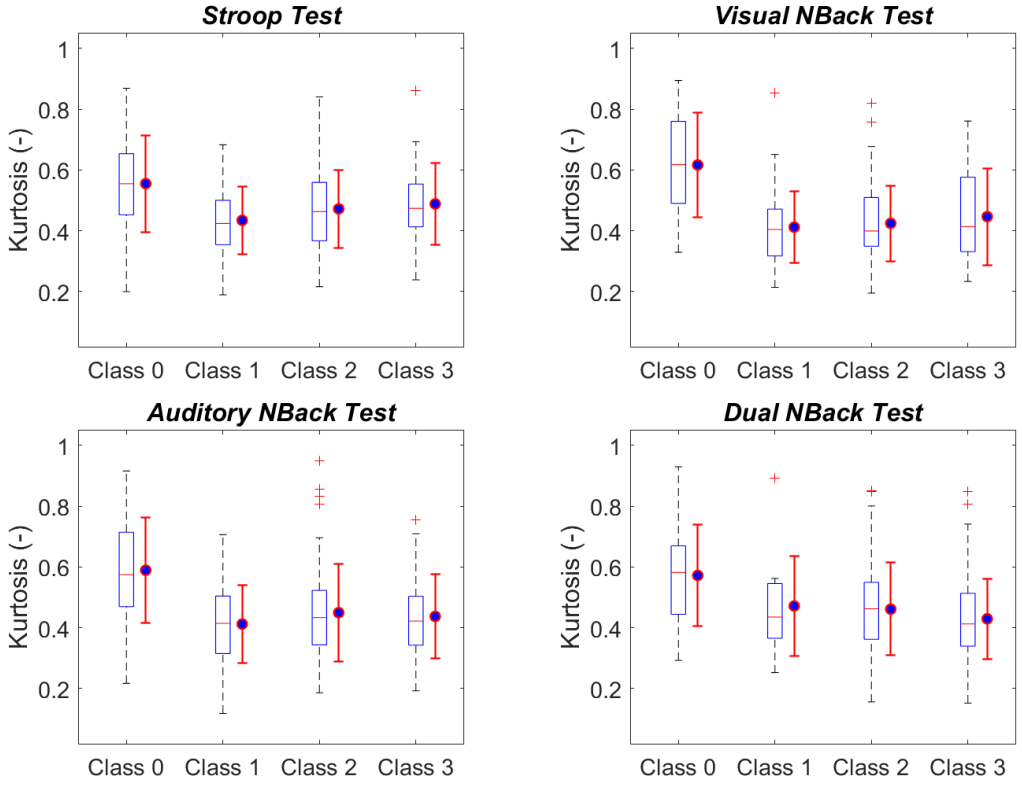

Figure B.7: Kurtosis feature

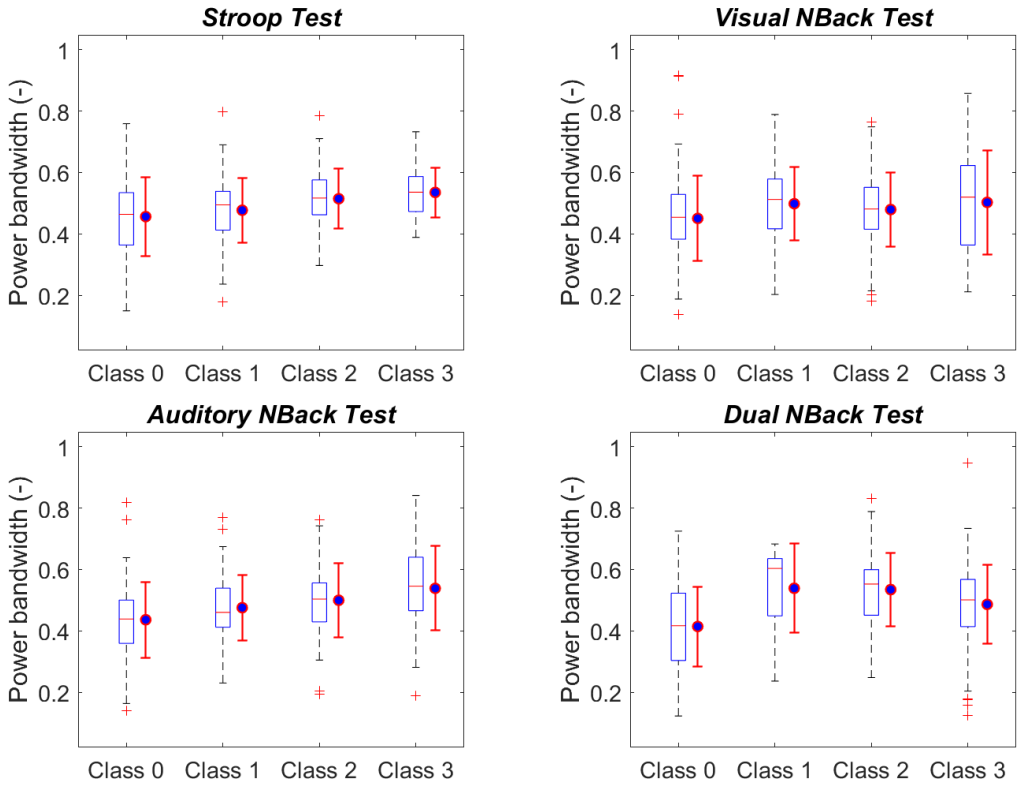

Figure B.8: Power bandwidth feature

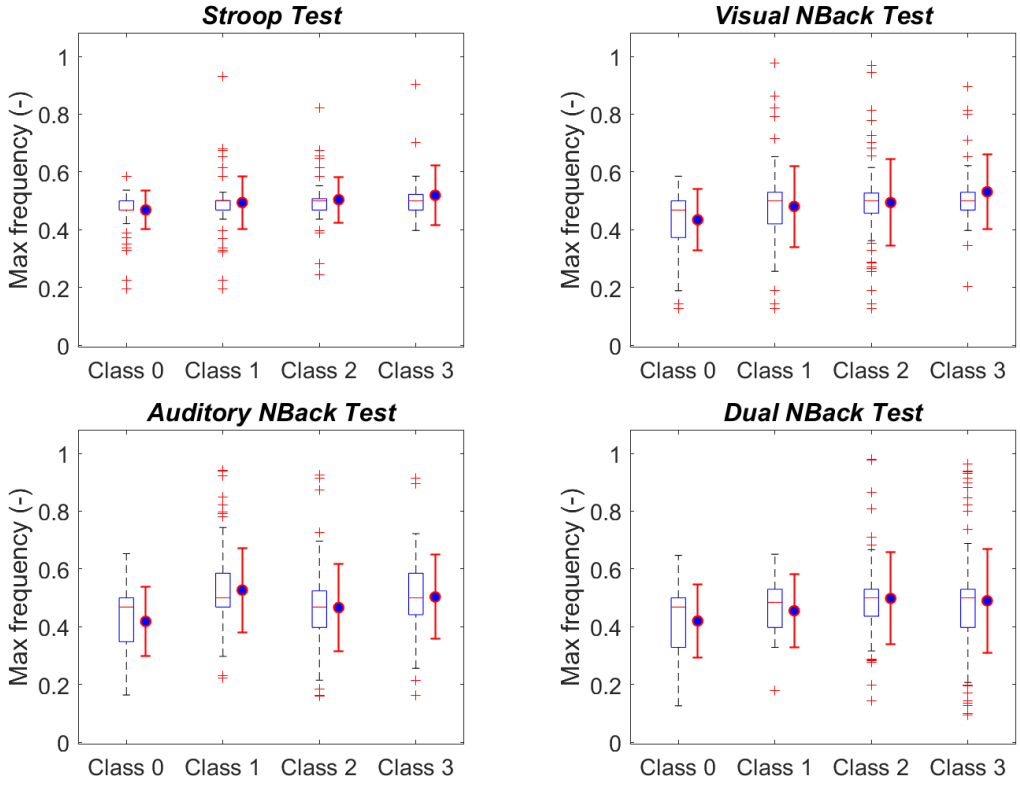

Figure B.9: Max frequency feature

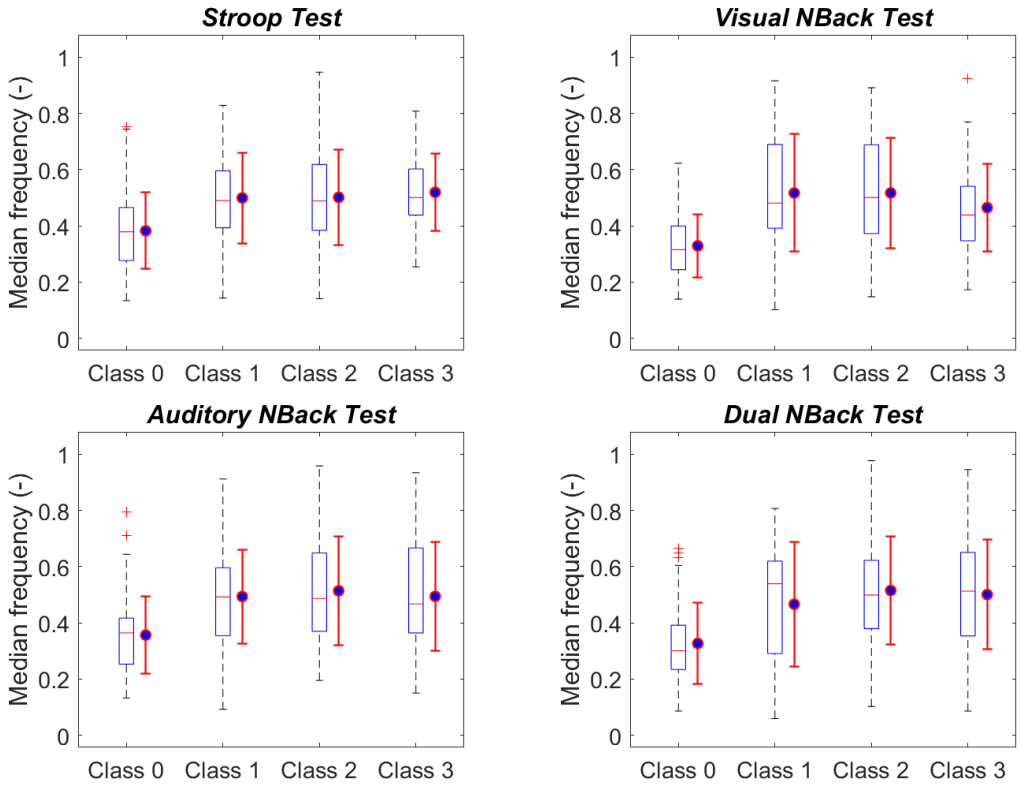

Figure B.10: Median frequency feature

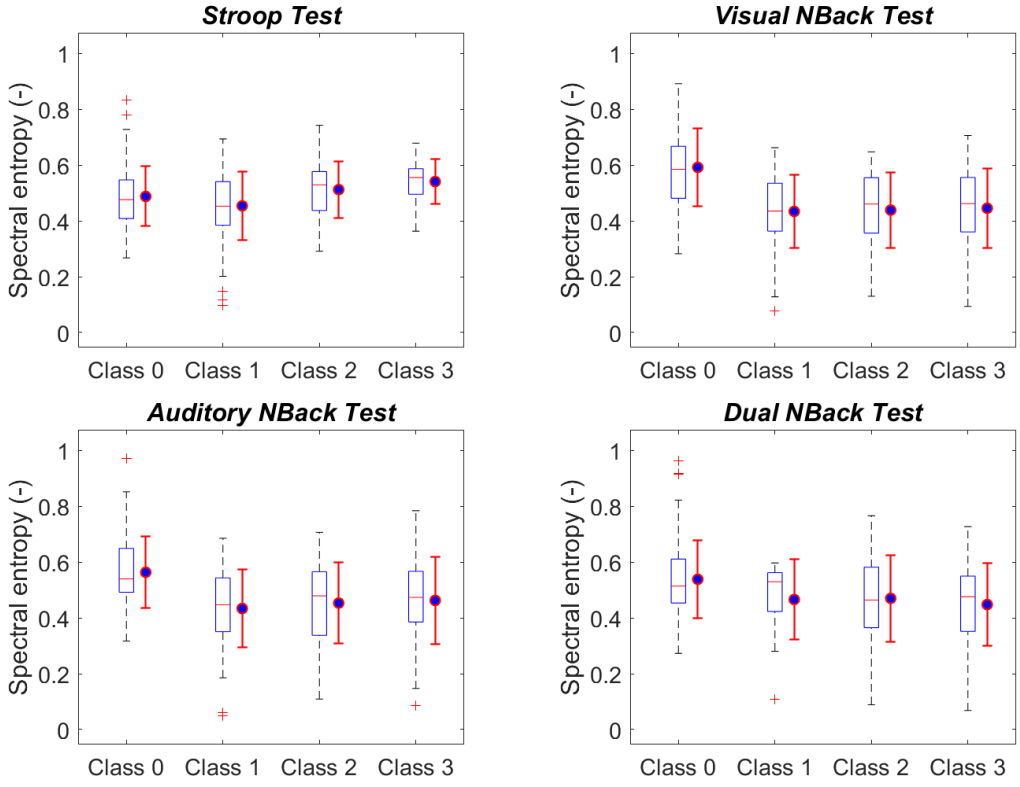

Figure B.11: Spectral entropy feature

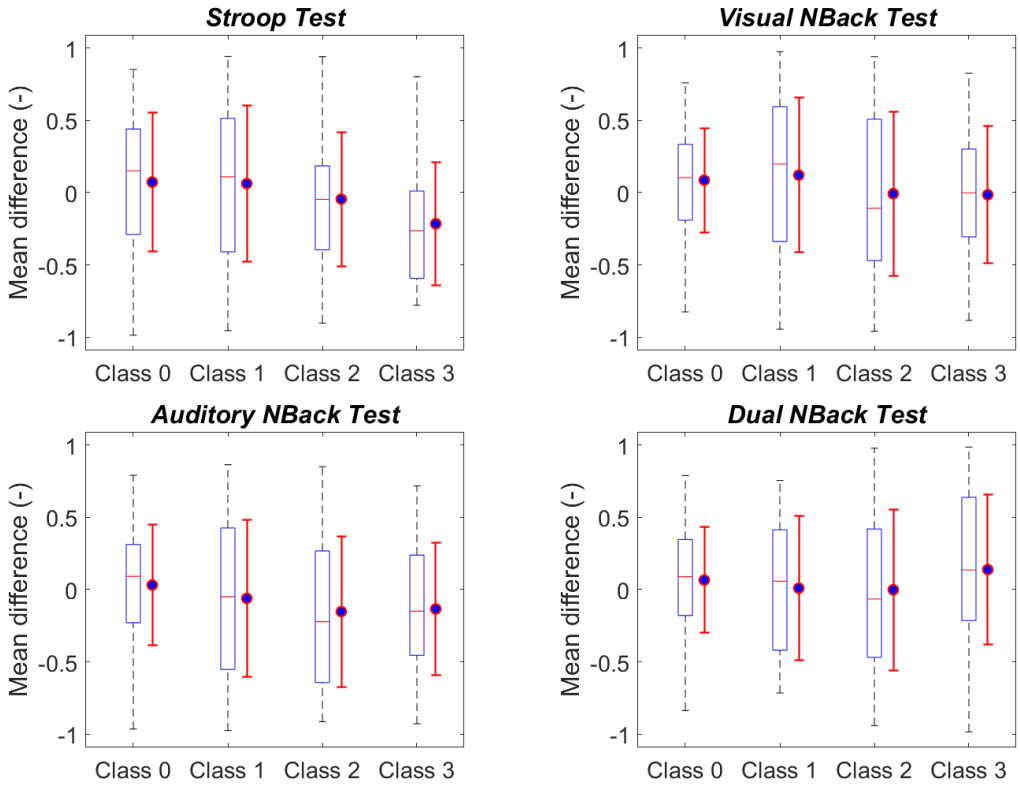

Figure B.12: Mean difference feature

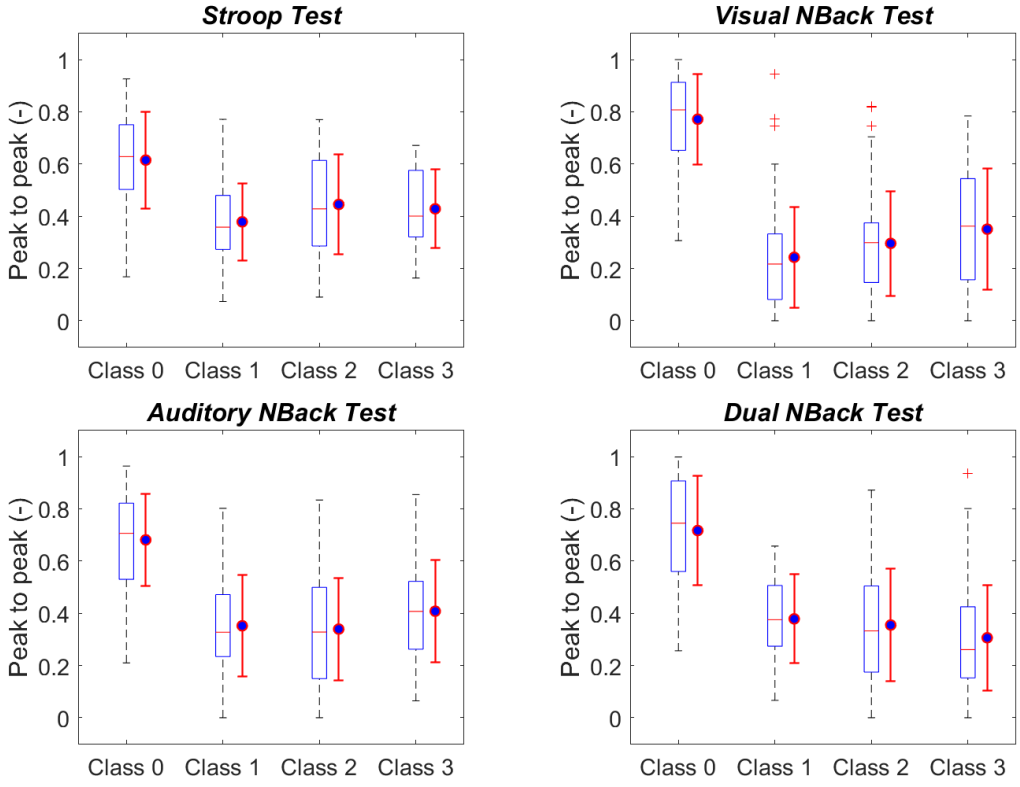

Figure B.13: Peak to peak feature

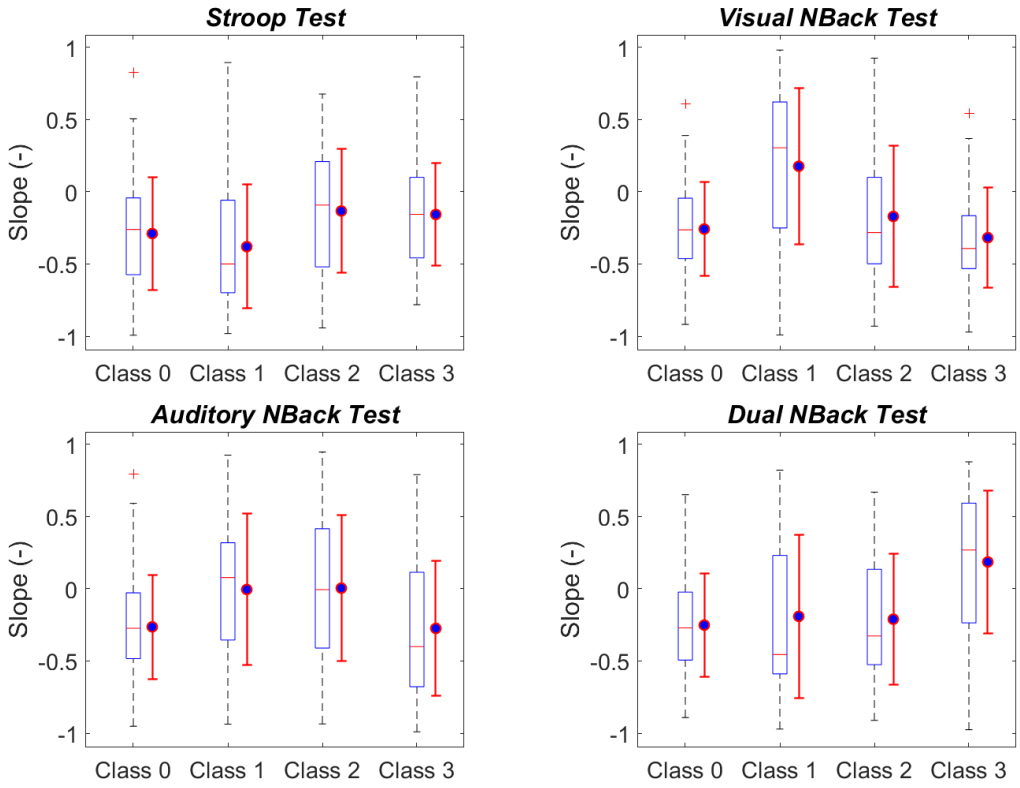

Figure B.14: Slope feature

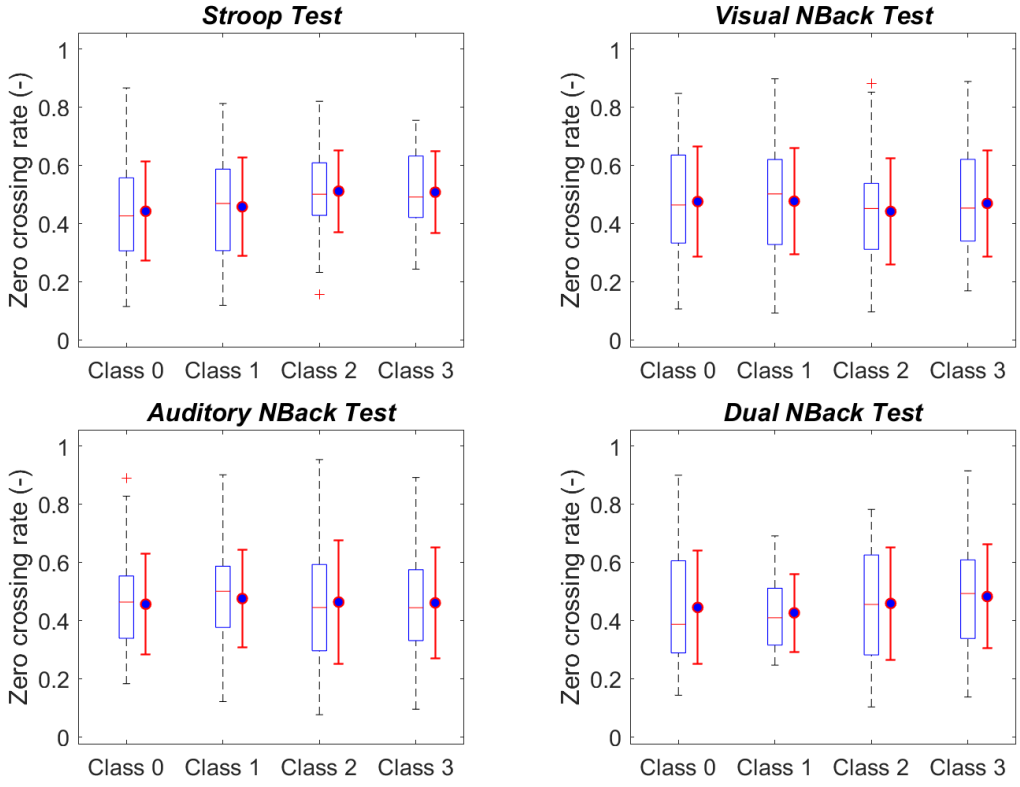

Figure B.15: Zero crossing rate feature

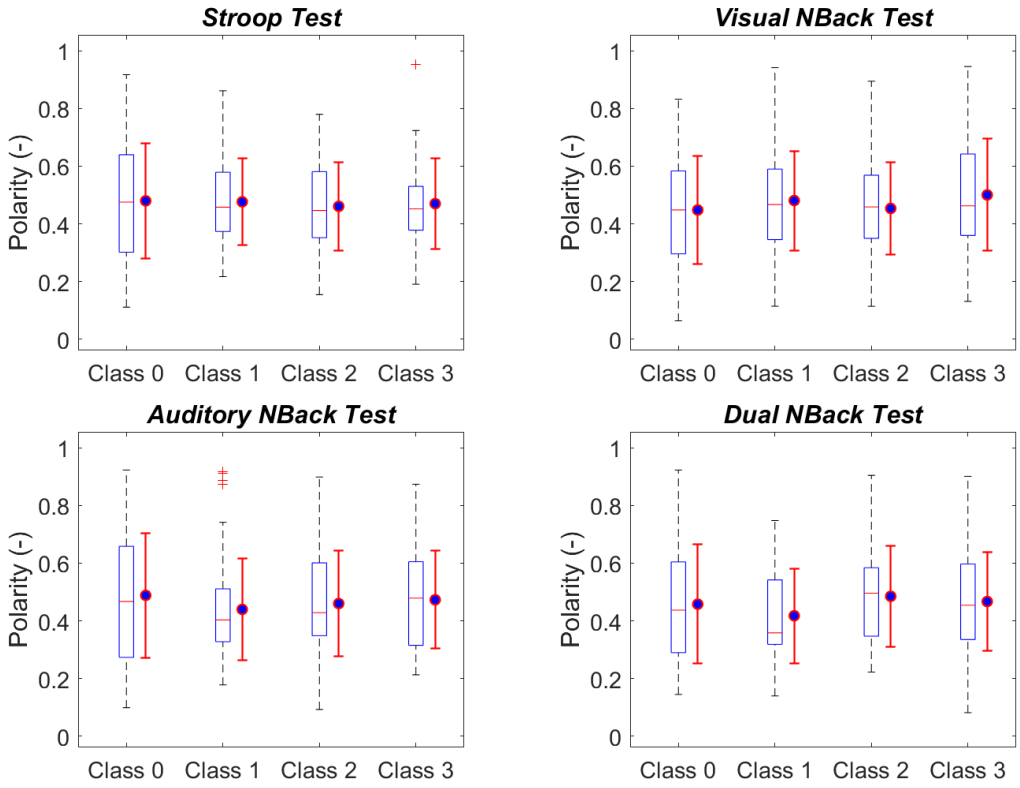

Figure B.16: Polarity feature

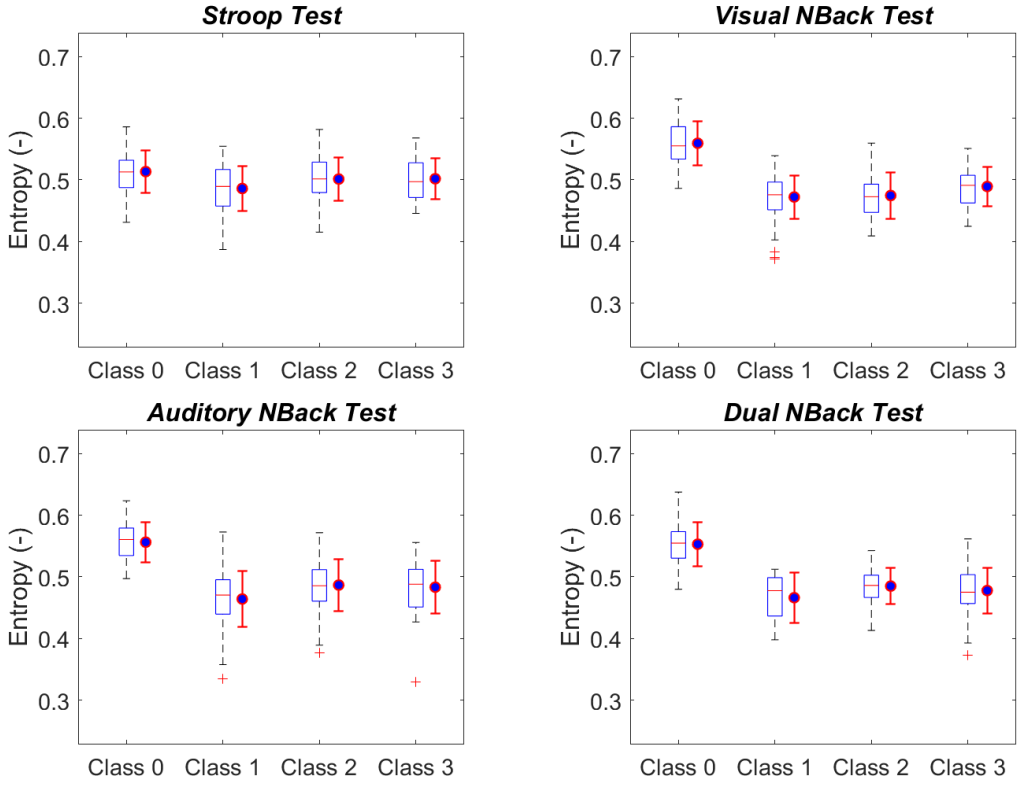

Figure B.17: Entropy feature

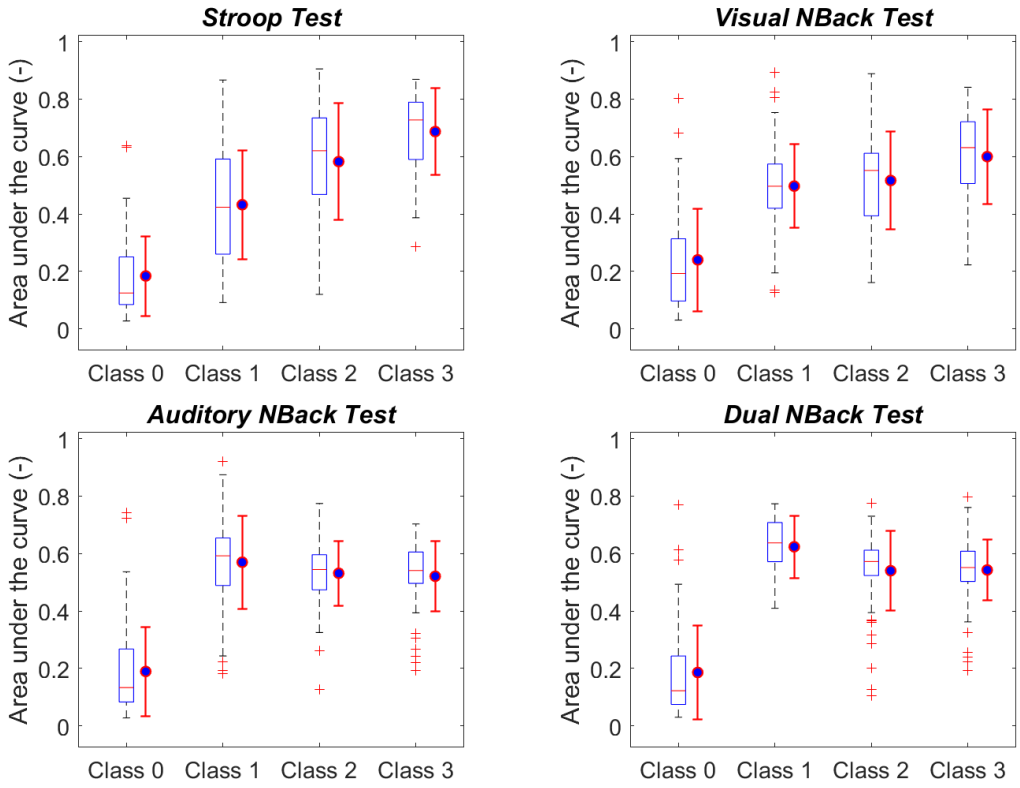

Figure B.18: Area under the curve feature

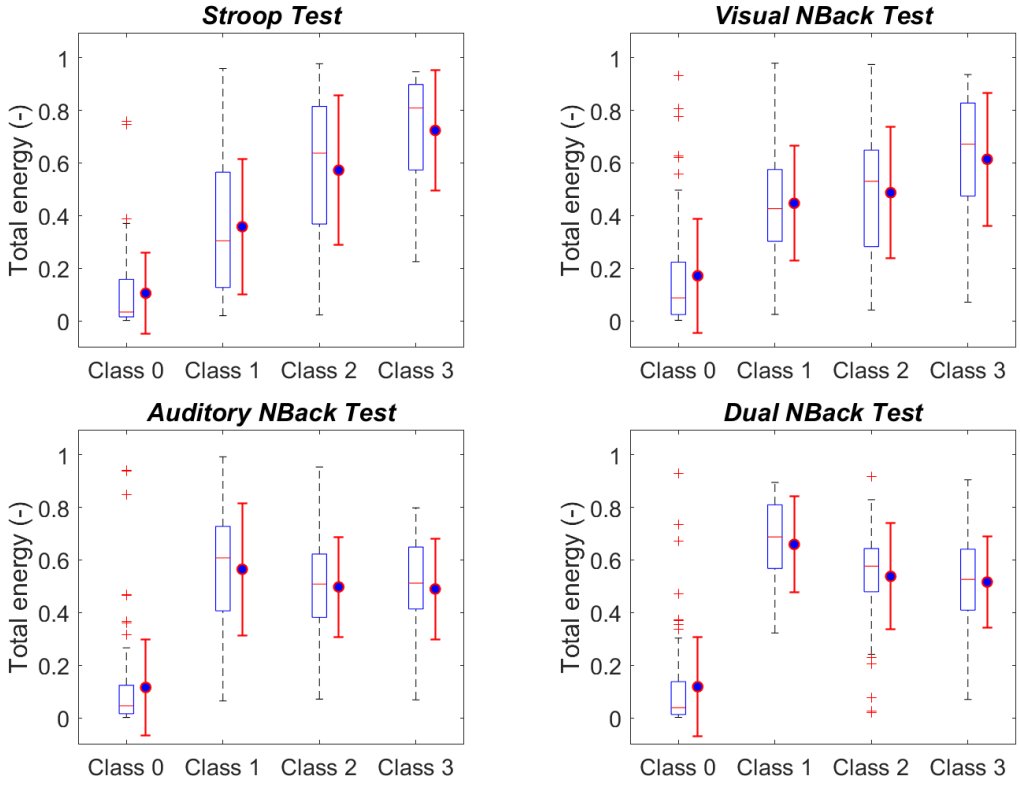

Figure B.19: Total energy feature

Bibliography

[1] Hans Selye. *Stress Without Distress*. Recording Services, 1972 (cit. on p. 6).

[2] Cofer and Appley. *Motivation: Theory and Research*. John Wiley, 1964 (cit. on p. 6).

[3] A. P. G. Martins. «A Review of Important Cognitive Concepts in Aviation». In: *Aviation* 20.2 (2016), pp. 65–84 (cit. on p. 6).

[4] Alice Baird, Lukas Stappen, Lukas Christ, Lea Schumann, Eva-Maria Meßner, and Björn W Schuller. «A physiologically-adapted gold standard for arousal during stress». In: *Proceedings of the 2nd on Multimodal Sentiment Analysis Challenge*. Cited on pages 3–5. 2021, pp. 69–73 (cit. on p. 6).

[5] D. R. Morse and M. L. Furst. *Stress for Success: A Holistic Approach to Stress and Its Management*. New York: Van Nostrand Reinhold, 1979 (cit. on p. 6).

[6] Allan V. Horwitz and Teresa L. Scheid. *A Handbook for the Study of Mental Health: Social Contexts, Theories, and Systems*. cit. on pp. 1, 4, 5. Cambridge University Press, 1999 (cit. on p. 7).

[7] I. Hoang, M. Ranchet, R. Derollepot, F. Moreau, and L. Paire-Ficout. «Measuring the Cognitive Workload During Dual-Task Walking in Young Adults: A Combination of Neurophysiological and Subjective Measures». In: *Frontiers in Human Neuroscience* 14 (2020). DOI: 10.3389/fnhum.2020.592532. URL: https://doi.org/10.3389/fnhum.2020.592532 (cit. on p. 8).

[8] H. Maior, M. Pike, S. Sharples, and M. L. Wilson. «Examining the reliability of using fNIRS in realistic HCI settings for spatial and verbal tasks». In: *CHI '15 Proceedings of the 33rd Annual ACM Conference on Human Factors in Computing*. 2015, pp. 3807–3816 (cit. on p. 8).

[9] R. F. Rojas, E. Debie, J. Fidock, M. Barlow, K. Kasmarik, S. Anavatti, M. Garratt, and H. Abbass. «Electroencephalographic Workload Indicators During Teleoperation of an Unmanned Aerial Vehicle Shepherding a Swarm of Unmanned Ground Vehicles in Contested Environments». In: *Frontiers in Neuroscience* 14 (Feb. 2020). DOI: 10.3389/fnins.2020.00040. URL: https://doi.org/10.3389/fnins.2020.00040 (cit. on p. 8).

[10] G. Young, L. Xavelina, and V. D. Hooper. «Assessment of Workload Using NASA Task Load Index in Perianesthesia Nursing». In: *Journal of PeriAnesthesia Nursing* 23.2 (2008). DOI: 10.1016/j.jopan.2008.01.008 (cit. on p. 8).

[11] H. Maior, M. Pike, M. L. Wilson, and S. Sharples. «Continuous Detection of Workload Overload». In: *Contemporary Ergonomics and Human Factors 2014*. Taylor & Francis, 2014, pp. 450–457. DOI: 10.1201/b16742-79. URL: https://doi.org/10.1201/b16742-79 (cit. on p. 8).

[12] M. Mazher, A. A. Aziz, A. S. Malik, and H. U. Amin. «An EEG-Based Cognitive Load Assessment in Multimedia Learning Using Feature Extraction and Partial Directed Coherence». In: *IEEE Access* 5 (2017), pp. 14819–14829. DOI: 10.1109/access.2017.2731784. URL: https://doi.org/10.1109/access.2017.2731784 (cit. on p. 8).

[13] Gerard Mulder. «The Concept and Measurement of Mental Effort». In: *Energetics and Human Information Processing*. Ed. by G.R.J. Hockey, A.W.K. Gaillard, and M.G.H. Coles. Vol. 31. NATO ASI Series. Springer, 1986. DOI: 10.1007/978-94-009-4448-0_12. URL: https://doi.org/10.1007/978-94-009-4448-0_12 (cit. on p. 8).

[14] Ima Pereira da Silva. «Mental workload, task demand and driving performance: what relation?» In: *Procedia-Social and Behavioral Sciences* 162 (2014), pp. 310–319 (cit. on p. 9).

[15] Gabriele Luzzani, Irene Buraioli, Danilo Demarchi, and Giorgio Guglieri. «Preliminary Study of a Pilot Performance Monitoring System Based on Physiological Signals». In: (2023). Presentato alla Aerospace Europe Conference 2023 – 10 EUCASS – 9 CEAS, p. 14. DOI: 10.13009/EUCASS2023-349. URL: https://doi.org/10.13009/EUCASS2023-349 (cit. on pp. 9, 31).

[16] J. H. et al. Tulen. «Characterization of stress reactions to the Stroop Color Word Test». In: *Pharmacology, biochemistry, and behavior* 32.1 (1989), pp. 9–15. DOI: 10.1016/0091-3057(89)90204-9 (cit. on p. 10).

[17] Mahdi Malakoutikhah, Reza Kazemi, Hadiseh Rabiei, Moslem Alimohammadlou, Asma Zare, and Soheil Hassanipour. «Comparison of Mental Workload with N-Back Test: A New Design for NASA-Task Load Index Questionnaire». In: *International Archives of Health Sciences* 8.1 (2021), pp. 7–13 (cit. on p. 10).

[18] J Ridley Stroop. «Studies of interference in serial verbal reactions.» In: *Journal of experimental psychology* 18.6 (1935), p. 643 (cit. on p. 10).

[19] J. Mark G. Williams, Andrew Mathews, and Colin MacLeod. «The emotional Stroop task and psychopathology». In: *Psychological Bulletin* 120.1 (1996), pp. 3–24. DOI: 10.1037/0033-2909.120.1.3. URL: https://doi.org/10.1037/0033-2909.120.1.3 (cit. on p. 11).

[20] Maura Mitrushina, Kyle B Boone, Jill Razani, and Louis F D'Elia. *Handbook of Normative Data for Neuropsychological Assessment*. cit. on pp. 32, 33. Oxford University Press, 2005 (cit. on p. 11).

[21] Susanne M Jaeggi and et al. «The concurrent validity of the N-back task as a working memory measure». In: *Memory (Hove, England)* 18.4 (2010), pp. 394–412. DOI: 10.1080/09658211003702171 (cit. on p. 11).

[22] W. K. Kirchner. «Age differences in short-term retention of rapidly changing information». In: *Journal of Experimental Psychology* 55.4 (1958), pp. 352–358. DOI: 10.1037/h0043688 (cit. on p. 11).

[23] J. F. Mackworth. «Paced memorizing in a continuous task». In: *Journal of Experimental Psychology* 58.3 (1959), pp. 206–211. DOI: 10.1037/h0044706 (cit. on p. 11).

[24] J. Au, E. Sheehan, N. Tsai, G. J. Duncan, M. Buschkuehl, and S. M. Jaeggi. «Improving fluid intelligence with training on working memory: a meta-analysis». In: *Psychonomic Bulletin & Review* 22.2 (2015), pp. 366–377. DOI: 10.3758/s13423-014-0699-x (cit. on p. 11).

[25] Susanne M. Jaeggi et al. «Does excessive memory load attenuate activation in the prefrontal cortex? Load-dependent processing in single and dual tasks: functional magnetic resonance imaging study». In: *NeuroImage* 19.2 Pt 1 (2003), pp. 210–225. DOI: 10.1016/s1053-8119(03)00098-3 (cit. on p. 11).

[26] Paul Ayres, Joy Y. Lee, Fred Paas, and Jeroen J. Van Merriënboer. «The Validity of Physiological Measures to Identify Differences in Intrinsic Cognitive Load». In: *Frontiers in Psychology* 12 (2021), pp. 1–16. DOI: 10.3389/fpsyg.2021.702538. URL: https://doi.org/10.3389/fpsyg.2021.702538 (cit. on p. 12).

[27] Ehsan Debie, Roberto F. Rojas, Jonathan Fidock, Matthew Barlow, Kassandra Kasmarik, Sreenatha Anavatti, and Matthew Garratt. «Multimodal Fusion for Objective Assessment of Cognitive Workload». In: *IEEE Transactions on Cybernetics* 51.3 (2021), pp. 1542–1555 (cit. on p. 12).

[28] PN Ainslie and P Brassard. «Why is the neural control of cerebral autoregulation so controversial?» In: 6 (2014), p. 14. DOI: 10.12703/P6-14 (cit. on p. 13).

[29] S. S. Kety and C. F. Schmidt. «The determination of cerebral blood flow in man by the use of nitrous oxide in low concentrations». In: *Amer. J. Physiol.* 143 (1945), p. 53 (cit. on p. 14).

[30] Payne Stephen. «Clinical Conditions». In: *Cerebral Autoregulation: Control of Blood Flow in the Brain*. Cham: Springer International Publishing, 2016, pp. 75–119 (cit. on p. 14).

[31] Frans F. Jobsis. «Noninvasive, infrared monitoring of cerebral and myocardial oxygen sufficiency and circulatory parameters». In: *Science* 198 (1977), pp. 1264–1267 (cit. on p. 17).

[32] Arno Villringer. «Non-invasive optical spectroscopy and imaging of human brain function». In: *Trends in Neurosciences* 20.10 (1997), pp. 435–442. DOI: 10.1016/s0166-2236(97)01132-6. URL: https://doi.org/10.1016/s0166-2236(97)01132-6 (cit. on p. 17).

[33] Franz Herold, Patrick Wiegel, Felix Scholkmann, and Norbert Müller. «Applications of Functional Near-Infrared Spectroscopy (fNIRS) Neuroimaging in Exercise–Cognition Science: A Systematic, Methodology-Focused Review». In: *Journal of Clinical Medicine* 7.12 (2018), p. 466. DOI: 10.3390/jcm7120466. URL: https://doi.org/10.3390/jcm7120466 (cit. on pp. 17, 22).

[34] Paola Pinti, Ilias Tachtsidis, Antonia Hamilton, Joy Hirsch, Clarisse Aichelburg, Sam Gilbert, and Paul W. Burgess. «The Present and Future Use of Functional Near-Infrared Spectroscopy (fNIRS) for Cognitive Neuroscience». In: *Annals of the New York Academy of Sciences* (2018). DOI: 10.1111/nyas.13948 (cit. on pp. 17, 18).

[35] Lun-De Liao et al. «Neurovascular Coupling: In Vivo Optical Techniques for Functional Brain Imaging». In: *BioMedical Engineering OnLine* 12 (2013), p. 38. DOI: 10.1186/1475-925X-12-38 (cit. on p. 17).

[36] Felix Scholkmann, Steffen Kleiser, Andreas J. Metz, Rolf Zimmermann, Jose M. Pavia, Ursula Wolf, and Martin Wolf. «A review on continuous wave functional near-infrared spectroscopy and imaging instrumentation and methodology». In: *NeuroImage* 85 (2014), pp. 6–27. DOI: 10.1016/j.neuroimage.2013.05.004. URL: https://doi.org/10.1016/j.neuroimage.2013.05.004 (cit. on pp. 17, 21–23).

[37] P. T. Fox and M. E. Raichle. «Focal physiological uncoupling of cerebral blood flow and oxidative metabolism during somatosensory stimulation in human subjects». In: *Proceedings of the National Academy of Sciences of the United States of America* 83.4 (1986), pp. 1140–1144. DOI: 10.1073/pnas.83.4.1140 (cit. on p. 18).

[38] Meltem Izzetoglu, Scott C. Bunce, Kurtulus Izzetoglu, Banu Onaral, Pourrezaei, and Kambiz. «Functional brain imaging using near-infrared technology». In: *IEEE Engineering in Medicine and Biology Magazine* 26.4 (2007), pp. 38–46. DOI: 10.1109/MEMB.2007.384094 (cit. on p. 18).

[39] Panteleimon Ekkekakis. «Illuminating the Black Box: Investigating Prefrontal Cortical Hemodynamics during Exercise with Near-Infrared Spectroscopy». In: *Journal of Sport and Exercise Psychology* 31.4 (2009), pp. 505–553. DOI: 10.1123/jsep.31.4.505. URL: https://journals.humankinetics.com/view/journals/jsep/31/4/article-p505.xml (cit. on p. 18).

[40] D. T. Delpy and M. Cope. «Quantification in Tissue Near-Infrared Spectroscopy». In: *Philosophical Transactions: Biological Sciences* 352.1354 (1997), pp. 649–659. URL: http://www.jstor.org/stable/56499 (cit. on p. 19).

[41] W. Cui, C. Kumar, and B. Chance. «Experimental study of migration depth for the photons measured at sample surface». In: *Time-Resolved Spectroscopy and Imaging of Tissues*. Ed. by Britton Chance. Vol. 1431. International Society for Optics and Photonics. 2005, pp. 180–191. DOI: 10.1117/12.44189. URL: https://doi.org/10.1117/12.44189 (cit. on p. 20).

[42] D.T. Delpy, M. Cope, P. van der Zee, et al. «Estimation of optical pathlength through tissue from direct time of flight measurement». In: *Phys. Med. Biol.* 33.12 (1988), pp. 1433–1442 (cit. on p. 21).

[43] Ferrari Marco and Quaresima Valentina. «A Brief Review on the History of Human Functional Near-Infrared Spectroscopy (fNIRS) Development and Fields of Application». In: *NeuroImage* 63.2 (Nov. 2012), pp. 921–935 (cit. on p. 23).

[44] Fares Al-Shargie, Masashi Kiguchi, Nasreen Badruddin, Sarat C. Dass, Ahmad Fadzil Mohammad Hani, and Tong Boon Tang. «Mental stress assessment using simultaneous measurement of EEG and fNIRS». In: *Journal of Neuroscience Methods* (2023) (cit. on p. 25).

[45] Yuta Murayama, Lizhen Hu, and Kaoru Sakatani. «Relation between prefrontal cortex activity and respiratory rate during mental stress tasks: a near-infrared spectroscopic study». In: *Oxygen Transport to Tissue XXXVIII*. Springer International Publishing. 2016 (cit. on p. 25).

[46] Matthias L Schroeter, Stefan Zysset, Thomas Kupka, Frithjof Kruggel, and D Yves von Cramon. «Near-infrared spectroscopy can detect brain activity during a color-word matching Stroop task in an event-related design». In: *Human brain mapping* 17.1 (2002), pp. 61–71 (cit. on p. 25).

[47] Y. Ogawa, K. Kotani, and Y. Jimbo. «Relationship between working memory performance and neural activation measured using near infrared spectroscopy». In: *Brain and Behavior* 4.4 (2014), pp. 544–551. DOI: 10.1002/brb3.238. URL: https://onlinelibrary.wiley.com/doi/abs/10.1002/brb3.238 (cit. on p. 26).

[48] Evan M Peck, Beste F Yuksel, Aryk Ottley, Robert J K Jacob, and Remco Chang. «Using fNIRS brain sensing to evaluate information visualization interfaces». In: *CHI 2013*. 2013 (cit. on p. 26).

[49] Hasan Ayaz, Patricia A Shewokis, Scott Bunce, Meltem Izzetoglu, Barry Willems, and Banu Onaral. «Optical brain monitoring for operator training and mental workload assessment». In: *NeuroImage* 59.1 (2012), pp. 36–47 (cit. on p. 26).

[50] Christian Herff, Dominic Heger, Ole Fortmann, Johannes Hennrich, Felix Putze, and Tanja Schultz. «Mental workload during n-back task—quantified in the prefrontal cortex using fNIRS». In: *Cognitive Systems Lab, Institute for Anthropomatics, Karlsruhe Institute of Technology, Karlsruhe, Germany* (2014) (cit. on p. 27).

[51] Ivan Kesedžić et al. «Classification of cognitive load based on neurophysiological features from functional near-infrared spectroscopy and electrocardiography signals on n-back task». In: *IEEE Sensors Journal* 21.13 (2020), pp. 14131–14140 (cit. on p. 27).

[52] *PLUX Biosignals*. URL: https://www.pluxbiosignals.com/products/professional-kit (cit. on p. 28).

[53] *tobii*. URL: https://www.tobii.com/products/eye-trackers/wearables (cit. on p. 28).

[54] William H. Kruskal and W. Allen Wallis. «Use of Ranks in One-Criterion Variance Analysis». In: *Journal of the American Statistical Association* 47.260 (1952), pp. 583–621. DOI: 10.1080/01621459.1952.10483441 (cit. on p. 37).

[55] The MathWorks Inc. *MATLAB version: 9.13.0 (R2022b)*. Natick, Massachusetts, United States, 2022. URL: https://www.mathworks.com (cit. on p. 39).

[56] Jiapu Pan and Willis J. Tompkins. «A Real-Time QRS Detection Algorithm». In: *IEEE Transactions on Biomedical Engineering* BME-32.3 (1985), pp. 230–236. DOI: 10.1109/TBME.1985.325532 (cit. on p. 42).

[57] Shekoufe Barahimi, Zahra Einalou, and Mehrdad Dadgostar. «Evaluation of hemodynamic response function during mental arithmetic task in fNIRS data using GLM method». In: *Neuroscience Informatics* (2023). URL: https://www.elsevier.com/locate/neuri (cit. on p. 44).

[58] Nguyen Thanh Hai, Ngo Q Cuong, Truong Q Dang Khoa, and Vo Van Toi. «Temporal hemodynamic classification of two hands tapping using functional near—infrared spectroscopy». In: *Frontiers in human neuroscience* 7 (2013), p. 516 (cit. on p. 45).

[59] Jaeyoung Shin and Jichai Jeong. «Multiclass classification of hemodynamic responses for performance improvement of functional near-infrared spectroscopy-based brain–computer interface». In: *Journal of biomedical optics* 19.6 (2014), pp. 067009–067009 (cit. on p. 45).

[60] Rui Varandas, Rodrigo Lima, Sergi Bermúdez I Badia, Hugo Silva, and Hugo Gamboa. «Automatic Cognitive Fatigue Detection Using Wearable fNIRS and Machine Learning». In: *Sensors* (2023) (cit. on pp. 45, 48).

[61] S. Matcher, C. Elwell, C. Cooper, M. Cope, and D. Delpy. «Performance Comparison of Several Published Tissue Near-Infrared Spectroscopy Algorithms». In: *Anal. Biochem.* 227 (1995), pp. 54–68. DOI: 10.1006/abio.1995.1275 (cit. on p. 47).

[62] Felix Scholkmann and Martin Wolf. «General equation for the differential pathlength factor of the frontal human head depending on wavelength and age». In: *Journal of Biomedical Optics* 18.10 (2013), p. 105004. DOI: 10.1117/1.JBO.18.10.105004 (cit. on p. 47).

[63] Paola Pinti, Felix Scholkmann, Antonia Hamilton, Paul Burgess, and Ilias Tachtsidis. «Current Status and Issues Regarding Pre-processing of fNIRS Neuroimaging Data: An Investigation of Diverse Signal Filtering Methods Within a General Linear Model Framework». In: *Frontiers in Human Neuroscience* 12 (2019). DOI: 10.3389/fnhum.2018.00505. URL: https://www.frontiersin.org/articles/10.3389/fnhum.2018.00505 (cit. on p. 48).